Swingarm and Rear Suspension Design in an Electric Reverse Trike

Hannes Nilsson

DIVISION OF PRODUCT DEVELOPMENT | DEPARTMENT OF DESIGN SCIENCES
FACULTY OF ENGINEERING LTH | LUND UNIVERSITY
2022

MASTER THESIS

Swingarm and Rear Suspension Design in an Electric Reverse Trike

A topology optimisation-based approach

Hannes Nilsson

LUND
UNIVERSITY

Swingarm and Rear Suspension Design in an Electric Reverse Trike

A topology optimisation-based approach

Published by

Department of Design Sciences
Faculty of Engineering LTH, Lund University
P.O. Box 118, SE-221 00 Lund, Sweden

Subject: Technical Design (MMKM10)
Division: Product Development
Supervisor: Per Kristav
Examiner: Axel Nordin

Abstract

OMotion AB is developing a new model of their vehicle that will house a more powerful motor than the current model, which uses a hub motor in the rear wheel. The motor will be mounted behind the seats in the rear of the vehicle, entailing that drive by either chain or belt will be necessary. This poses a few challenges, but also facilitates beneficial adjustments to vehicle dynamics. This project intends to tackle these challenges and opportunities.

The elaborate teachings of Tony Foale in *Motorcycle Handling and Chassis Design* are used as guidance regarding vehicle dynamics, while the process created by Karl T. Ulrich and Steven D. Eppinger in *Product Design and Development* was used during the conceptual phase.

Topological optimisation is used to reach a theoretically optimal swingarm design in terms of stiffness-to-weight, which subsequently becomes the basis of inspiration for a welded, more easily manufacturable design. This welded design is then improved iteratively based on its performance in several edge cases that the swingarm must be able to withstand.

Keywords: Topological/topology optimisation, swingarm, suspension, anti-squat, SolidWorks, finite element analysis, simulation

Sammanfattning

OMotion AB utvecklar en ny modell av deras fordon som ska ha en mer kraftfull motor än den aktuella modellen med navmotor i det bakre hjulet. Motorn ska monteras bakom sätena i bakre delen av fordonet, vilket medför att kedje- eller remdrift krävs. Detta utgör ett par utmaningar, samtidigt som det även plats åt gynnsamma justeringar till fordonsdynamik. Detta projektet ämnar att tackla dessa utmaningar och möjligheter.

Tony Foales detaljerade lärdomar i *Motorcycle Handling and Chassis Design* används som vägledning gällande fordonsdynamik, medan processen skapad av Karl T. Ulrich och Steven D. Eppinger i *Product Design and Development* användes under den konceptuella fasen.

Topologisk optimering används som en metod att nå en teoretiskt optimal svingarmdesign gällande styvhet-mot-vikt, vilket därpå blir en inspirationsbasis för en svetsad, mer tillverkningsbar design. Denna svetsade designen är sedan förbättrad iterativt baserat på dess prestationer i flera specialfall som svingarmen måste klara av.

Nyckelord: Topologisk/topologioptimering, svingarm, fjädringssystem, anti-squat, SolidWorks, finita elementmetoden, simulering

Acknowledgements

I want to thank Ola at OMotion for the opportunity that was this project, and for his patience—the patience to answer my seemingly endless questions, and for putting up with the added hurdles of SolidWorks license issues, and scheduling hours of Zoom time as the project ended up having to be done remotely given the absence of a powerful enough laptop.

To my girlfriend, my family, my cats, and Deftones.

I could not have done this without you.

The cats I probably could have done it without,

but they are loved no less because of it.

There's probably a typo somewhere in this report they directly caused…

Lund, October 2022

Hannes Nilsson

Table of contents

Introduction

1.1 Preface

Originally founded in 2013 in Lund, OMotion AB is developing a new model of their ‘electric reverse trike’. The currently retailing model, OMOTION 2, houses a hub motor in the rear wheel. The version currently in development which this project hopes to support in this endeavour, OMOTION 300, will have its motor upgraded to one mounted in the rear of the vehicle instead. This placement implies that drive by either chain or belt will be required. Opting for chain drive allows for beneficial changes to vehicle dynamics, but in doing so there are a few obstacles to overcome.

Due to confidentiality, some details in this report might be omitted or not explained in full detail.

1.1.1 **Objective**

The mission is to explore possible configurations of a swingarm construction, drive train, and suspension with regard to said redesign. The best concept is then further improved on, and by the end of the project hopefully supplies OMotion with a model based on a solid foundation for continued development of the vehicle.

1.1.2 **Scope & delimitations**

While recommended (or required) materials for the parts have been suggested, the specific retailers have not been chosen. If time had permitted, a model in a program such as Adams Car could have been used for this specific vehicle to simulate and measure the edge case forces during hard bumps and similar more accurately.

The actual settings of springs and dampers have been left in the hands of someone with more experience in driving the vehicle in question, namely OMotion themselves.

A thorough economic analysis was not included but was done ‘intuitively’ when sketching concepts and further designing the constituents of the construction.

Specific fittings for the motor mounting location were not designed as the actual placement of the motor, as will be shown, allows for some variance. The wheel hub and rim were also not modelled; in this case, time constraints were the reason.

1.2 Methodology

The project, being a development of a product and modification of the architecture within which it resides, drew on the guidelines by Ulrich et al. in *Product Design and Development* [1]. Their teachings encompass a much wider area regarding general product development than applicable to this project. As such, only a small portion of the process guidelines was used; chapter 3 details said parts.

The development process of the swingarm in this thesis can be divided into four main parts:

1. Developing a concept, detailed in chapter 4.
2. Using topology optimisation to yield a result that serves as a basis of inspiration for a subsequent welded design, detailed in chapter 5.
3. Modelling said welded design in SolidWorks (SW), detailed in chapter 6.
4. Simulating extreme cases that the swingarm must be able to withstand through finite element method (FEM) simulations, detailed in chapter 7.

There is also a 5th step, not entirely integral to the design of the swingarm itself, but rather an indirect necessity for it to function desirably. This consists of constructing a jackshaft subjected to high torsional stresses and possibly fatigue failure.

2 Product development process

In this project, the ‘Ulrich & Eppinger methodology’ of product development is used. The entire methodology is of course not fully applicable as there is a magnitude of segments either completely out of reasonable scope, or simply bear little relevance to the process in this project. Figure 2.1 shows the six phases of the generic product development process as described by Ulrich et al.

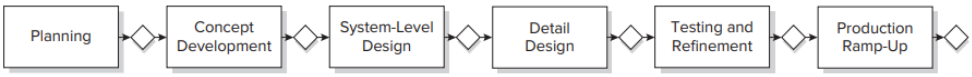

Figure 2.1 The six phases of the generic product development process (adapted from [1, p. 14]).

While the phases *Detail Design* and *Testing and Refinement* might suggest some activities that sound similar—or even equal—to the activities that will be performed in this project, most of the entire process resides in the *Concept Development* phase. Further, the full concept phase is not fully applicable, and as such adjustments to the process were made. These are detailed below.

2.1 Adaptation of process

The product in question in this project is a swingarm, a stiff structural link between frame, rear tyre, suspension fittings and brake calliper; there is no debate on what these core functions are, only how they are achieved. This ‘wiggle room’ manifests in that the product development process instead focuses on configurations in mounting positions and subsequent adjustments of affected parts, instead of conceptually different products. Henceforth, *concepts* refer to different configurations in this report rather than theoretical solutions born from thinking outside the box. In addition to this adaptation, the scope of this project sets limitations on how much of the process is applicable. No surveys or interviews with customers were made, manufacturing cost estimates were purely intuitive, and no physical prototype was made. Interviews were done informally, with OMotion themselves, which lays the basis for the ‘customer’ needs in this case. Described below are the main parts of their process that have been followed.

2.2 Concept development phase

Ulrich et al. list three overarching activities in Figure 2.2 that are meant to be performed in support of the many front-end activities of the concept development phase: *perform economic analysis*, *benchmark competitive products*, *build and test models and prototypes*. The extent of the economic analysis is as mentioned mostly intuitive, meaning that design choices whose economic impact is immediately apparent as too large are discarded promptly. A more thorough analysis was deemed out of scope. The benchmarking aspect mostly manifests in using competitors' products as guidance and inspiration—in this case swingarm configuration, suspension location, and other structural aspects. It is not feasible for this project to travel and rent one of the competitors' vehicles for actual numerical benchmarking. In any case, that time (and money) would be better spent on other parts of the project. The prototype testing was done in its comprehensive, analytical form (detailed further in 2.2.5.).

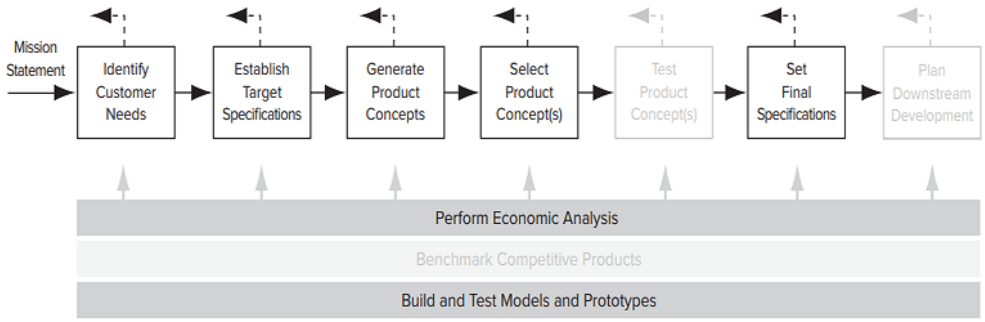

Figure 2.2 A view of Ulrich & Eppinger's concept development phase, modified for relevance (adapted from [1, p. 16]).

2.2.1 **Identifying customer needs**

No customer statements or large amounts of raw data were gathered. OMotion is the 'customer' in this case, and the needs and wants were mostly selected through discussion. The remaining needs and wants, perhaps not explicitly stated in these discussions, are of an obvious enough nature to not warrant mentioning.

2.2.2 **Establish target specifications**

The target specifications were not established conventionally, as the nature of this project, and given limited expertise in vehicle design especially at the initiation of it, made it difficult to pinpoint exact values. There are a few implicit binary

conditions that need to be met—the swingarm must not break during normal use for instance—and most of the rest are set through minimum manageable loads and torques in chapter 7.

2.2.3 **Generate product concepts**

In the concept generation phase, a few different configurations were made. A very rough sketch with pen and paper first, and then inside SW using references from the vehicle assembly.

2.2.4 **Select product concepts**

Ulrich et al. suggests several methods of concept selection, one of which is simply intuition [1, p. 151]. Discussions with OMotion about principal differences in different design layouts and subsequently going by intuition were the primary selection methods. A concept scoring matrix was also used, but with difficulty in confidently assessing an accurate grade for some selection criteria, it was mostly used as guidance and verification that the intuitive choice and the scored choice aligned.

2.2.5 **Further front-end activities**

The continuous activity *building and testing models and prototypes* and main activity *set final specifications* are what chapters 7 and 8 in this report entail. Ulrich et al. mention two different dimensions a prototype falls within: *physical–analytical* and *comprehensive–focused* [1, p. 297]. The prototype in this thesis is analytical and comprehensive—it is a CAD model of the swingarm, tested comprehensively, namely against all edge cases it must be able to withstand during everyday use (although one would hope that some of the more extreme edge cases do not occur *every day*). The testing for the jackshaft is done through strength and fatigue calculations for the jackshaft.

The final specifications are essentially set for the swingarm when the simulations show promising results, and for the jackshaft when the calculations show that the geometry and material choice is sufficient.

Something of note is that *Test Product Concept(s)* is greyed out in Figure 2.2. Judging by the title of this activity it sounds like the testing mentioned above would fall into this step, but Ulrich et al. describe it rather as market-response testing, or *resonance testing*, which was not done during this project.

2.3 Topology optimisation phase

Before being able to proceed with the TO, several necessary modifications were made to the rear of the frame so that the fittings for swingarm and suspension had rigid places to be welded onto. These changes are described below.

Removed:

- A horizontal tube spanning the entire width of the rear.
- Two short vertical tubes supporting the bar mentioned above.

Added:

- Two vertical rectangular tubes supporting the swingarm fittings and jackshaft bearings.
- Two smaller tubes supporting them laterally near the fitting.
- A laterally spanning rectangular tube at the top of the rear frame, to which the frame fittings for the rear suspension will be welded.

Moved:

- A laterally spanning tube at the top of the frame. It was moved forward a very small distance for the newly added vertical rectangular tube to attach to.

With the selected concept, and the frame now modified accordingly, the reference points from the vehicle assembly were used as boundary conditions for the TO and subsequent FEM simulations. The TO study itself included many cases with different types of loads, mimicking real-life scenarios.

2.4 FEM phase

The result from the TO was superimposed into a new part file to aid in modelling a welded design while attempting to stay true to said TO result. After this, a few FEM simulations were done on the initial design to evaluate its strengths and weaknesses.

Many iterative redesigns were then conducted to better comply with the forces and torques of more detailed edge cases, after which a finalized design was reached.

3 Vehicle Dynamics

The topic of vehicle dynamics is vast and complex; for the purposes of this project, mostly large-scale vehicle dynamic effects were considered. This was done partly due to some areas adding far too much complexity for the small benefit in simulation accuracy. Mostly, however, it was due to the time frame within which the project was carried out and considering a limited experience regarding said dynamics at the start of the project. An example of a highly complex part present (hopefully) on all normal road vehicles is the tyre; springing and damping forces acting in several different directions all at once, different internal plies in different orientations made of different materials, slip angles and pneumatic trails [2]. A similar area of slightly larger scale is the suspension itself: springs and dampers. These impact the driver comfort significantly and are more easily modelled in software such as the Adams Car package. Compare this to tyres that instead might use both several springs and dampers spread out over the contact patch [3]. Time constraints hindered using any such software, and ultimately the choices regarding driver comfort—spring rate and damping ratio, etc.—were considered better left in the hands of someone with large amounts of experience in driving the actual vehicle (i.e., left for OMotion to decide for themselves).

3.1 Load transfer

Sometimes misnomered as weight transfer, load transfer is the shifting of load either to the front or the rear of the vehicle because of braking or acceleration, respectively. If 100% of the load is transferred to the rear a ‘wheelie’ occurs. There are four main sources of load transfer: inertial, aerodynamic, attitude-dependent and torque-reaction-dependent [2, p. 9:1]. Only inertial load transfer is considered in this project since it is of greatest magnitude (unless, of course, future models include for example massive aerofoils).

Aerodynamics is a highly complex field and the load transfer relating to it needs to be simulated with a very true-to-life design; it is far outside the scope of this project. Attitude-dependent load transfer is the difference in front vs rear loading when driving up- or down-hill. Since the vehicle will be driven on public roads, very seldom going into double digit degrees of incline—at least for speeds and distances where load transfer could be regarded as something of concern—this type of load

transfer was ignored. Load transfer due to torque reaction could have a discernible effect for the driver during regular use and might be an area of interest for further development, but the magnitude of it was not calculated. For the scope of this project, moving the torque-reaction away from the inside of the rear wheel when using a hub motor (directly making the swingarm pivot, and thus lifting or lowering the rear of the frame) to affecting the entire frame instead (both due to motor and jackshaft) was deemed enough of an improvement.

3.2 Squat, dive, rise

When a vehicle accelerates and subsequently has load transferred from the front to the rear, the rear suspension is loaded and thus compressed. Consequentially, the front suspension is unloaded and extended. This pitching motion is called *squat*. Aerodynamic forces also add to this effect, whereas dive—the front suspension compressing and the rear extending—is typically only caused by braking [2, p. 9:4].

Since the rear brake calliper is mounted to the swingarm, the torque created due to braking has some pro-squat tendency. This is however largely counteracted by load transfer dive and significantly reduced due to *brake bias* (what percentage of braking is done by the front or rear wheels) not being 100% rear-wheel-bias.

3.3 Anti-geometry

The pitching motions mentioned above are rather intuitive and have been felt by anyone who has ridden in a car, or mountain bike. There is however sometimes an advantage to countering some, or even all, of this pitching. Most notably, *anti-squat* (AS) geometry is a very commonly used method; *anti-rise* also exists but is much less common. There is also a type of anti-geometry known as anti-dive, which is the prevention of forward pitching under braking. This is largely dependent on the front suspension and was thus not a part of this project.

3.3.1 **Anti-squat**

Anti-squat can be determined in different ways depending on the type of drive used, ‘paralever’ or single link swingarm, diameters of wheel and sprockets—the list goes on. Only the specific case that concerns the OMOTION 300 will be explained in this report: a single link swingarm, using rear wheel chain drive. Without going into too much detail, as only the surface-level method of geometrically determining the anti-squat will be referred to, there are simply a few reference points needed.

The approximate centre of gravity (CoG) is easily determined in the SW assembly of the vehicle. A horizontal line is drawn from the CoG to a line extending vertically from the front axle. The *instantaneous force centre* (IFC) is determined by extending the line along which the swingarm links the rear wheel to the frame and finding its intersection with the line extending from the driving chain run (i.e., the upper run during acceleration). A line is then drawn from below the rear wheel axle, extending through the IFC to the vertically extending line. How far up this line intersects the vertical line determines the magnitude of anti-squat. More specifically, if it intersects the vertical line at the same height as the CoG, 100% AS is achieved; if it instead intersects the line at 80% of this height, 80% AS is achieved. See Figure 3.1 for a visualisation. The example uses a motorcycle instead, but the method is identical since it has the same type of swingarm and chain drive.

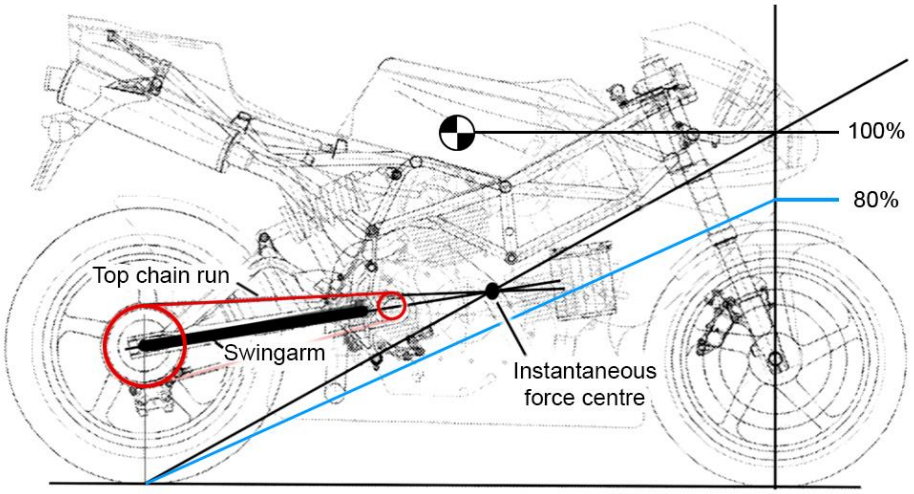

Figure 3.1 A visualisation of anti-squat determination (adapted from [2, p. 9:14]). The larger red circle is the rear wheel sprocket, the smaller sprocket is the driving sprocket.

3.3.2 **Anti-rise**

Braking causes load transfer, and under normal braking with both front and back wheel(s) this is highly utilised; using brake bias to brake harder with the wheels that get additional load makes perfect sense. The specific case of 'rear braking only' is more troublesome. In most cases, this is avoidable by not using *only* rear braking. The case with OMOTION 2 is not so simple, using a hub motor inside the rear wheel where regenerative braking is a necessity. This type of braking is essentially just a torque countering the rotation of the wheel. The swingarm is then also subjected to this torque, causing the front of the swingarm to rise, pushing the whole rear of the vehicle up. This can create an 'unintuitive' rider experience; in some cases, this

unloading of the braking wheel can sometimes cause the tyre to intermittently leave the ground [2, p. 9:43].

A method of countering this must be employed. To our advantage, chain drive has easier methods of accomplishing this. Much like in the case of anti-squat, anti-rise is calculated using the IFC and the chain run that is under load [2, p. 9:16]. During regenerative braking with chain drive, the bottom chain run is in tension. As long as the extended line of this chain run and the swingarm line create an IFC that yields an acceptable percentage, rise during regenerative braking will not be an issue. As we will see in chapter 4, this will be achieved. A visualisation of the aforementioned lines is shown in Figure 3.2.

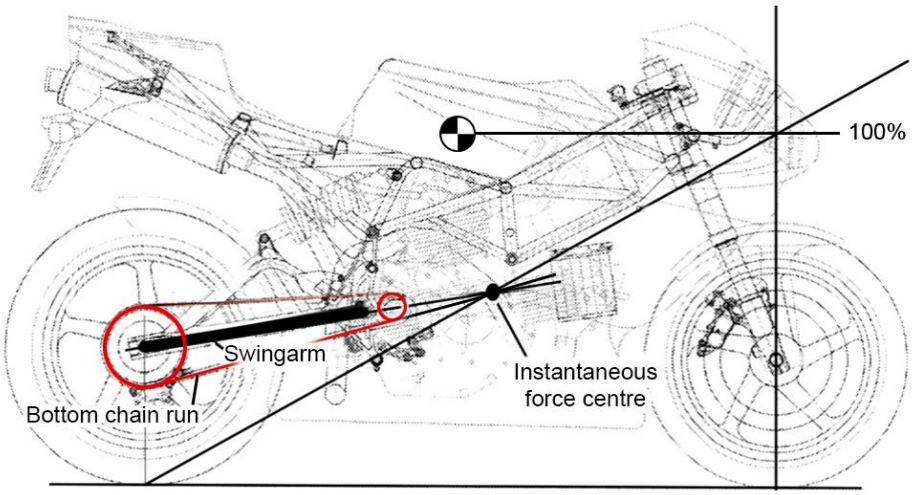

Figure 3.2 A visualisation of anti-rise determination (adapted from [2, p. 9:14]).

3.4 OMOTION 300

Whenever the weight or the mass of the OMOTION 300 is referred to, a dummy mass of 80 kg is added through a simply modelled driver sitting in the driver's seat. This puts the total combined mass, or *laden mass*, at roughly 455 kg (subject to change). For all calculations and weight-dependent results in the report, unless otherwise specified, this is the mass and the subsequent CoG placement that is used.

3.4.1 **Initial goals**

An initial target of being able to accelerate from 100 km/h from a standstill in five seconds was set, which supposedly required a total gear ratio of roughly 6. Upon

further consideration, reaching a higher top speed had its priority increased, sacrificing some maximum attainable acceleration. The total gear ratio eventually became 4,77 after selecting sprockets, whose choice was largely guided by frame clearance. This is further elaborated below.

A specific motor was selected for the new trike model. This motor had a peak torque of 130 Nm, which with a total gear ratio of 4,77 means the rear wheel will exhibit a peak torque of 620 Nm. Taking the rear wheel diameter into account, a theoretical maximum force at the rear wheel contact patch of 2400 N is achieved. With a rough measurement of the total weight of the new model, a maximum acceleration of 5,27 m/s^2 is suggested, which would put the new 0-100 km/h at a—coincidentally similar—value of 5,27 s. This is of course still a simplified scenario, not considering things like the inertia of jackshaft and wheels, air drag and the total weight not being fully accurate, to name a few.

As previously mentioned, OMotion decided on a target value of 100% AS.

3.4.2 **Anti-squat implications**

In order to achieve said AS percentage, the SW assembly of the vehicle was used so the CoG could be referenced. This meant that, for a given set of sprockets, a sketch could easily be made that fully adhered to the AS percentage. This yielded a problematic sketch; no combination of reasonable sprockets allowed for direct mounting from rear wheel sprocket to the driving sprocket[1]. The solution was to use a *jackshaft* (or *countershaft*), an intermediate axle that would allow redirection of chain forces so that the forces in the chain 'pulling the swingarm' instead are directed in a purposefully chosen direction; see Figure 3.3.

[1] 'Reasonable' in this case perhaps makes it sound like the choices were very limited—they were not. A multitude of configurations were considered, but immediately obvious spatial concerns inside the frame, or extreme sizes obviously not permissible were disregarded, for example.

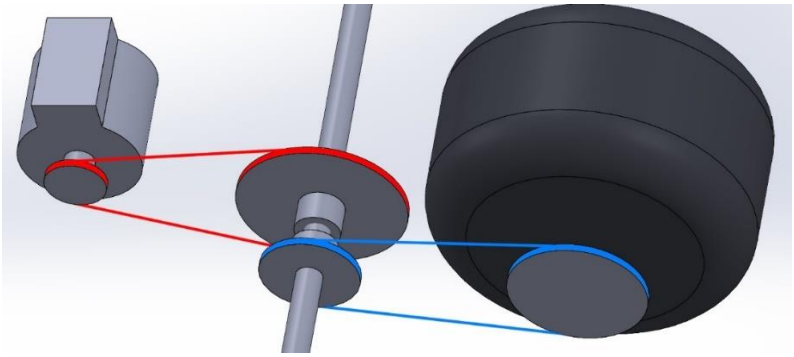

Figure 3.3 A visualisation of the jackshaft (middle), allowing for the driven sprocket on the motor (left) to transfer torque to the wheel sprocket on the wheel (right). Note the ability to mount different sprocket sizes on the jackshaft. Both ends of the jackshaft are mounted in bearings (not pictured). The sprockets and respective chains have been coloured for clarity.

This can be thought of as placing the driving sprocket in the specifically required location to achieve 100% AS—for example like the driving sprocket in Figure 3.1—and then simply driving this now-correctly-placed sprocket through other means, which can be rigidly attached to the frame. This allows for subjecting the frame to loads instead of the suspension.

Some additional benefits follow when opting for a jackshaft design. First, if this jackshaft is mounted close to and in-line with the swingarm, the chain tension also becomes very consistent. If mounted fully concentric, the tension remains completely unchanged when the swingarm pivots (during suspension travel). Second, the jackshaft also enables the total gear ratio to be reached in two steps instead of one. Instead of going directly from a very small sprocket to one with 4,77 times the diameter, two smaller steps can be taken instead. Third, a desirable value of anti-rise is easily achieved. Furthermore, this allows a large degree of freedom in motor mounting location, aiding in either some slight CoG manipulation or in making space for other vital parts.

The shaft itself is simply an axle, whose dimensions and material required are determined in chapter 8. The sprockets are, more specifically, hub sprockets. The sprockets and shaft transfer torque through the use of a key. Figure 3.4 below shows one such transmission element (on the jackshaft, the part on the right with is instead replaced with a hub sprocket), as well as an example of a hub sprocket.

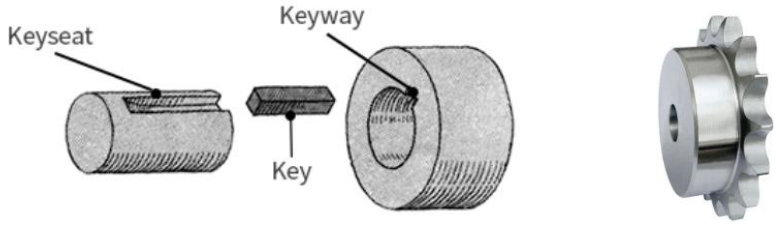

Figure 3.4 Left: nomenclature of keyed joint [4]. Right: hub sprocket (without keyway) [5].

Depending on the placement in the frame, the shaft itself might become long, as it requires mounting in bearings on both sides. An exception would be if the shaft was large enough in diameter and short enough in length to resist bending. For future development, one such shaft using splines instead of keys might be considered. This is also discussed further in chapter 8.

Despite the jackshaft allowing for a higher degree of flexibility in mounting positions, all the positions allowing for 100% AS were rather close to the bottom of the frame. A specific set of sprockets were chosen to stay clear of it. For example, a quite large sprocket on the jackshaft connected by chain to the driving sprocket on the motor had to be chosen (the 'red' sprocket in Figure 3.3). It would have been preferable to increase the diameter of the driving sprocket to reduce the load it experiences, reduce the diameter of the larger jackshaft sprocket to reduce its inertia, and shift some of the gear ratio towards the jackshaft sprocket–rear wheel sprocket. This very quickly caused a 'bottoming out' where the larger jackshaft sprocket collided with the bottom of the frame.

3.4.3 **Load transfer**

The inertial load transfer towards the rear is calculated as

$$\Delta W_r = \frac{mah}{L}$$

Where m is the mass, a is the acceleration, h is the CoG height, and L is the wheelbase[2] [2, p. 9:2]; the load transfer towards the rear is the same value but negative. During hard braking when the acceleration is negative, the load transfer *towards the rear* is as well, unloading the rear, and vice versa for the front of the vehicle. These variable values are fetched from the non-final OMOTION 300 assembly and are thus not fully accurate. The maximum load transfer due to either maximum acceleration or hard braking was averaged for simplicity and set to the

[2] The longitudinal distance from the centre of the front wheels to the centre of the rear wheel.

same absolute value. It must be commented that the maximum positive acceleration is lower than the negative acceleration during the approximated hardest braking, further detailed in 7.1.2. An approximated load transfer of 725 N was calculated[3]; a thorough analysis of a more accurate value would not deviate much from this.

3.4.4 **Other improvements**

An advantageous consequence of the new, higher mounting location of the swingarm is that bumps in the road (when travelling forward, specifically) cause the rear wheel to deflect upward at slight backward angle. This results in a less harsh experience for the driver; see Figure 3.5.

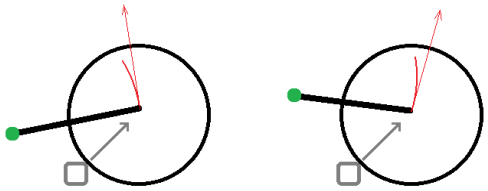

Figure 3.5 Travel direction is to the left; the swingarm pivot is marked by a green dot. Left: lower swingarm pivot requiring the wheel to 'overcome' the obstacle (visualised by a small, red circular arc). Right: higher swingarm pivot letting the wheel deflect at a backward angle.

Further, the change from hub motor to frame-mounted motor reduces the unsprung weight of the vehicle which will improve the vehicle handling and driver comfort.

[3] Listing the exact variable values used was deemed unnecessary and might not reflect the final values of the OMOTION 300 anyway.

4 Concept Development

4.1 Identifying customer needs

OMotion is regarded as the customer in this case, and the needs and wants are determined accordingly. Instead of customer statements and interpreted needs as suggested by Ulrich et al. [1], discussions laid the ground for a few ‘core needs’, and some additional wants; most of the needs and wants are obvious, and the specific extra wants were few:

The product needs	**to link the rear wheel axle rigidly to the swingarm fitting on the frame**
	to withstand a certain amount of load and torque, in certain directions
	to not deform excessively under high load and/or torque
	a way to mount coil-over shock absorber suspension
	a place to fasten a brake calliper at an exact height
	to allow for an acceptable amount of anti-squat
The product hopefully	allows mounting a coil-over shock absorber on both lateral sides
	allows for an exact amount of anti-squat
	has a considerably long lifetime
	adheres to spatial concerns
	is not too expensive
	is easily installed
	looks good

The spatial concerns are mostly regarding a future battery compartment, roughly 100 mm in height, covering most of the bottom of the frame in the rear. This compartment is not finalised in geometry and could be redesigned if required. It is desirable but not completely necessary for swingarm, jackshaft, sprockets and chains to stay fully clear of it. Further, there are other obvious ‘spatial wants’, in the sense that the construction does not become obstructive to other parts without adding much value. If a redesign suggests a structure where the swingarm becomes only slightly more rigid while sacrificing a considerable amount of space, it is not a worthwhile change.

4.2 Establish target specifications

With limited expertise in the field, the target specifications were not thoroughly explored and defined. A focus was put on the structural capabilities of the swingarm construction itself, and subsequent iterative design if it proved too weak; the same was done for the jackshaft. The target specifications regarding exact forces and torques are further detailed in the FEM simulations listed in chapter 7, and chapter 8 for the swingarm.

4.3 Generate product concepts

The concepts were generated by initially thinking about principally different mounting configurations, and then further refined using reference points and trying different sprocket size combinations inside the SW assembly (because changing the sizes while keeping the total gear ratio consistent, changes the mounting locations required to maintain the chosen AS percentage). The 'optimal' sprocket sizes were chosen by simultaneously considering conflicting properties:

- **Clearance to frame**. In concepts A and B, shifting more of the gear ratio from motor-jackshaft to jackshaft-rear wheel might make the sprocket sizes look more 'coherent', but the clearance to the bottom of the frame at the jackshaft quickly diminishes.
- **Other sprocket size concerns**. Making the larger jackshaft sprocket even larger in concepts A and B does result in a higher clearance to the bottom of the frame, at the cost of taking up space where other things might eventually have to be mounted. In concept A it also further reduces the space a crossbar might be built. In concept C, clearance is needed to the back of the seats, the top of the battery compartment, and other things that needs to be mounted close to the motor as well such as the inverter.
- **Inertial changes**. Adding more mass to the sprocket at an increasing diameter, the construction rapidly starts acting like a small flywheel. This means the vehicle not only becomes slower to accelerate, but also increases the stopping distance during hard braking. No calculations detailing this were made, as it would be difficult to effectively compare the values to the other conflicting properties.
- **Aesthetics**. Given a choice of sprockets close in size, the one that makes the whole configuration most coherent is preferably chosen.

The visualisations of the concepts shown below all use the same sprockets sizes. For concept A and B this makes little difference as the sizes needed to be kept very similar for the reasons listed above. In concept C the sizes could have been modified slightly, so the visualisation of the concept is simply showing the configuration principle and has an ability to move the jackshaft location to some degree.

As mentioned, all three concepts make use of a jackshaft with two sprockets on them, acting as a redirection of forces to reach a certain AS percentage. Initially the concepts were roughly sketched on paper, after which they were evaluated further inside the SW assembly. The concepts are shown below in Figures 4.1, 4.3, and 4.5.

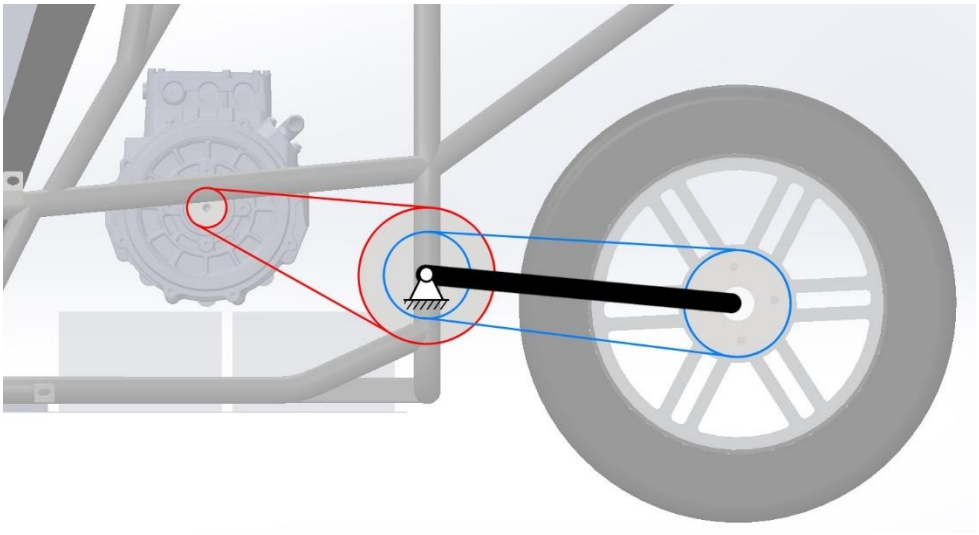

Figure 4.1 Concept A. The motor–jackshaft sprockets and chain are shown in red; the jackshaft–rear wheel sprockets and chain are shown in blue. Note that this is a very simplified picture taken from the assembly with all parts removed except the ones needed to show the concept. The two rectangular objects near the bottom left are part of the battery compartment.

Concept A is the clear winner in AS consistency during suspension travel[4] (this consistency is explained below). The concentricity of swingarm and jackshaft mounting keeps the anti-rise equally consistent and guarantees a chain tension that is unchanged when the swingarm pivots. The design does however require a redesign of the battery compartment due to the large jackshaft sprocket colliding with it.

[4] 100% AS becomes roughly 78% when both wheels are displaced upward 20 mm. Displacing only the rear wheel this distance instead puts it closer to 79%.

Worse yet, a very significant drawback is the other spatial changes the concept necessitates. The jackshaft sprockets are both hub sprockets, which requires much more space along the jackshaft axis, pushing the bearings it would be mounted in further apart. The larger jackshaft sprocket also protrudes quite a bit from the back of the frame, which could look quite odd. This also means the space for a 'crossbar' (laterally extending bar, connecting both sides of the swingarm) is more restrictive in this concept, and it would likely have to pass either over the upper chain run or below the bottom one.

A visualisation of the aforementioned AS consistency is visualised in Figure 4.2. Note how the instantaneous force centre moves forward with rear suspension compression; likewise, it moves rearward with rear suspension extension.

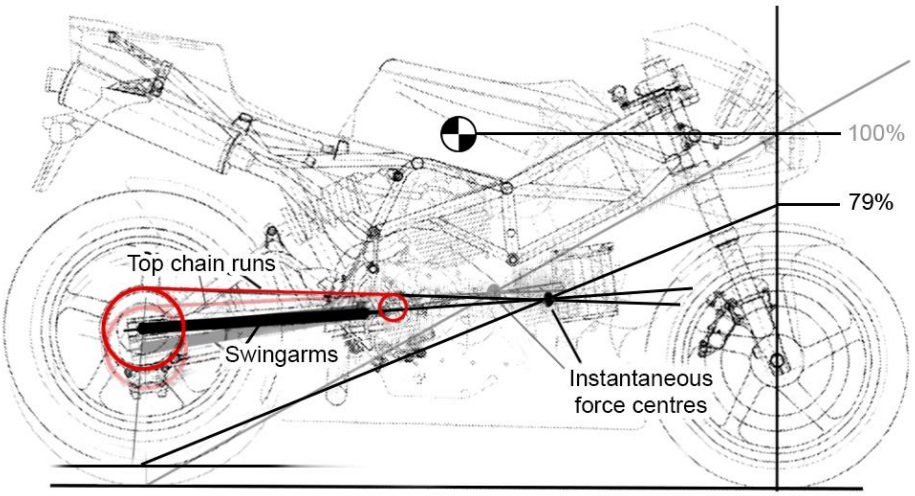

Figure 4.2 An example of how the AS percentage changes with suspension compression. The configuration is the same as in Figure 3.1 and the suspension is compressed an arbitrary amount just for this explanation. The normal driving scenario is superimposed with some transparency, and the compressed-rear-suspension-scenario is shown fully opaque.

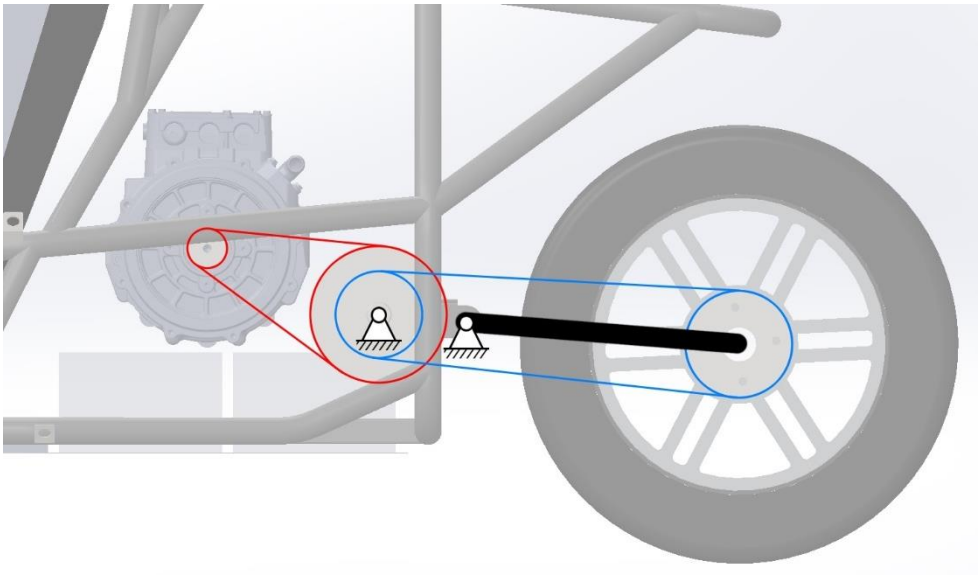

Figure 4.3 Concept B. Comments regarding visualisation are the same as in Figure 4.1.

Concept B was created as a variance on concept A described above. It is reminiscent of many motorcycle and reverse trike designs, placing a sprocket slightly forward of the swingarm mounting position (like in Figure 4.2). The AS percentage consistency is worse[5] than concept A but still passable, and the same goes for its anti-rise capabilities. The chain tension is no longer fully consistent as the distance between the centres of the 'blue sprockets', and the length of the swingarm, create two unequal radii. The smaller radius created by the swingarm length veers away from the 'vertical' path (when the swingarm pivots) quicker than the radius created by the blue-sprocket-centres-distance. The shortened distance during swingarm pivot means that a chain—which obviously does not change its length—becomes less tensioned, resulting in more slack.

This design also requires a redesign of the battery compartment, but this is starting to look unavoidable. The design is more easily manufactured and is likely more rigid than concept A could be. This is because, instead of oval flanged bearings whose base exceeds the width of the vertical tubes they would be mounted on, it allows using *plummer block bearings* (or *pillow* block bearings) See Figure 4.4 for examples of these bearings.

[5] 100% AS becomes roughly 42% when both wheels are displaced upward 20 mm. Displacing only the rear wheel this distance instead puts it closer to 43%.

Figure 4.4 Left: plummer block bearing [6]. Right: oval flanged bearing [7].

The design tucks the jackshaft further into the frame, which looks better. There is also more space for a potential crossbar which might mean higher lateral stiffness.

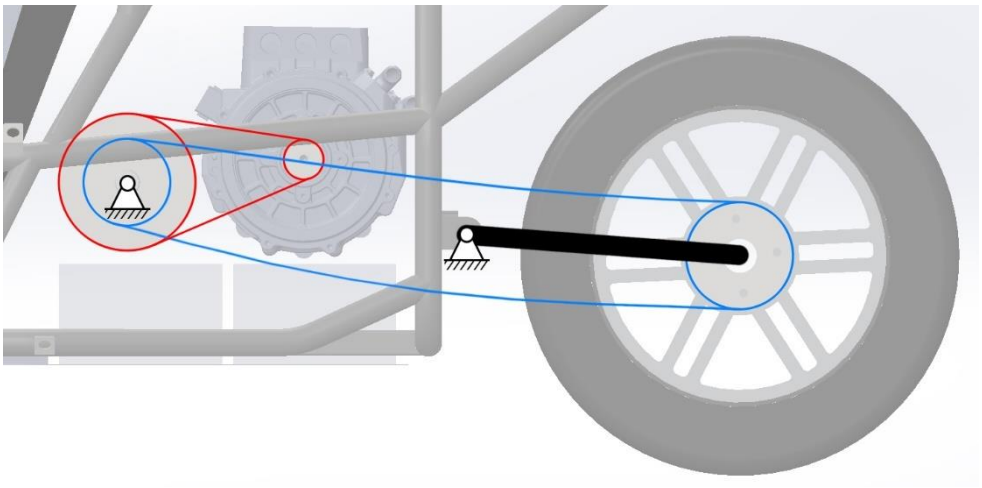

Figure 4.5 Concept C. Comments regarding visualisation are the same as in Figure 4.1.

Although not immediately apparent in the figure, Concept C was born as the only alternative that theoretically could allow for a mounting where both jackshaft sprockets and chains all avoid hitting the preliminary battery compartment. With chain slack, however, the margin becomes very small and even collides when the suspension is extended. The core idea of this concept might have initially looked good, but eventually proved not entirely feasible.

It might look ‘cooler’ than the other concepts, but it sports an atrocious AS consistency. It *very* quickly becomes pro-squat even during very little weight transfer. The anti-rise consistency is equally poor—perhaps even worse.

4.4 Select product concepts

Proceeding with a design that seems to harbour fewer potential points of failure—both in manufacture and function—felt like the correct solution. This seemed to favour concepts A and B. While concept A was the first one to be sketched out in the SW assembly as it looked most promising regarding AS consistency with suspension travel, spatial constraints regarding the jackshaft were certainly highly concerning. Namely, since hub sprockets were needed for the jackshaft, a significant amount of lateral space was required compared to using sprockets without hubs (initially considered but scrapped due to concerns regarding strength).

Without undergoing a drastic redesign, concept A simply did not fit. A case where additional changes to the frame would be made that might have allowed this was not completely ruled out, but not preferred.

Table 4.1 shows the concept scoring matrix used as a ‘second opinion’ to verify if what felt best intuitively also scored the highest when using some other selection criteria. The emphasis on fewer points of failure means that a design which might look exceptional with regards to one aspect, but appear questionable in another *crucial* aspect, will be highly scrutinised.

Table 4.1 The concept scoring matrix for the three different 'concepts' [1, pp. 160-165]. Weight is truncated as 'Wt.', and weighted score is abbreviated as 'WS'.

		Concept A		Concept B		Concept C	
Selection Criteria	**Wt.**	**Rating**	**WS**	**Rating**	**WS**	**Rating**	**WS**
AS consistency[a]	25%	4	1,00	2	0,50	1	0,25
Ease of manufacture	15%	3	0,45	4	0,60	2	0,30
Spatial concerns	20%	2	0,40	4	0,80	2	0,40
Chain tension consistency	10%	4	0,40	3	0,30	1	0,10
Weight[b]	5%	2	0,10	2	0,10	3	0,15
Aesthetics	5%	2	0,10	3	0,15	4	0,20
Rigidity	20%	3	0,60	4	0,80	3	0,60
Total Score		3,05		3,25		2,00	
Rank		2		1		3	

[a] *During suspension travel.*
[b] *1 = heavy, 5 = light.*

The scoring matrix reaffirms the selection of concept B instead of A and favours it significantly more than C. Concept A was largely carried by its near-exceptional AS consistency as predicted but fell short in other areas such as the aforementioned spatial concerns and ease of manufacture. Concept C was initially created to circumvent having to redesign the battery compartment. When briefly modelled inside the SW assembly, it was the only concept out of the three that managed to stay fully clear of said compartment. When factoring in chain slack, however, especially in the bottom chain run, it does not perform much better. During suspension extension, it performs even worse. Furthermore, structural members or a large fastening structure would have to be added to mount the jackshaft at this forward location, in a place where spatial concerns are likely already high.

An early idea was to compare the configurations more thoroughly to each other based on the AS consistency, in which case concept A likely would have cemented its highest ranking even further. It adds little value as a comparison, however, seeing as the spatial concerns almost dismiss the concept immediately.

4.5 Further refinement

As mentioned in 3.4.2, it would have been preferable to increase the diameter of the driving sprocket on the motor, to reduce the load it will be subjected to; this would in addition also reduce the subsequent wear. A small increase in size was tested, which unfortunately proved unfruitful. It either placed the jackshaft mounting location too far down or further increased the already large size of the connecting sprocket on the jackshaft. The exact sprocket dimensions were thus determined, in accordance with a small interval in possible total gear ratio.

This determined the final locations of swingarm mounting and centre of jackshaft axle, which were then used as references for the topology optimisation study.

5 Topology Optimisation

Topology optimisation simply put, is the process of modifying—in most cases by subtractive means—a given volume, or *design space*, while adhering to a rule of maximising one property while minimising another. In this project the property to maximise is stiffness, and the weight is to be minimised; another way to phrase this is to simply maximise the ratio of stiffness-to-weight. As such, the power of using a TO program is that it is a reasonably quick way of reaching a highly optimised, often very complex geometry for a very specific purpose. Some complex geometries are practically impossible to design completely by intuition and would take an excessive amount of time if designed iteratively through trial and error of trusses or lattices. One additional benefit of TO is that there might be alternative configurations not immediately apparent if a part was designed simply through intuition and experience.

5.1 Input

5.1.1 **Design space**

As with most topology optimisations, the design space in this project was made as large as possible within reasonable realms. Had this volume been widened beyond the points where the fittings are welded to the frame, the results might have yielded a slightly different result than if said points were the furthest ones in the lateral direction. There were still spatial constraints at play, however. Any swingarm wider than the fittings might just prove detrimental in the future. Thus, a maximum width was set.

The maximum height was determined through a couple of factors. Firstly, it was important to allow a space where a crossbar could form to stiffen the swingarm against lateral forces. Secondly, towards the back, the volume is tapered off. There was little point in allowing much material in the upward direction as it would have collided with the suspension, and excessive material in the downward direction might result in inadequate ground clearance.

The length was largely decided by having to adhere to keeping the wheelbase unchanged. Some extra material was however added in front of the frame mounting position, limited by clearance to frame during suspension travel, see Figure 5.1. When pivoting downward (extending the suspension) the only potential collision is with the frame. When pivoting upward (contracting the suspension) the upper 'potential crossbar' might eventually collide with the frame, or the larger jackshaft sprocket and its chain.

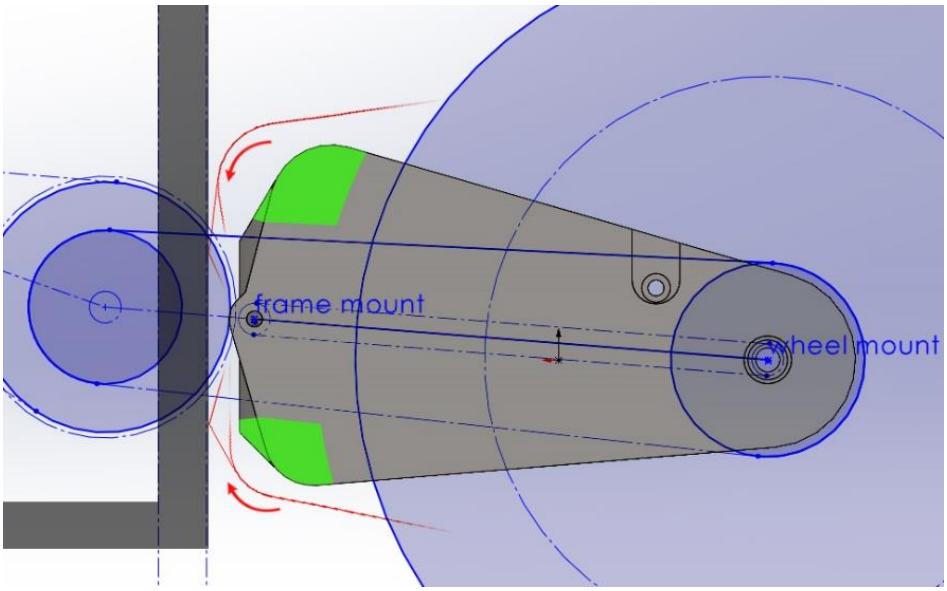

Figure 5.1 A simplified side-view of the frame, sprockets, wheel and swingarm design space, showing areas highlighted in green where a potential crossbar could exist without collision. The red lines show the side view edge of the design space if pivoted about the frame fitting, showing potential collision during suspension travel, acting as a limiting boundary.

Appropriate cuts from the design space volume were made to remedy this, visible in the top view in Figure 5.2.

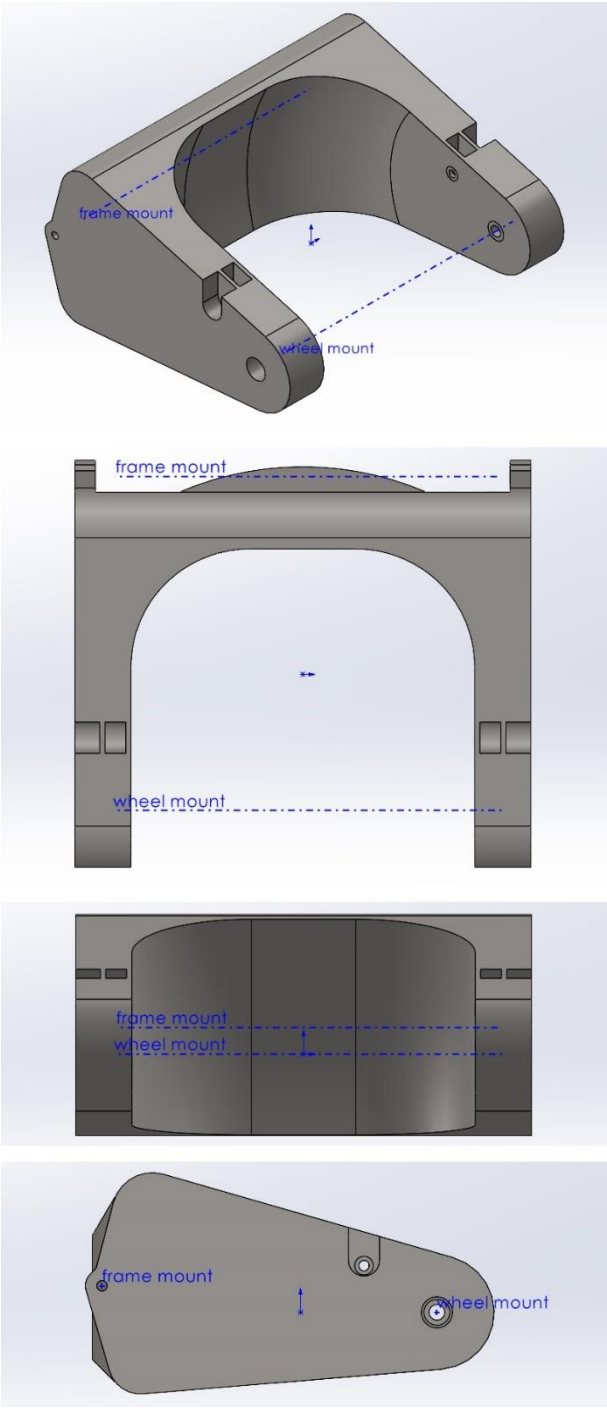

Figure 5.2 The design space for the TO. Views: angled, top, back, left.

Some properties did not immediately require a specific configuration, and whose placement and design might have had an impact on the TO results. The placement of the suspension fitting was the main variable in this category. A longitudinal change of a few centimetres might give slightly different results, and as the fitting placement is not entirely crucial to its function (albeit not unimportant), this required a few different configurations. If the results from the configurations all were to look similar, any reasonable configuration could be picked, such as the most easily manufactured one, or maybe the one that seemed the least prone to have high stress concentrations. If it was difficult to say for certain which configuration is best, receiving similar results would at least mean that whatever placement the suspension fitting ends up in—if forced by other constraints or modifications to the design—is likely satisfactory.

While the suspension fitting doesn't call for a highly specific placement, there is however definitely an area within which it can be said beyond reasonable doubt that it should reside. For example, a suspension fitting mounting point rearward of the wheel mounting will likely give high bending and shear stresses close to the wheel mounting position, not to mention the collision with the brake calliper mounting plate, or the brake calliper itself. A mounting position placed too forward would give unnecessary bending forces in the resulting swingarm, in addition to ending up almost vertical which furthermore would be less aesthetically pleasing—a slight forward tilt is preferred for a sportier and more aggressive look (as well as making the suspension progressive). See Figure 5.3 for the first of three suspension mounting configurations used for the topology optimisation.

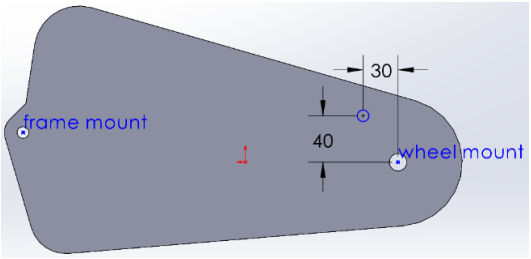

Figure 5.3 Configuration 1 of the suspension mounting location. see Table 5.1 for all configurations.

The three suspension mounting configurations are listed in Table 5.1. The height is increased slightly with increasing distance from the wheel mounting position, to leave sufficient room material to build underneath the suspension mounting position.

Table 5.1 The three different suspension mounting location configurations.

Configuration	1	2	3
Horizontal distance (mm)	30	50	70
Vertical distance (mm)	40	43	45

As mentioned above, a crossbar will likely be formed in the TO result. This has the potential to collide with the chain. There is however no cut-out in the design space for the path the chain will take. This is intentional as the vertical distance of the chain above and below the swingarm mounting points can be adjusted by changing the sizes of said sprockets—while making sure to keep the gear ratio unchanged. A few things must be kept in mind if this adjustment is employed. Firstly, the upper and lower runs of the chain cannot be changed independently; they are both roughly equidistant and from the middle of the swingarm as they join at the same, circular sprocket[6]. Secondly, it is important to note that a change of sprockets, even with unchanged *ratio*, will cause both a translation and rotation of the chain force vector. More importantly, the swingarm mounting point changes if the anti-squat value is to be kept consistent. A larger change thusly warrants running a new TO study.

The hope is that one of two things will be true. The first case is that there will naturally be space for the chain, or that very minor changes to the resulting volume must be made that doesn't affect the structure too much. The second case is that if a large change in sprocket sizes is needed to avoid chain-crossbar collision, said change—which subsequently yields a new configuration in mounting points for swingarm and jackshaft, and thus requires a new simulation to be run—doesn't alter the new result so much that the change gives a solution that immediately invalidates the newly chosen sprocket sizes. A perpetual state of leapfrogging could potentially occur, which would simply be solved by making a more radical change in crossbar placement and geometry.

A single step up or down in diameter and subsequent new mounting points will have a negligible effect[7] on performance and tuning of the vehicle. A large change, however, might warrant a reconsideration in design—a large step up in diameter, and thus mass, would likely affect the performance by means of extra unsprung weight. It might also have a structural effect, since accommodating ever larger sprockets might eventually become unfeasible, given spatial constraints. Extra consideration must be taken when a change results in higher torsional shear forces

[6] There's an emphasis on 'roughly' in this case, since the swingarm might not be a perfectly straight line, the chain will certainly not be infinitely tensioned, nor the sprocket perfectly circular.

[7] Adding an extra 100 grams to the jackshaft would only move the CoG roughly 0,12 mm backward and 0,01 mm down; a change minuscule enough to be overshadowed by other variances in manufacturing, weight of driver, extra baggage, road unevenness, driver skill, etc.

as this is a limiting factor in jackshaft material choice. This is detailed further in chapter 8.

Another choice is to simply keep the sprocket sizes and design the crossbar to avoid the chain runs. Perhaps the best solution is to use a crossbar that runs higher above or further below the upper or lower chain runs, respectively (as shown through the green areas in Figure 5.1). Otherwise, taking notes from conventional design where the crossbar runs in between the chain runs is likely a safe bet.

5.1.2 **Boundary conditions**

Using the Load Case Manager tool in SW, a few edge cases were set up that the swingarm must withstand. This tool allows for several different scenarios to be simulated independently of each other and then automatically combined into one result. Any form of vertical force in this TO was modelled through the suspension mounting location reaction force, which is angled away from vertical, using reference points from the assembly. The angle and exact position of this force may vary in the welded design. This potential change was deemed small enough to not warrant deeper analysis at this stage, but this must be reconsidered if a larger change is required.

5.1.2.1 Fixtures

The swingarm has two different types of fixture constraint. The first is a fixed hinge constraint at the two frame mounting holes visible along the ‘frame mount’ axis in Figure 5.2. The second is a reference geometry constraint only hindering the internal surfaces of the wheel axle mounting holes from moving vertically. Had these two surfaces also had the fixed hinge constraint, the swingarm could not have extended either longitudinally or axially and would yielded much different results. This would have been equivalent to fixing both the frame and wheel mountings to two infinitely stiff axles, locked in space, with infinite friction in the axial direction.

In practice, the swingarm will bend when subjected to a higher weight, either lengthening or shortening the total distance from frame mounting to wheel mounting depending on final geometry. This effectively means that the wheel would roll forward or backward—an ability that must be reflected in the wheel mounting in the TO.

5.1.2.2 Hard bump

The hard bump is likely the most demanding case, as the vertical load to design for is highly uncertain in both magnitude and angle. In racing motorcycle design, you might simply use the whole weight of the vehicle, as the front wheel frequently leaves the ground during hard acceleration, leaving the rear to bear the whole weight of the bike. For cases of hard cornering even higher vertical loads are achieved (vertical in this case meaning with respect to the bike, not the ground). This makes

sense for a racing motorcycle as they are seldom taken for a high-speed ride where there might be debris on the road.

This isn't as applicable for the OMOTION 300, which will frequently be driven on public roads and in cities. A pothole at medium speeds or some debris at higher speeds are probably the worst cases of vertical max load. Both scenarios also have an innately coupled rearward load, the magnitude of which depends on the height of the object. More accurately the height determines the ratio of horizontal-to-vertical reaction force since when a wheel hits an obstacle the reaction force from said obstacle always points towards the centre of the wheel, and a height increase means a decrease in angle of the reaction force. See Figure 5.4 below.

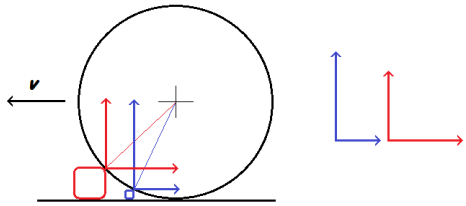

Figure 5.4 A simple visualisation of the ratio change of force components depending on the height of the object hit. Left: the wheel and the different heights of object creating different angles of the resultant force, causing different ratios of horizontal-to-vertical reaction components. Right: The forces components compared next to each other.

Given the large difference in reaction force and angle dependent on type of bump—road bump at high speeds, or pothole as lesser speeds—it is difficult to find a be-all and end-all. In this TO, inspiration was taken from another project similar in character wherein a comparison to the total weight was made, applied vertically upward to a remote point in the middle of a simulated wheel axle [8]. As mentioned previously, vertical forces instead are angled along the implied suspension, applied downward in the suspension mounting location. More specifically, the actual surfaces this force was applied to is done in the same fashion as in the maximum acceleration case, explained below. A value of 5000 N was chosen for this force (for comparison, the approximate mass of vehicle plus driver being 455 kg, the total weight is roughly 4470 N).

This vertical component of this value was then calculated and multiplied by a factor of 1,5 for a horizontal component of 6850 N, applied to the wheel mounting location. These values might seem rather arbitrary; remember that this form of slightly erring on the side of caution effectively gives this case a higher weighting for the results, which is desirable. The TO study will not produce an immediately manufacturable structure—only a basis on which to build a welded design.

This hard bump case eliminates the need for a regenerative braking case, as the longitudinal forces caused by this also act along the same path the much greater-in-

magnitude longitudinal force in the hard bump case does. Any case with duplicate, but smaller forces, is redundant for the results and only impact the study through its increase in run time. Granted, the hard bump case varies in that it has additional vertical forces as well, but this was still deemed similar enough to ignore a regenerative braking case. An actual hard brake calliper-braking case should ideally have been included but was not. This is commented on in chapter 7.1.1.

5.1.2.3 Maximum acceleration

We get the force from acceleration through Newton's second law; it reaches a maximum of approximately 2400. It is applied along the horizontal plane (top plane) in the direction of forward travel, acting on the surface where the wheel axle will contact the swingarm, as well as on split surfaces modelling the area a washer on the wheel axle would be tightened onto the swingarm. These split surfaces are modelled on both sides of the wheel mounting location, on both lateral sides of the swingarm, for a total of four split surfaces. See Figure 5.5 for a visualisation of the force direction and the surfaces to which it is applied.

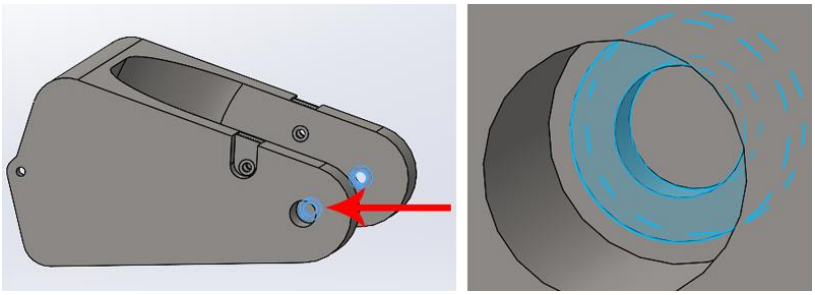

Figure 5.5 Left: the swingarm is from an angled left view, with the force direction shown with a red arrow. Right: A zoomed-in view of the left side wheel mounting location (which the force direction arrow coincidentally points to). Highlighted are the two surface split areas, in addition to the cylindrical area the wheel axle will be in contact with.

Realistically, the longitudinal force due to the chain pull during acceleration on the left arm of the swingarm is larger than that on the right side. The acceleration force was however intentionally kept equal on both sides in the study; the finished, welded design will be a laterally symmetrical one, both for aesthetic reasons and to keep unexpected forces due to asymmetry at a minimum. Unfortunately, load transfer was left out due to negligence. This was luckily taken care of to a great extent by the hard bump case.[8]

[8] Albeit in a very slightly different manner, as the bending moments caused by the downward force in the suspension mounting location affect the swingarm differently in the two cases.

5.1.2.4 Hard cornering

During normal driving conditions is Depending on type of vehicle, suspension, tyres, driver, the maximally attainable lateral g forces vary quite a bit, and the different sources claim different numbers. 'Street tyres' might typically lose traction at around 0,7 g [9], many modified street cars land in the 0,9-1 g range [10], and FSAE vehicles reach upward of 1,4 g [11] [12]. A value of 0,9 g was used as a means of precaution against any potential overzealous drivers. For reference, R. Thomas Bundorf of General Motors characterizes normal driving conditions as those with lateral acceleration under a third of that of normal gravity, or roughly 0,33 g [13, p. 6].

Assuming the rear tyre takes half of the load if the vehicle's CoG is centred along the wheelbase[9], this approximates a lateral force of 2000 N, applied to an area modelling the surface a washer would contact the wheel mounting plate. This was done for two separate cases, one for each lateral direction. This could also have been done using symmetry control (but this crashed the software a few times and was thus abandoned).

5.2 Output

The result is a structure that bridges the best of all worlds through the load case manager—roughly. It is not perfect, as without great scrutiny the results might show a local optimum rather than a global one. Furthermore, weightings are not considered in the load case manager but was done manually to some extent by using very high bump case forces.

As the study aimed to maximise the stiffness-to-weight ratio, the weight of the results can now be adjusted, with a coupled stiffness for any given weight. The initial results had a quite arbitrarily set amount of material to be kept, which yielded results that did not reveal much of the internal structure deemed most important. The results, shown in Figure 5.6 have had this material amount reduced until the internal 'skeleton' was exposed. Note that only a few select parts are shown here, and with a smoothed mesh. The non-smoothed TO results of all three configurations are shown in Appendix A.

[9] This assumption is not completely true. This is discussed further in chapter 9.1.

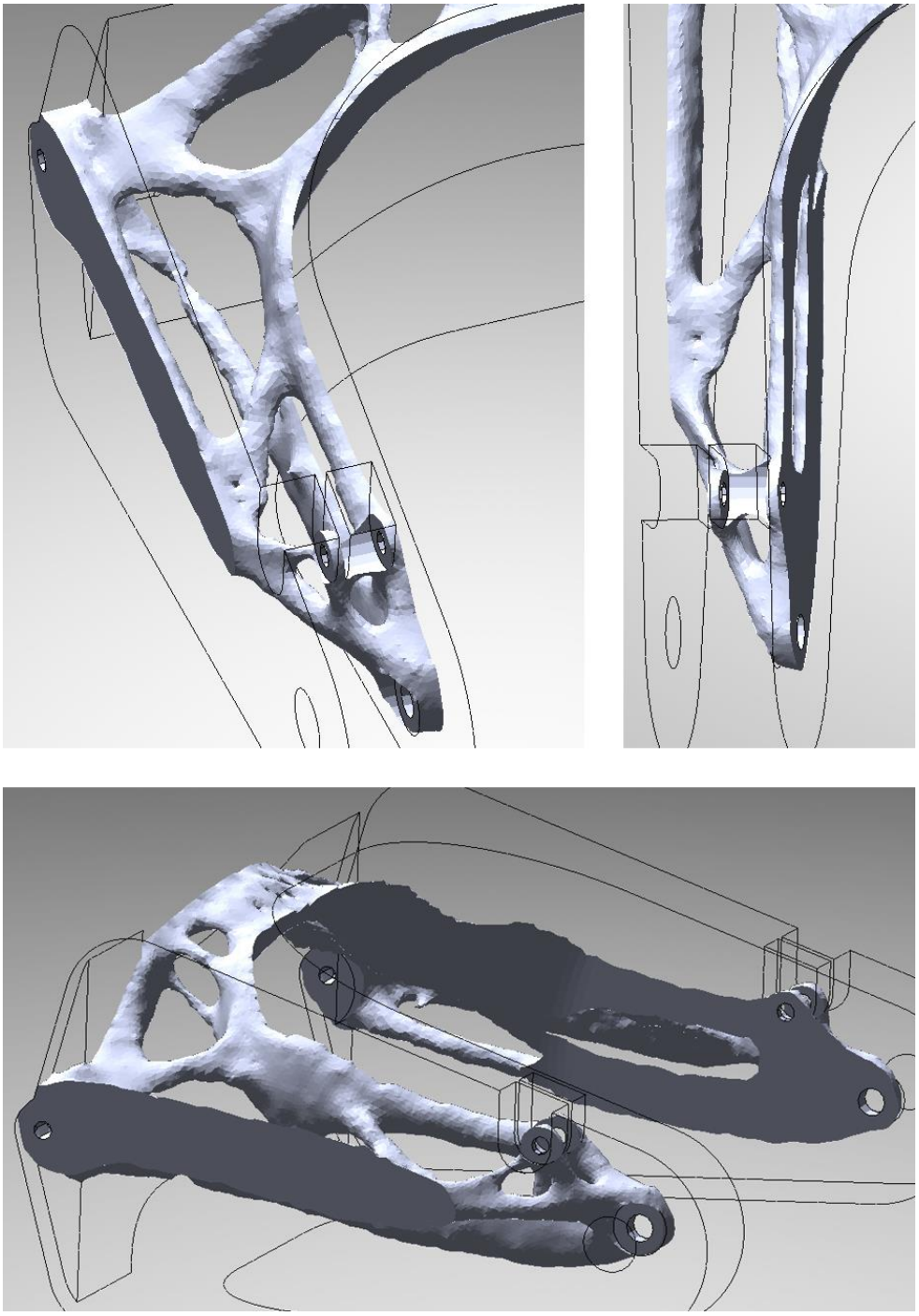

Figure 5.6 A smoothed-mesh version of the topology optimisation results, configuration B.

If the result of a TO study was feasible to manufacture directly, the engineer could immediately call it a day. This is obviously not true for almost all cases as the variety of manufacturing methods able to replicate the geometry closely are limited. Additionally, the costs of the methods that *can*, are often not within budget. Metal 3D printing is likely the best method of attaining the highest topological similarity, and while it certainly can be the cheapest way to manufacture a specific complex part, it is still costly. Casting can typically create complex enough geometry, albeit does not offer a wide range of materials, and boasts a hefty price tag at lower production volumes.

If you randomly skipped to this part of the report and are currently at the edge of your seat: the 'name of the game' in this project is to create a welded design, inspired by the results of this TO study.

5.2.1 Interpretation and adaptation of results

A structure consisting of beams creating a truss-like net can be seen where the innermost structural member also constitutes part of the arching transverse crossbar that resists bending in the lateral case, the outermost member in conjunction with the lower member constitutes a rigid longitudinal structure for the bump case as well as the acceleration case. This structure is aptly replaced either directly by circular bent steel tubes following the suggested path closely, or by a rectangular tube oriented such that it maximises the resistance to bending, induced by the weight (at the location where the suspension fitting will be). In this project, the rectangular tube[10] was chosen for a couple of reasons. Firstly, the TOs seemed to suggest a slightly thicker outermost member running along the edge of the allowed volume with an almost parallel thinner circular member further inward and downward. Both members could reasonably be replaced with a single, larger rectangular tube. Secondly, using circular tubing of smaller dimension would introduce some concern through thermal weakening close to welds, especially near the suspension fitting. If this top longitudinal tube were to yield, the remaining bottom longitudinal tube would not be able to withstand the forces by itself. A single, larger tube—and thus hopefully less prone to failing—felt safer.

Something to note is the upward inclination of said crossbar. The slope can likely be explained by considering why the crossbar was required in the first place. Without any lateral forces there would be little need for a large and stiff crossbar, with only a smaller one likely sufficing. However, during use the car might be subjected to quite large lateral forces during cornering. The TO creates results that are the stiffest with respect to weight, and the geometry that best resists bending is

[10] Henceforth referred to as *longitudinal bar(s)*.

a bar that has all its material shifted the furthest from the plane of bending [14, p. 346], which explains the shape of the generic I-beam. Of course, in practice *all* the weight cannot be shifted to the flanges, since without a web to keep the flanges separated the result would just be two separate sheets in an orientation in which they resist bending the *least*. Using the thinned result from configuration 2 a plane can be superimposed on which the arch that best resists bending in the lateral force-case would exist, and an imagined I-beam in the middle, see Figure 5.7.

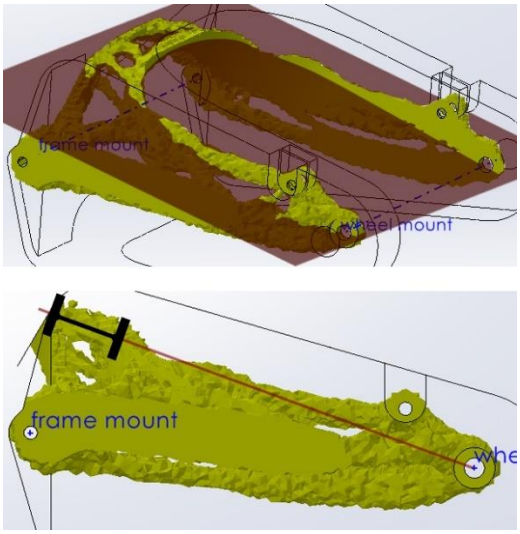

Figure 5.7 The plane on which the arch that best resists bending has been created, and the imagined I-beam created by the TO.

The bump force case, containing the largest force, is the reason the main structure runs almost straight, directly from the wheel mounting to the frame mounting. This gives a geometry where the crossbar looks to arches upward, away from the main structure.

As it looks like the longitudinal structure is best composed of a (mostly) straight rectangular bar, and thus not naturally creating a 'flow' upward for the slanted crossbar, the actual slant might even be detrimental in the welded version. Two main crossbar configurations, flat versus slanted, will be modelled and tested through FEM simulations. In any case, the slanted design will not incorporate the sharp peak in the arch seen when viewed from the back view, as this will certainly be weaker than if the design would look like a gradually bent arch.

6 Welded Design

The designs are based on rectangular and circular steel tubes, with a material specified in SW as *plain carbon steel*. This steel has a yield limit of 220,6 MPa and is what OMotion uses currently.

6.1 Constructing the initial design

The TO result was imported into the assembly to check for chain clearance, which showed troublesome results. With the sprocket sizes used, the crossbar and upper chain run collided. As mentioned in 5.1.1. some options were available at this point.

Instead of exploring the already rather restrictive selection of sprockets, two different configurations whose crossbars did not collide were instead created. The TO result was superimposed into a new SW part file and used as guidance for creating the welded designs, as shown in Figure 6.1.

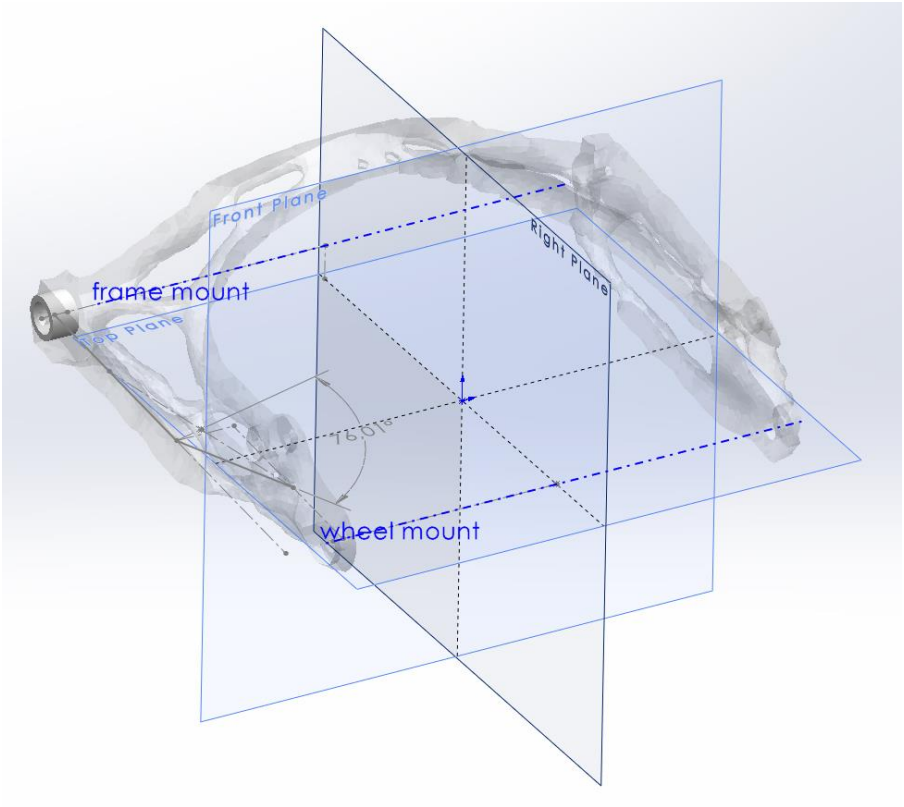

Figure 6.1 The TO result superimposed to aid in creation of the welded design.

The designs were rather closely modelled after the TO result, with some additional restraints and modifications for ease of manufacture, etc. One such thing is the wheel mounting consisting of a plate. This means that the longitudinal bar must be shaped in such a way that the connection can give a rigid weld. Furthermore, the rectangular longitudinal bar connects to the 'frame mounting cylinder' in a straight line as this allows the widest bar possible to be used. See Figure 6.2 for a visualisation of this.

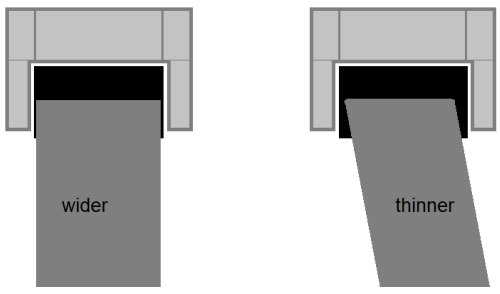

Figure 6.2 The straight or angled join from longitudinal bar to frame mounting cylinder.

If FEM simulations later show that a wider bar is required, the frame-swingarm fitting would have to be widened. This fitting is however already as wide as the vertical bar is, on which the fitting is welded. This would thus require either using an even wider bar, or welding on a piece of sheet metal to the side of it, adding width in that specific location. If simulations show that the width instead is superfluous, angling the rectangular bar inward could be considered as this means that the bar doesn't have to be cut and welded in the middle, or bent, but instead can run 'straight' from frame mounting to wheel mounting plate.

The two different variants are shown in Figures 6.3 and 6.4 below. The suspension mounting point ended up being placed slightly higher, and slightly more forward, than configuration 3 of the design space.[11] This changes the vector along which the compressive forces in the suspension act slightly and as such alters the actual force experienced in the springs (because the straight *downward* force from weight is counteracted by the suspension, mounted at a *non-vertical angle*, meaning that the suspension instead feels the force of the weight divided by the sine of the angle between suspension axis and horizontal plane).

The change in the initial design did not change the angle much and thus kept the compressive forces consistent. The angular change does however also affect the induced torque under the fitting since the fitting is angled in respect to the suspension. The angle is shallow in this construction and thus the lever arm (the perpendicular distance to the line along which the force applies) is short. The resulting torque is minimal enough to not warrant a change in design at this stage. Were the angle steeper the perpendicular distance would increase, and the torque as well, in proportion to said distance. Neglecting this could prove troublesome if the design needs large changes later. This is usually intuitive when changing the design and is unlikely to necessitate a completely new TO study.

The wheel mounting plate used a wheel removal method inspired by the design usually found on city bikes. Upon further consideration later in the project, another configuration was sketched out that was deemed superior. This is discussed in 9.1.

[11] The height change was mostly due to misjudging the height of the suspension fitting. The more forward change was made to place the fitting centred laterally on the longitudinal bar, meaning that when viewed from above, the bottom face of the fitting protruded an equal amount on both sides of the longitudinal bar.

Figure 6.3 The initial design of the high crossbar variant. Views: angled, top, back, left.

Figure 6.4 The initial design of the flat crossbar variant. Views: angled, top, back, left.

6.2 Comments on initial design

Both variants initially had longitudinal bars consisting of two half-length straight bars, cut and welded at an angle in the middle—a configuration used in the high crossbar variant. Making these two straight bars a single bent bar instead removes the risk of a weld break where a weld wasn't necessary to begin with. The flat crossbar variant was created after the first few simulations of the high crossbar variant had already been made, highlighting said risk, hence why the flat crossbar variant already has this modification in Figure 6.4.

6.2.1 **High crossbar variant**

Quite an unusual angle of joining the crossbar to the longitudinal bar was used. The forwardmost smaller bar joins at an angle connecting it to both the top and the inner surfaces of the longitudinal bar, and the longer, main bar connects only to the inner surface. Intuitively this feels like it poses a risk of buckling when heavily loaded with a lateral force, and other methods of joining the two longitudinal bars together would be superior. The project proceeded with this design anyway, to check if staying as true as possible to the TO result would prove more important than instead paying attention to how structural members are usually fastened to each other. Methods of fastening of structural members is a field of its own, so haphazardly slapping together something like this is unlikely to be the best solution. Regardless, the project proceeded, and the problem would be tackled again after the initial FEM simulation results.

6.2.2 **Flat crossbar variant**

The risk of buckling is potentially greater in this case, as not only is the crossbar bonded to the middle of the side face of the longitudinal bar, but the shorter additional tube is also as well. Thus, a very shallow angle between longitudinal bar and main crossbar was employed to spread out the lateral force on the side face of the longitudinal bar to minimise said risk. Immediate concerns regarding manufacturability arose in doing so however, as this shallow angle might reduce the weld quality in the sharp corner. The project proceeded however, with the same reasoning as with the high crossbar variant.

7 FEM Simulation

As a means of testing how well both configurations of the swingarm holds up in practice, different cases were devised. These attempting to model real-life scenarios the swing arm must be able to withstand. These are highly similar to the cases in the Load Case Manager for the TO although some have been adjusted, and others added. These modifications are detailed below. Furthermore, a wheel axle reference and suspension bolt references were modelled, to which forces could be applied directly for greater realism.

Initially, a very simple large diameter axle was modelled. It was thicker towards the middle to better model the increased stiffness a wheel hub would provide but was otherwise very simple. During the case testing cornering forces, the wheel axle reference was made thinner along its entire length and received a radius leading up to the point where it contacts the wheel mounting plate[12]. At some point most cases simply proceeded with the thinner wheel axle as the results yielded less unpredictable stress concentrations. This is certainly one of the parts of the topology optimisation that could have been improved upon given more time, and knowledge of FEM simulation in general. The results are not listed below in chronological order, and thus the variant of wheel axle used might appear random.

Both configurations had the exact same boundary conditions for each case, but the mesh sizes might differ, mostly through choice of mesh control area. This is explained for each case in the boundary-condition-and-mesh-size tables. The mesh control is typically set on a case-by-case basis through having run the simulation once, and if areas prone to stress concentrations arise, the mesh control is applied and/or further refined in the affected area. Note that all mesh controls are applied to both sides symmetrically; if the mesh control on a detail on the left side is described, it is applied the same way on the right side. No mesh control is applied to the brake calliper (the only asymmetrical part).

The mesh size is set rather coarse for most of the initial simulations. This is because the hard cornering case described below yielded troublesome enough results by itself to necessitate a redesign. As such, this is the only case with a finer mesh

[12] It is no surprise that sharp corners give stress concentrations, but the highest stress values were at times placed on seemingly random nodes. It shall be noted that this occurred where there was no change in boundary condition, no change in mesh size, and no force directly applied to the area.

quality, because allowing multiple hours for the other cases when the design was set to be changed anyway was a poor use of time. This is also why the initial flat crossbar variant only had this specific case simulated.

The FEM simulation results displaying stress are always displayed with a maximum value set to that of the yield limit of SW's plain carbon steel (220,6 MPa), unless specifically stated. This makes the results of one case easier to compare to that of another one. Anything completely red exceeds this value and areas with orange-reddish hue are, supposedly, close to yielding. This of course must be interpreted on a case-by-case basis, as some simulations have some oddities in their results, as we will notice. The bluest tint is not equal to a specific value, but any area bluish in colour experiences practically no stress worth considering. The displacement results however are not displayed with a consistent deformation scale, as some results deform very little and whose deformation model thus would not add anything of value. The deformation scale has therefore been allowed to automatically detect an appropriate value, which aids in analysing potential problems either with the design itself or with the FEM simulation study that yielded the results in question.

7.1 Boundary conditions

7.1.1 **Hard cornering**

Only a right turn was simulated as the swingarm is entirely symmetrical apart from the brake calliper, which had no boundary conditions specified for this case. A summary of boundary conditions and mesh sizes can be found in Table 7.1.1, where the 'washer' surfaces the lateral cornering force is applied to is the same as described in 5.1.2.3. Note that the wheel axle contact surface is not part of this surface. Additionally, only the side that experiences the *pushing* force from cornering has the force applied to it; there is no *pulling* force on the opposite side. For a right turn this means the centripetal force (countering the centrifugal force) is placed on the outer side on the left arm and inner side on the right arm.

Table 7.1.1 Hard cornering boundary conditions and mesh settings.

Fixtures	**Location**	**Direction**	**Magnitude**
Fixed hinge	Frame mounting cylinder	Lateral (axis)	-
No translation	Middle of wheel axle	Vertical	-
External loads			
Force, weight	Middle of susp. bolt	Susp. angle downward	2235 N
Force, cornering	Wheel axle washer	Lateral right	2000 N

Mesh type	**Mesh size (mm)**	**Mesh location**
Standard	3,00	Entire model
Mesh control	1,00	Wheel axle contact and washer areas
Mesh control	0,75	Frame mounting cylinders, lateral faces
Mesh control	2,00	Frontmost inner face of longitud. bar

The mesh controls are visualised below in Figure 7.1. As mentioned, these mesh controls are applied with lateral symmetry; the frontmost inner face of the left longitudinal bar is still applied to the *inner* face on the right side, for example.

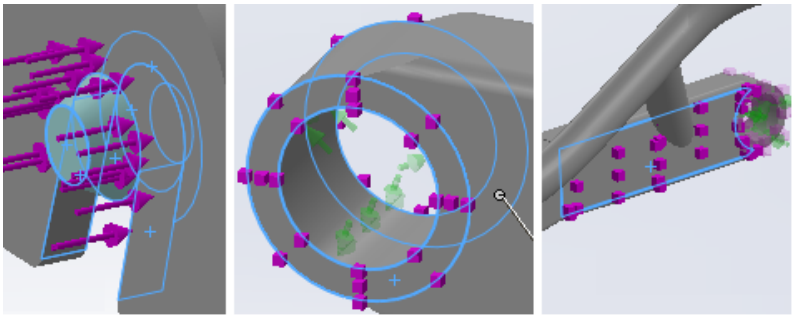

Figure 7.1 The mesh control areas are highlighted in blue. Left: wheel axle contact and washer areas (left washer area is accidentally deselected in this figure). Middle: lateral faces of frame mounting cylinder. Right: Frontmost inner face of longitudinal bar.

7.1.2 **Hard braking**

This case should ideally have been included in the TO cases as well but was at the time deemed lenient enough on the swingarm to not be needed, for a couple of reasons. Different sources claim different values of brake bias. According to [15] a maximum of 40% of the total braking should be done by the rear tyres, and according to [16] as little as 20% may be done by rear brakes for front wheel drive vehicles, whereas rear wheel drive instead puts this number at 30-40%. As the OMOTION 2 only sports a single rear tyre (as its successor will as well) the percentage was approximated at 32% for this case. The rear tyre is of course wider than a single front tyre, but narrower than two.

Going by data for passenger cars from [17] and [18] a maximum deceleration of 0,75 g forces (7,365 m/s^2) was used. This, in conjunction with the more rearward placement of the suspension fitting in the TO (meaning it had a higher resistance against bending) meant that the only forces likely posing any danger was the torque from the brake calliper. This torque was considered small enough to neglect so that it would not affect the TO result, especially since the load transfer forward would further reduce some of the stresses inside the swingarm. Now that we are modelling real life scenarios it is necessary, especially as the currently more forward placement of the fitting compounds the torque from the brake calliper.

As mentioned, load transfer will cause the front of the vehicle to dive when braking, and the rear suspension to extend. This means that the reaction force applied to the contact patch of the wheel due to weight will decrease, by 725 Nm more specifically. The pitch change of the vehicle also causes a small change in the angle of the suspension and thus the vector of the force it applies. This change is small enough to have been neglected in the simulations (in the acceleration case as well).

Using all the necessary data, we calculate the resulting longitudinal force through Newton's second law, taking the brake bias percentage into consideration:

$$455 * 7{,}365 * 0{,}32 \approx 1072 \text{ N}$$

The torque that must be resisted by the brake calliper is then calculated similarly, simply by a multiplication with the wheel radius, which equals 277 Nm of torque. In rare cases, tyre slip might be induced upon losing traction, perhaps due to wet or icy ground. The stiction force under the tyres is then replaced with friction. The force from kinetic friction is less than stiction, which means a lower braking deceleration, and thus the braking force and torque are lower. The values used in this case is therefore case of maximum, non-slip deceleration, rarely occurring during normal usage. See Table 7.1.2 for a summary of boundary conditions and mesh sizes.

Table 7.1.2 Hard braking boundary conditions and mesh settings.

Fixtures	**Location**	**Direction**	**Magnitude**
Fixed hinge	Frame mounting cylinder	Lateral (axis)	-
No translation	Brake callip. mounting	Lateral	-
No translation	Middle of wheel axle	Vertical	-
External loads			
Force, weight[a]	Middle of susp. bolt	Susp. angle downward	1510 N
Force, braking	Middle of wheel axle	Longitud. rearward	1072 N
Torque, braking	Brake callip. bolt holes	CW around wheel axle[b]	277 Nm

Mesh type	**Mesh size (mm)**	**Mesh location**
Standard	5,65	Entire model

[a] *Reduced due to load transfer.*

[b] *Clockwise when viewed from the left (countering the rotation of the wheel).*

7.1.3 **Maximum acceleration**

Much like in maximum braking, load transfer was considered in this case. The longitudinal force was also increased to 2800 N, 'futureproofing' against a higher maximum acceleration, should OMotion decide to alter gear ratios slightly. See Table 7.1.3 for a summary of boundary conditions and mesh sizes.

Table 7.1.3 Maximum acceleration boundary conditions and mesh settings.

Fixtures	**Location**	**Direction**	**Magnitude**
Fixed hinge	Frame mounting cylinder	Lateral (axis)	-
No translation	Brake callip. mounting	Lateral	-
No translation	Middle of wheel axle	Vertical	-
External loads			
Force, weight[a]	Middle of susp. bolt	Susp. angle downward	2960 N
Force, accel.	Middle of wheel axle	Longitud. forward	2800 N

Mesh type	**Mesh size (mm)**	**Mesh location**
Standard	5,65	Entire model

[a] *Increased due to load transfer.*

7.1.4 **Road bump**

This case was hastily modelled for the initial high crossbar variant, but unfortunately not documented properly. At the time, a redesign was already planned, and the result from the quick simulation yielded high stress concentrations at critical areas that would be addressed with the redesign anyway. More specifically, one of these areas was the inner corner of the cut and welded longitudinal bar, visualised in Figure 7.2.

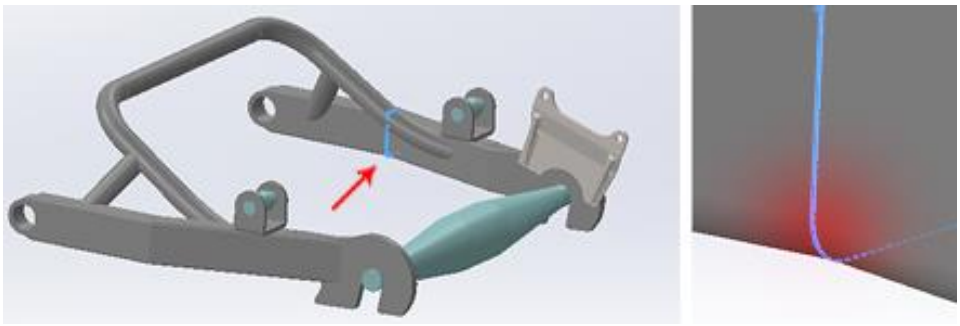

Figure 7.2 An area of excessive stress in the road bump case. The image is a recreation visualising a stress concentration and does not describe an accurate FEM simulation.

As mentioned in 6.2, this area does not have to be cut and welded, but is better constructed by a single, bent bar (and similarly on the left side of the swingarm).

The final iterations do include this case, however. The values have been changed from the TO study, as it is now supposed to model a real-life scenario more accurately (where in the TO, higher values were used as a means of adding weighting towards the case). The case was split into two similar cases: road bump, whose boundary conditions and mesh sizes likely very similar to those in Table 7.3.4; and full weight, inspired by the racing motorcycle wheelie scenario (even if unlikely to occur on the OMOTION 300), shown later on in 7.3.5.

In the hard bump case, instead of the setting a geometry constraint of no vertical displacement to the wheel axle, this was simplified by being applied to the suspension mounting location, with the reason that a hard enough bump stiffens the shock absorber. For future development, this case should be more accurately modelled with real spring and shock values, perhaps by used of the Adams Car package, or similar. In the full weight case, the force in the suspension from the weight of half the car was simply doubled.

7.2 Analysis of results, first iteration

See Appendix B for all cases' FEM simulation results of the first design iteration. Specific stress concentrations and other things of note are shown in their respective subchapter below.

7.2.1 **Hard cornering**

See Figure 7.3 for troublesome stress concentrations. Note that since welds are not modelled in this case, the join of crossbar to longitudinal bar becomes much harsher than it realistically should be. On the other hand, it is unwise to have a stress concentration where a weld should be as the weld, and nearby area, is usually weaker than the material welded on. It must be remembered that the highly localised stresses near the frame mounting cylinder will likely decrease quite a bit in a realistic scenario, since this connection will be by rubber bushing, instead of infinitely stiff, fixed axle.

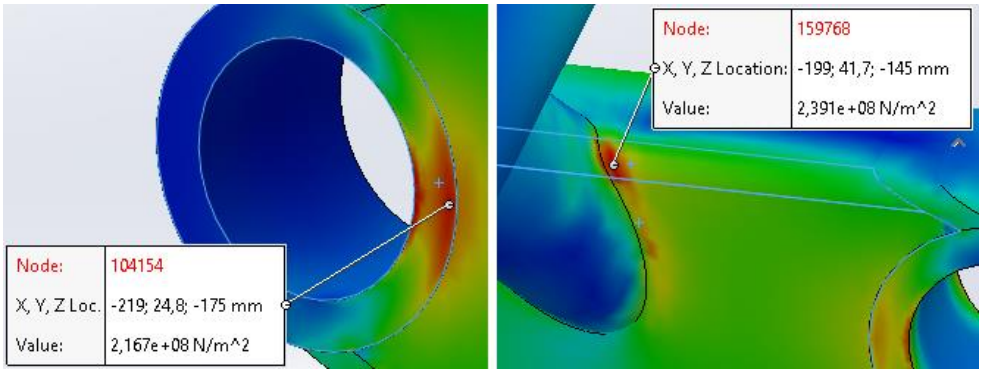

Figure 7.3 Stress concentrations near the front, hard cornering case. Left: frame mounting cylinder. Right: smaller supporting strut for the crossbar, joining into the longitudinal bar.

Figure 7.4 displays some very high stresses near the wheel axle contact area. This is a result of two things: first, the mesh control changes the mesh size slightly at the edge of the circular surface split; second, the forces are applied to said surface split (attempting to model a washer fastened by a nut). This is a very unreliable result and would need much scrutiny if proceeded with.

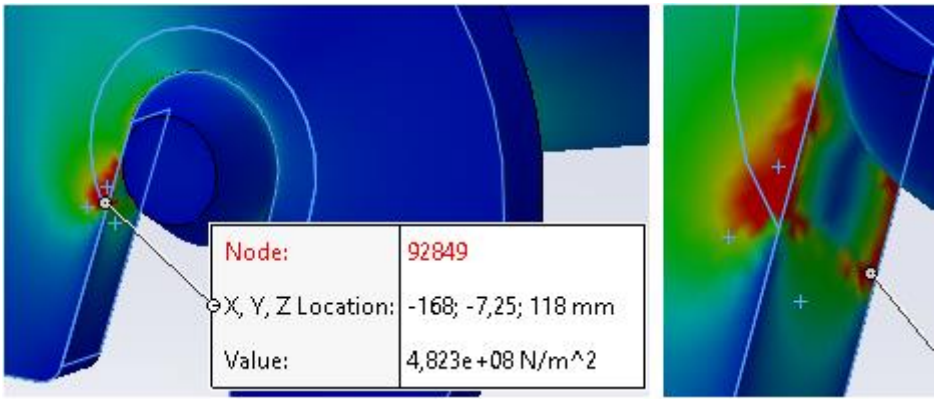

Figure 7.4 Left: stress concentrations at the wheel axle contact area. Right: zoomed in view of the same area, angled slightly upward; note the edge near which the highest stress concentration resides.

Note that this is not one of the cases referred to in footnote 6, as this stress concentration coincides with the change in mesh size and area with applied force very well and is very likely caused in conjunction with this. The ‘seemingly random nodes’ mentioned were located further down than in the right picture in Figure 7.4, on an area devoid of any rapid changes in boundary conditions or mesh size.

The hard cornering case reveals the shortcomings of the slanted design's angled crossbar connection points, in that they cause stress concentrations due to applying a directed load in a direction against which the rectangular bar is weaker. This might be remedied in two different ways that coincidentally stays true to the two different configurations of crossbar.

The first method is to connect the crossbar on top of the longitudinal bar instead, converting what would be a *lateral* load to a *torsional* one. The second option is to rethink how to connect a flat—or in-line, rather—crossbar so that the stress concentrations shown here are avoided. This could be done by using gussets. See 7.3 for a further elaboration on both these options.

7.2.2 **Hard braking**

As mentioned in the introductory paragraphs of chapter 7, the hard cornering case yielded results worrisome enough on its own to warrant a redesign. The rest of the cases in 7.2 thus have less trustworthy results (because of the much coarser mesh size).

The longitudinal force seems to not affect the design much at all, but the torque does impart significant stresses, especially when coupled with the weight through the suspension fitting. This must be carefully monitored in future design iterations.

7.2.3 **Maximum acceleration**

A very low-stress case regarding the swingarm. The only stressed areas that look slightly concerning are under the suspension fittings, which also can be seen in the other cases. A larger longitudinal bar 'height' might be a smarter option at this stage.

7.3 Iterations on design and boundary conditions

Both designs were iterated upon a few times, with either small or large changes. Listing all of these changes and showing the FEM simulation results for all small changes would add little of value. The changes listed below are therefore the changes made in creating the final iterations. First, both variants had the height of the longitudinal bar increased (the vertical dimension of the bar itself, not the placement). The other changes were unique to both variants, explained below.

The high crossbar variant was modified as suggested, to run higher instead and join the longitudinal bar from above, converting what was lateral loads on the less resilient side faces to a torsional load, in a manner that does not weaken the structure as much.

The flat crossbar was initially modified simply by employing angular changes of the bent crossbar to spread out the lateral forces over a larger area. If this method was to be used, internal stiffening plates would likely have been needed, which is more difficult if the longitudinal bar is bent, not to mention perhaps being near impossible to do at a certain internal depth. Instead, a similar longitudinal bar was used as a crossbar, fastened by a *gusset*. The gusset was modelled as a simple triangle for the first cornering simulations (the most problematic case), which still showed high stress concentrations. It was then given a radius, gradually slimming it towards the rear, causing the lateral stiffness reduce in a manner that spread the stress out much more evenly. This type of 'exponential slimming' was also used by Eklund [19] as a means of reducing the maximum stress in a welded beam bracket, see Figure 7.5.

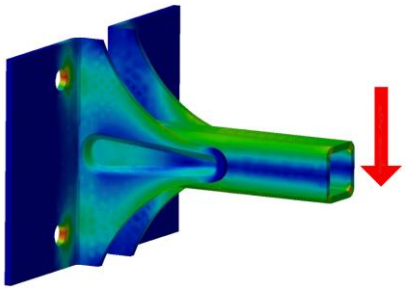

Figure 7.5 FEM simulation results of improved version of welded bracket for beam in bending (adapted from [19]). A red arrow has been added to show the load direction. Note the bracket geometry.

In order to make the simulation more realistic, the gusset had makeshift welds created, as this method of fastening it is integral to its function. Briefly explained, a simply supported beam in bending—the longitudinal bar during cornering—has one side in compression, and one side in tension. The gusset is to be welded in the very middle of the line that splits these two sides, where there is very little stress (note the deep blue middle of the beam in Figure 7.5). This means the weld experiences very little stress compared to if it had been welded furthest out on either the compressive or the tensile side. An error sometimes seen is to add a triangular gusset on the inside of the corner between the beams, in the middle of the side face. Without any support in the inside of the beams, the result is a very stiff reinforcement either pushing into or pulling out from a side face of a hollow beam, sometimes making it even weaker than if there was no reinforcement at all.

The gusset weld simulation and the lines along which they are bonded can be seen in Figure 7.6. If this is to be manufactured, a sheet metal variant would instead be modelled, which effectively means to simply remove the simulated welds.

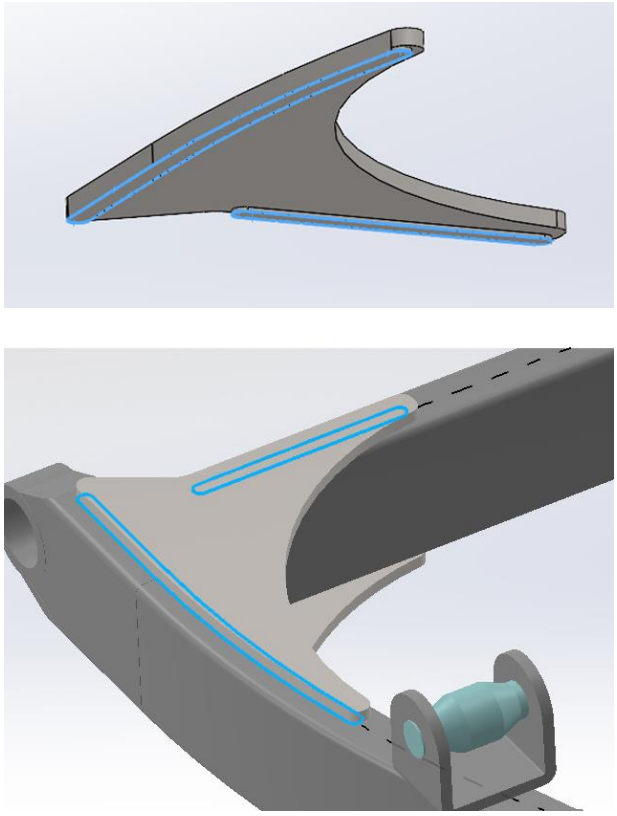

Figure 7.6 Gusset weld simulation. 1 mm extra material thickness has been added to the areas outlined in blue to act as a weld.

The two variants' final design iterations are shown below, in Figures 7.7 and 7.8.

Figure 7.7 The final design of the high crossbar variant. Views: angled, top, back, left.

Figure 7.8 The final design of the flat crossbar variant. Views: angled, top, back, left.

The mesh size and mesh controls were kept consistent for all simulations on the final iterations. Both designs used the same general mesh size: a curvature-based mesh, maximum element size 5,00 mm, minimum element size 2,00 mm, a minimum of 8 elements in a circle, and an element growth size ratio of 1,4.

The mesh controls differ slightly in the two cases, however. Instead of listing them in every table below, they are visualised and explained in Figures 7.9 to 7.12. All figures show the full view of the model to the left and zoomed-in views to the right. The specific mesh control areas were selected in a similar fashion to that previously described; test simulations were run and appropriate areas that needed more detail were subsequently chosen. Figure 7.13 shows both variants' resulting mesh.

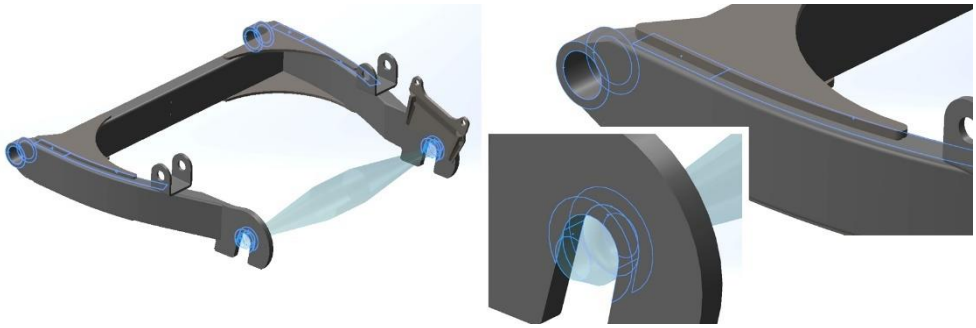

Figure 7.9 A 2 mm mesh control on the flat crossbar variant, ratio 1.2.

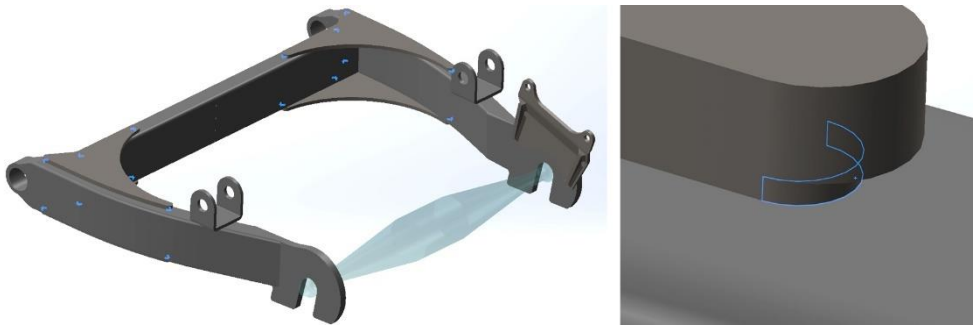

Figure 7.10 A 1 mm mesh control on the flat crossbar variant, ratio 1.4 (gusset 'weld' edges).

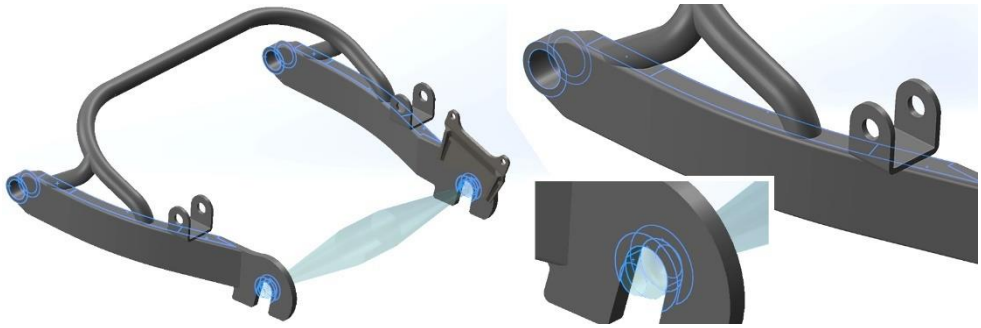

Figure 7.11 A 2 mm mesh control on the high crossbar variant, ratio 1.4.

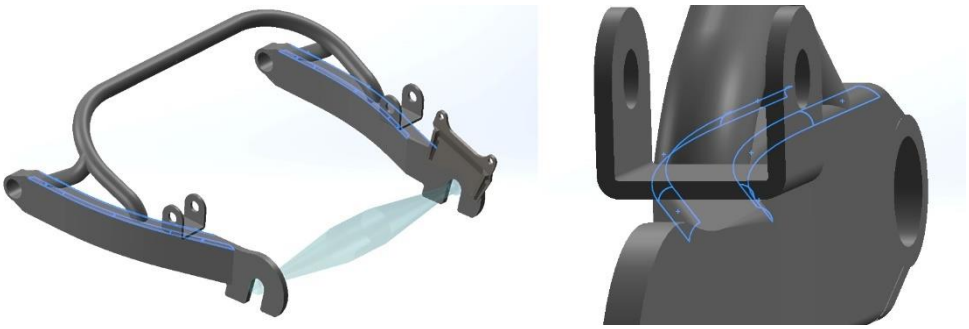

Figure 7.12 A 1,5 mm mesh control on the high crossbar variant, ratio 1.2.

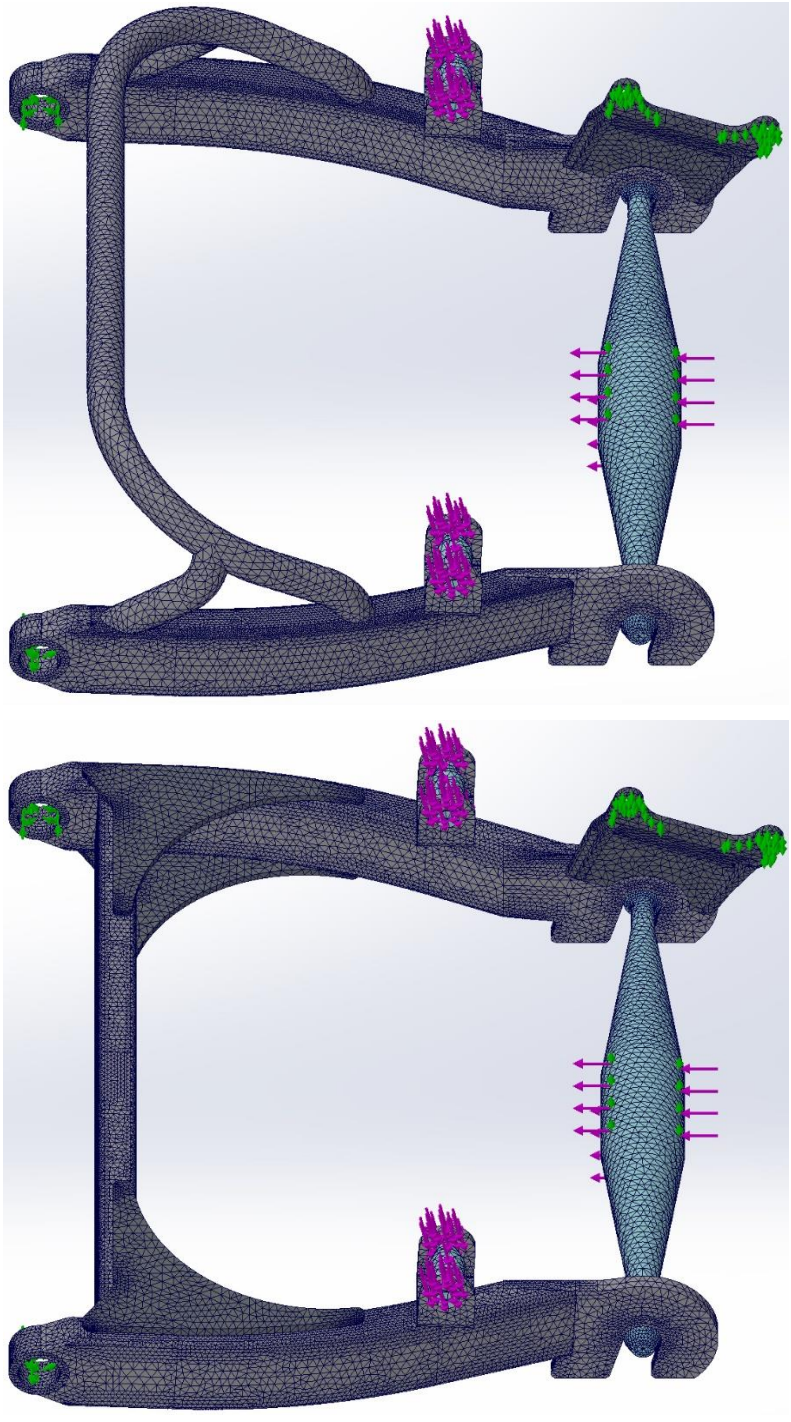

Figure 7.13 The resulting mesh after applying mesh control. Top: high crossbar variant. Bottom: flat crossbar variant.

7.3.1 **Hard cornering**

See Table 7.3.1 for a summary of boundary conditions (no changes were made from the first iteration).

Table 7.3.1 Hard cornering boundary conditions.

Fixtures	**Location**	**Direction**	**Magnitude**
Fixed hinge	Frame mounting cylinder	Lateral (axis)	-
No translation	Middle of wheel axle	Vertical	-
External loads			
Force, weight	Middle of susp. bolt	Susp. angle downward	2235 N
Force, cornering	Wheel axle washer	Lateral right	2000 N

7.3.2 **Hard braking**

See Table 7.3.2 for a summary of boundary conditions (no changes were made from the first iteration).

Table 7.3.2 Hard braking boundary conditions.

Fixtures	**Location**	**Direction**	**Magnitude**
Fixed hinge	Frame mounting cylinder	Lateral (axis)	-
No translation	Brake callip. mounting	Lateral	-
No translation	Middle of wheel axle	Vertical	-
External loads			
Force, weight[a]	Middle of susp. bolt	Susp. angle downward	1510 N
Force, braking	Middle of wheel axle	Longitud. rearward	1072 N
Torque, braking	Brake callip. bolt holes	CW around wheel axle[b]	277 Nm

[a] *Reduced due to load transfer.*

[b] *Clockwise when viewed from the left (countering the rotation of the wheel).*

7.3.3 **Maximum acceleration**

See Table 7.3.3 for a summary of boundary conditions (no changes were made from the first iteration).

Table 7.3.3 Maximum acceleration boundary conditions and mesh settings.

Fixtures	**Location**	**Direction**	**Magnitude**
Fixed hinge	Frame mounting cylinder	Lateral (axis)	-
No translation	Brake callip. mounting	Lateral	-
No translation	Middle of wheel axle	Vertical	-
External loads			
Force, weight[a]	Middle of susp. bolt	Susp. angle downward	2960 N
Force, accel.	Middle of wheel axle	Longitud. forward	2800 N

[a] *Increased due to load transfer.*

7.3.4 **Road bump**

Table 7.3.4 Road bump boundary conditions and mesh settings.

Fixtures	**Location**	**Direction**	**Magnitude**
Fixed hinge	Frame mounting cylinder	Lateral (axis)	-
No translation	Brake callip. mounting	Lateral	-
No translation	Middle of susp. bolt	Vertical	-
External loads			
Force, bump	Middle of wheel axle	Longitud. rearward	3000 N
Force, bump	Middle of wheel axle	Vertical upward	4000 N

See Table 7.3.4 above for a summary of boundary conditions. In a road bump scenario, it is assumed here that the front wheels have just contacted the bump. With the front suspension loaded from the bump, the CoG is currently in motion at a slightly upward angle, leaving less remaining load to be handled by the rear suspension. It should be noted that the pitch change of the vehicle could in some cases, due to speed and geometry of bump, counter this decrease in load. It is for this reason a full weight case was included, as the values still are rather arbitrarily chosen. A comparison can be made to the case of two motorcycles travelling over a 50 mm drop at 100 km/h described by Foale, one with bump damping only, and one with rebound damping only. The rebound-damped motorcycle experienced a vertical force at the front tyre of roughly 3700 N, whereas the bump-damped experienced roughly 4500 N [2, p. 6:37]. It must be noted that while these values are for a motorcycle likely much lighter in weight, the bump is considerable in size, and hit at very high speed. As mentioned in 7.1.4, for future development this case benefits from modelling in software such as Adams Car, or similar.

7.3.5 **Full weight**

See Table 7.3.5 for a summary of boundary conditions.

Table 7.3.5 Full weight boundary conditions and mesh settings.

Fixtures	**Location**	**Direction**	**Magnitude**
Fixed hinge	Frame mounting cylinder	Lateral (axis)	-
No translation	Brake callip. mounting	Lateral	-
No translation	Middle of wheel axle	Vertical	-
External loads			
Force, weight×2	Middle of susp. bolt	Susp. angle downward	4470 N

7.4 Analysis of results, final iteration

As mentioned in the start of chapter 7, the wheel axle reference is a potential source of errors, given that its shape allows for elasticity that was not fully explored in this project. Still, given its relatively large diameter in comparison to the 2 mm thickness of the rectangular bars, the elasticity is kept reasonably low. Some results might appear to show the axle bending to a great degree; pay extra attention the deformation scale in these cases. An example is the road bump case, as will be shown below, wherein a no-vertical-displacement constraint is used for the modelled suspension bolt, effectively has the stiffness of the main swingarm structure increased by a lot. This leaves most of the displacement to instead happen in the simulated wheel axle.

This was still considered the best solution as this yielded more realism than other methods considered. It provided a rather rigid connection without being infinitely so, allowing the left mounting plate to be coupled with the right one while still allowing some deviation from both coplanarity and distance. Given the bonded contact used in the FEM simulations,[13] there are sometimes alarming, highly localised stress concentrations at the location where the wheel axle contacts the wheel mounting plate. These stresses have largely been neglected with the reasoning that an extremely concentrated stress (usually consisting of less than five nodes) at this location is exceedingly unlikely to be a point of failure in real life and is simply a consequence of FEM input of less-than-ideal quality.

It must be remembered that the FEM simulation output is only as valid as the input, and with nonperfect boundary conditions, the results must be ‘taken with a grain of

[13] This *can* be changed in SW but was not done for this project.

salt'. While this entails there is no all-encompassing proof that the concept is failsafe, it does give a great bit of insight into what areas are more problematic, and especially what to investigate further in future development.

See Appendix C for all cases' FEM results of the final design iteration. As with the first iteration, specific stress concentrations and other things of note are shown in their respective subchapter below.

7.4.1 **Comparing the designs**

7.4.1.1 Hard cornering

Judging by the maximum stress value in both cases, the high crossbar variant seems to be favoured. Taking a closer look reveals more information. See Figure 7.14 for a comparison of the two highest nodal stresses in both cases.

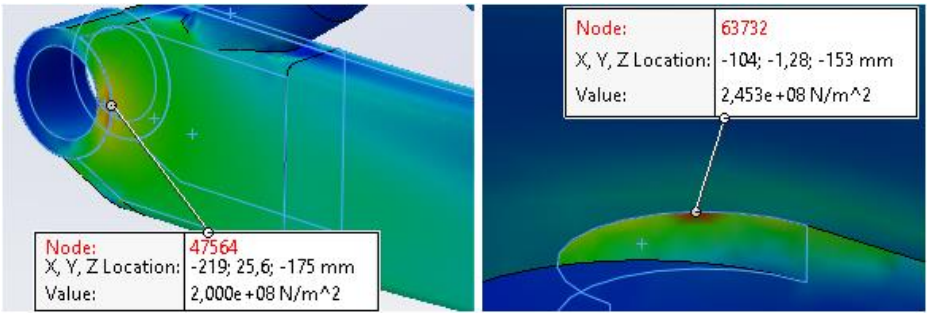

Figure 7.14 The highest nodal stresses in the hard cornering case. Left: high crossbar variant, stress located at frame mounting cylinder (at future weld location). Right: flat crossbar variant, stress located at crudely modelled weld, created simply to make the transfer of forces more realistic in the simulations.

After evaluation, this case speaks much more highly for the flat crossbar variant, showing most of the stress being more spread out in the longitudinal bars at more manageable levels. While high crossbar variant is rid of the stress concentrations it had on the first iteration where the crossbar meets the longitudinal bar, it does still show a high load near the frame mounting cylinders. In Figure 7.15 it can be noted that the stress is not highly concentrated (the plot is displaying stresses on *both* sides of the mounting cylinder and nearby longitudinal bar surface). As can be seen, the magnitude tapers off relatively slowly, meaning the stress is spread out over a larger area. This is true for both sides, although this is not specifically revealed by the nodal stress plot. The mounting cylinder will, as mentioned, house a rubber bushing which likely makes nearby stress concentrations more lenient. With how large the number of nodes close to the yield limit is, however, this case looks worrisome for the high crossbar variant.

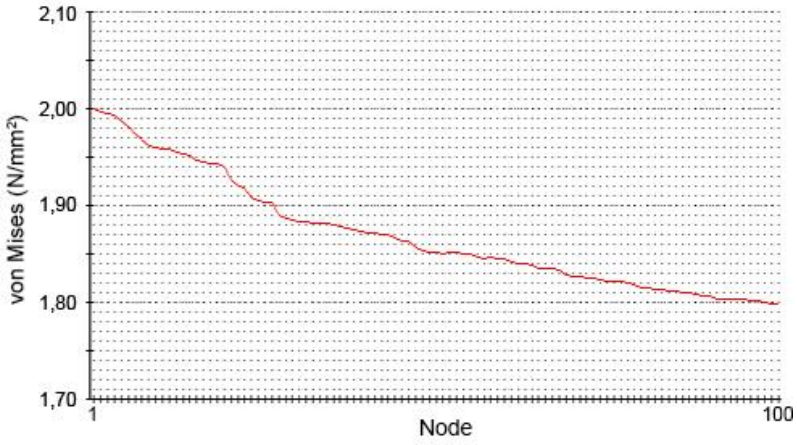

Figure 7.15 The 100 nodes with the highest stress on or near the frame mounting cylinder on the high crossbar variant, hard cornering case.

Looking instead at the flat crossbar variant, at the stress on the crudely modelled weld shown above, it appears extremely localised. Plotting all nodes on the highlighted surfaces and the ones nearby, we confirm this in Figure 7.16. It makes sense that this is a by-product of the overly simple weld simulation, as when looked at through a magnifying glass it is simply joined at a sharp, right-angled corner.

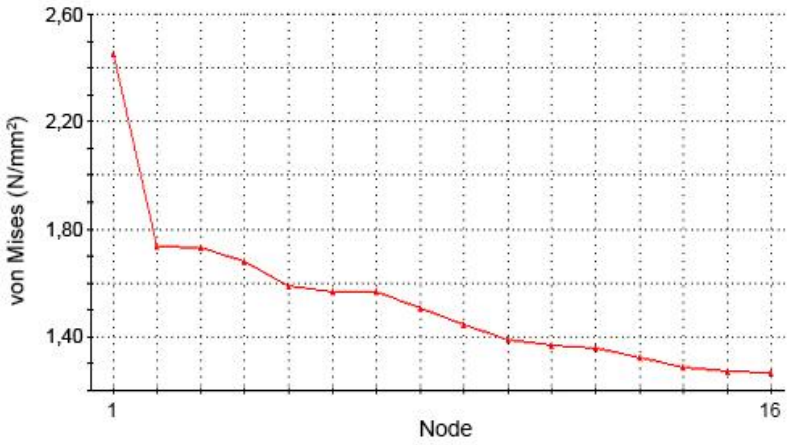

Figure 7.16 The 16 nodes with the highest stress on or near the frame mounting cylinder on the flat crossbar variant, hard cornering case.

With a single node over the yield limit, rapidly dropping off to safe levels, it is safe to say that the flat crossbar variant is preferable to the high one.

7.4.1.2 Hard braking

Very similar results in both cases. The one small area that exceeds the yield limit is the very sharp bonded corner at the brake calliper mounting plate, shown in Figure 7.17. This area, much like the simulated weld in the hard cornering case above, is extremely concentrated, and would be spread out much more evenly with the real-life welded design. This part could have been modelled with welds as well in an attempt to verify this, but ultimately time did not permit.

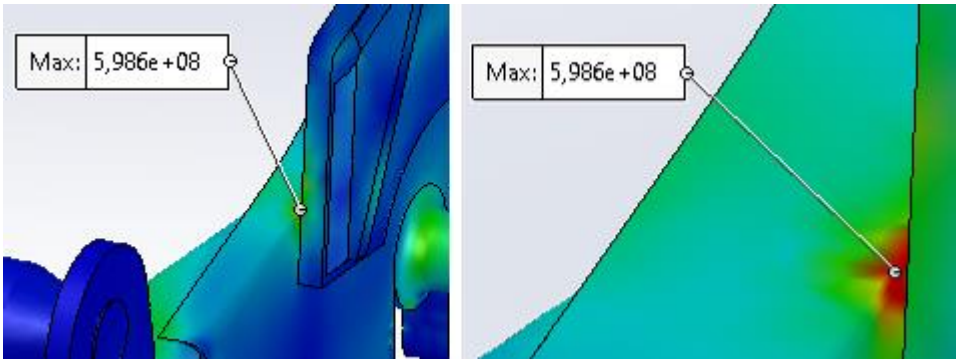

Figure 7.17 Stress concentration in the flat crossbar variant, hard braking. The high crossbar variant had a maximum nodal stress of similar magnitude.

In Figure 7.18 below, the maximum stress plot value was set to half of plain carbon steel's yield limit, to clarify which areas experience more concerning stress; this means completely red areas have a factor of safety value less than 2. Another way to visualise it is to imagine that all forces applied to the structure are doubled and the maximum plot value was left at 220,6 MPa.

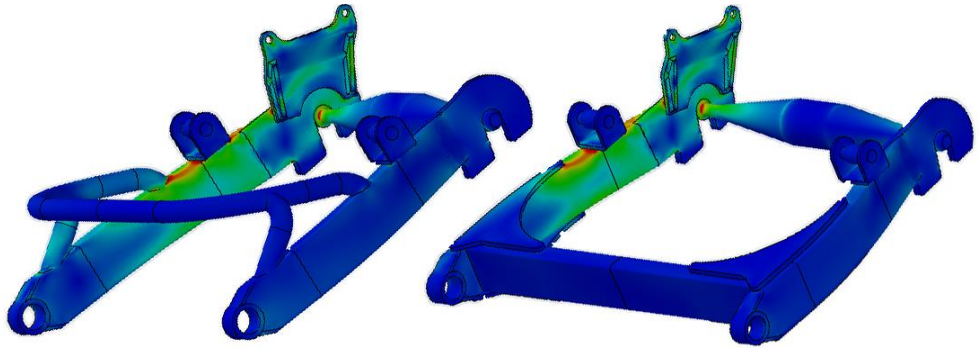

Figure 7.18 Stress result where the maximum plot value is halved (to 110,3 MPa), hard braking. Left: high crossbar variant. Right: flat crossbar variant.

The stresses are low enough to withstand, but not by a large margin. If the brake bias shifts towards the rear by a significant amount, this case might potentially prove problematic.

7.4.1.3 Maximum acceleration

All stress concentrations of any noticeable magnitude are in close proximity to areas where real-life welds would spread the force out. Even so, in this simulated model the stresses are low and of little concern.

7.4.1.4 Road bump

The results are not easily compared to the initial iterations in this report as those were not documented properly, but the increase in longitudinal bar dimensions had a significant positive effect on the stresses in both variants. As mentioned in 7.1.4 the case is perhaps simplified too much and would benefit from further evaluation.

In any case, the *overarching* appearance of the stress plots seem to suggest that this case is manageable for both variants, although zooming in shows a few stress concentrations in some expected places. Both cases had a very concentrated, high stress in one of the internal corners of the suspension fitting. The flat crossbar variant did however also have high stresses at the ends of the simulated welds on the longitudinal bar, above the limit of yielding.

Reflecting on the reason the gussets provided such a beneficial configuration (see 7.3), it is understood that their placement now unfortunately coincides with the location of *highest* tensile and compressive forces. The longitudinal bar is now effectively a beam in bending in the worst orientation regarding the gussets.

One way to remedy this is to attempt to reduce the bending caused by a road bump. This can be done by placing the suspension fittings further back, optimally as near the wheel axle mounting location as is allowed, without compromising other parts of course. A more reasonable placement—as they cannot completely coincide—is *above* the wheel axle mounting point, angled along the direction of the suspension. This would make the force from the suspension (or reaction force from the wheel, through the wheel axle, depending on how you want to visualise it) act purely compressively through the short distance of material between these mounting locations.

In this project, the suspension fittings OMotion uses currently was used for the design, and as mentioned, they were placed where they had equal amounts of overhang on either side of the longitudinal bar. A more space efficient solution that potentially enables a more rearward mounting location might be to instead use another type of fastening discussed further in 9.1.

The crossbar, predictably, was nearly completely free of stress.

7.4.1.5 Full weight

Both cases' plots show a very similar, rather safe result, with the only stresses of concern being inside the internal corner of, or under, the suspension fitting. These stresses, as commented on in earlier cases, is not of much concern.

7.4.2 **Recommended variant**

The flat crossbar variant looks very promising with how it handles the hard cornering case. Given the aforementioned potential suspension mounting change (see 9.1 for more details) I would recommend a further look into this design.

The high crossbar variant perhaps does not need the more rearward suspension mounting and is thus a worthy contender, on the condition that the hard cornering case can be improved. This can likely be done by widening the longitudinal bars from 20 mm to 25 mm; this does however require a change in frame fitting, in favour of a wider one. A wider fitting further requires a wider place to be welded onto, either by mounting an additional plate or two to the vertical frame tubes (highlighted in green in Figure 7.19 below), or by making the vertical frame tubes themselves wider.

This choice ultimately belongs to OMotion, depending on what is deemed best.

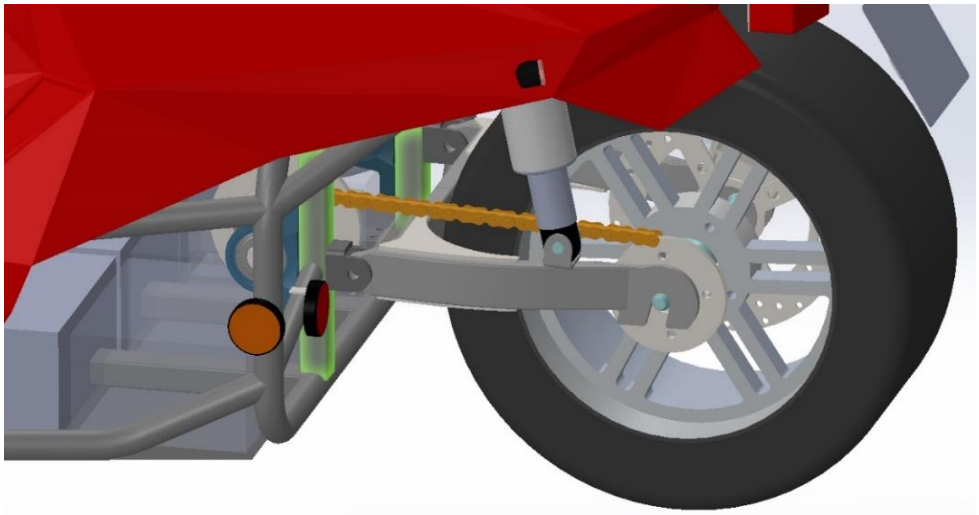

Figure 7.19 The vehicle assembly with the vertical frame tubes highlighted in green, to which the swingarm fittings are welded.[14]

[14] Note that this is not the final rendition, nor is it the representation of a currently commercially available OMotion product. It is simply to display the vertical frame members.

8 Jackshaft

The jackshaft will be subjected to high torsional shear during moments of high acceleration, and rotation bending (cyclic rotational loading) during *any* form of either acceleration or deceleration. Thus, the jackshaft needs to be dimensioned accordingly. A safety margin against maximum torsional shear stress will decide the material and diameter, after which the safety against fatigue is checked. Initially in this project, a rather low-strength ordinary steel and a diameter of 20 mm was selected, to check if it would suffice. A material with higher strength means higher difficulty in machining, and larger diameter further adds to this, in addition to extra cost and weight.

After the calculations it was concluded that both a change of material and an increase in diameter was necessary. Thus, the calculations shown in the following subchapters use material data and geometry attained from already having done the calculations (these initial calculations have not been included due to redundancy). The suggested material is SS 2225-04 (25CrMo4(+QT)[15]) and the diameter is 30 mm.

It is worth mentioning that if another configuration is to be explored in the future, a solution using a spline transmits torque very well and since the axle can be manufactured to have the spline teeth extend outward instead, the negative impact from the *stress concentration factor* (described below) can be minimised. A different material could perhaps also be used by locally hardening near the splines.

[15] Cr – Chromium, Mo – Molybdenum, Q – quenched, T – tempered.

8.1 Shear stress

The maximum amount of torsional shear stress will occur when the motor exhibits its peak torque, 130 Nm. With a motor-jackshaft gear ratio of 3,783, the peak torque at the jackshaft is 491,8 Nm. The shear stress for a linear, elastic material is expressed as

$$\tau = \frac{M_v}{W_v} \tag{8.1.1}$$

where $M_v = 491{,}8$ Nm as specified above, and

$$W_v = \frac{\pi r^3}{2} \tag{8.1.2}$$

for a circular, solid cylinder. Combining Equations (8.1.1) and (8.1.2) gives

$$\tau = \frac{2M_v}{\pi r^3}$$

which, with a diameter of 30 mm results in a torsional shear stress of 92,767 MPa. This is a nominal value, meaning that it is what the jackshaft would experience if it was perfectly cylindrical and without any defects, superficial or internal. However, the hub sprockets and jackshaft transmit torque by use of a key, and the keyseat imparts a very severe effect on the maximum allowed shear stress in the axle. More specifically it is the size of the internal fillet radius in the keyseat that needs to be of utmost scrutiny. This measurement is then compared to the axle diameter; assuming an internal fillet diameter of $\rho = 3$ mm the fillet radius to axle diameter ratio ρ/d becomes 0,1. With the graph shown in Figure 8.1 a stress concentration factor is approximated as $K_t = 2$.

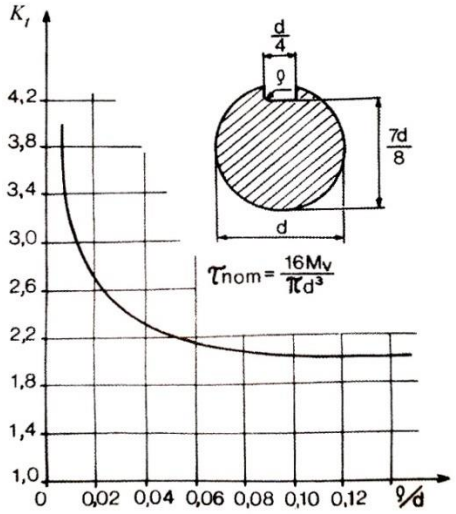

Figure 8.1 The graph showing the stress concentration factor K_t for different ratios of keyseat fillet radius to axle diameter. [14, p. 374]

This means that the actual maximum local stress in the axle instead will be

$$\tau_{max} = K_t \cdot \tau_{nom} = 2 \cdot 92{,}767 \text{ MPa} = 185{,}53 \text{ MPa}$$

For materials with no publicly tabulated torsional yield strength, it can be approximated as 60% of its tensile yield strength [14, p. 384]. The tensile yield strength varies slightly depending on source, but [14] lists a value of 590 MPa, which means that the torsional yield strength should be 354 MPa. This means that the jackshaft has a factor of safety of 1,91 against torsional yielding[16].

Quickly testing a case where the keyseat was incorrectly milled and instead ended up with an internal fillet radius of 0,6 mm, and thus a ρ/d ratio of 0,02, the stress concentration factor becomes $K_t = 2{,}7$. This increases our actual maximum local stress to 250,47 MPa, lowering the factor of safety to 1,41. This is likely still safe considering this is a scenario where there are few, if any, unpredictable momentary spikes in stress higher than those caused by the motor's peak torque. In addition to all this, there is also some hardening done when a material enters plasticity, or *work hardening*. This implies that the factor of safety against torsional yielding should be even larger than calculated here.

[16] The factor of safety is calculated by dividing the yield stress by the working stress (the maximum stress the part will experience during use).

8.2 Fatigue

With a material now known, the risk of failure through fatigue must be evaluated. Fatigue is simply put the onset of miniscule cracks, and their continued growth, which can potentially cause failure despite the maximum load applied at any point of the part's lifetime seemingly being within a safe margin [14, p. 287].

First, consider what cyclic events the jackshaft will be subjected to. There is *some* torsional cycling, but this only occurs when going to and from 'stepping on the gas'. This is arguably in low enough cycles to be ignored for a fatigue investigation. In any case, it occurs far less frequently than the bending moment caused by simply accelerating, with a cycle completed with every jackshaft revolution. Thus, the case of rotating bending fatigue is of highest importance. It should be mentioned that lower cycles with high loads still have fatigue failures, but the number of times actual peak torque is cycled is unlikely to shift this fatigue case to a higher priority.

First, the exact point along the length of the jackshaft that will be subjected to the highest bending moment is calculated. By extension this is the point that will have the highest stress amplitude. For this high cycle-case, the motor's *rated* torque of 50 Nm is instead considered. With a motor sprocket radius of 20,74 mm, this results in a tensile force $F_1 = 2410{,}8\ \mathrm{N}$ in the chain between motor and jackshaft. The torque transferred through the jackshaft, through the secondary smaller jackshaft sprocket with a radius of 48,23 mm, becomes a tensile force in the jackshaft-rear wheel chain $F_2 = 3921{,}9\ \mathrm{N}$, see Figure 8.2 and 8.3 for top-down views of the jackshaft assembly, and a free body diagram of the jackshaft, respectively.

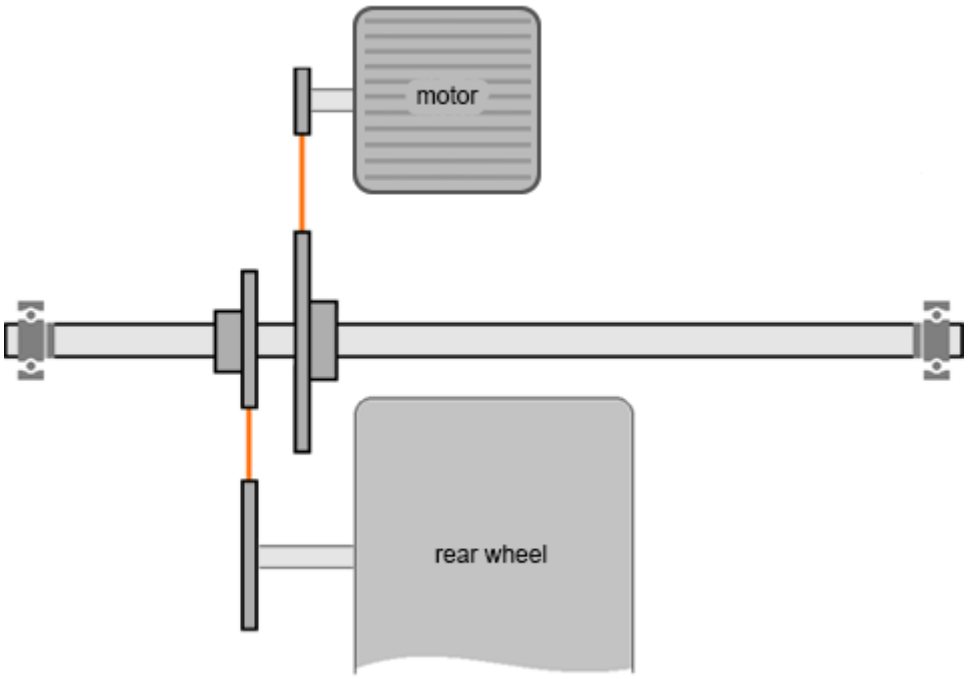

Figure 8.2 Top-down view of the jackshaft assembly. Not to scale.

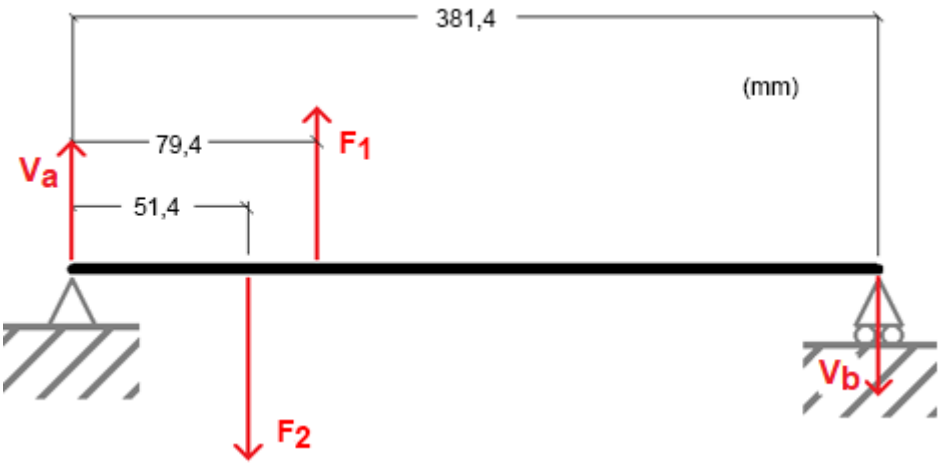

Figure 8.3 Free body diagram of the top-down view of the jackshaft assembly. Not to scale.

It is worth mentioning that these forces are very slight approximations, as the chains, and thus the corresponding forces, aren't perfectly aligned. They all run parallel to a 'median plane' (a plane splitting the vehicle in left and right halves) but have an angle of roughly 3º when viewed from an angle normal to said plane, see Figure 8.4.

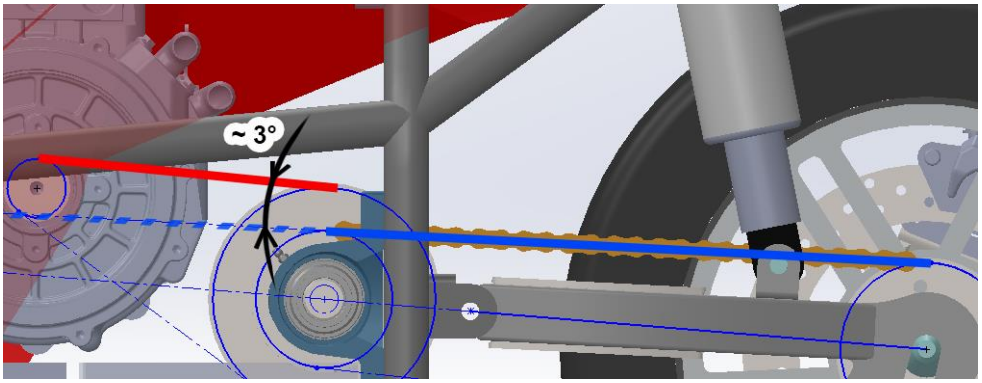

Figure 8.4 The vectors of the chain forces creating a shallow angle.

Equilibrium of forces and moments gives $V_a = 1484{,}4$ N and $V_b = 26{,}7$ N. Through cross-sectional moment diagrams the maximum bending moment of 76,3 Nm was calculated and determined to be located at the same point as F_1. With

$$\sigma = \frac{M_b}{W_b}$$

The maximum bending stress becomes 28,78 MPa. This value must now be compared to the material's *endurance limit* (the stress under which the material theoretically can be subjected to an infinite number of cycles without failure). For these calculations the methodology written in [14, pp. 295-301] is followed completely, and thus not referenced again during the rest of the calculations, unless specific references to pages outside of this interval necessitates it. Any other sources listed in this subchapter are only for the corresponding translations.

The process consists of initially acquiring a tabulated value of the endurance limit for the specific fatigue condition (in this case *rotating bending*), followed by reducing it by a set of factors that vary depending on how stress resistant the part is. This reduced endurance limit becomes the new endurance limit for any practical purposes. The tabulated values are slightly misleading, as they are calculated in controlled environments using samples of very high consistency in both dimensions and material quality.

The reduction factor in question is

$$\frac{\lambda}{K_f K_d K_r}$$

where λ is a size-dependent factor for cast products, K_f is a fatigue notch factor [20], K_d is a stress concentration factor for deep notches [21], and K_r a correction factor dependent on the roughness of the surface. The material is not cast, so

$$\lambda = 1$$

The fatigue notch factor is expressed as

$$K_f = 1 + q(K_t - 1)$$

where q is the notch sensitivity [20], established through linearly interpolating the ultimate stress of the steel, R_m in Figure 8.5, using the fillet radius established in the shear stress calculations.

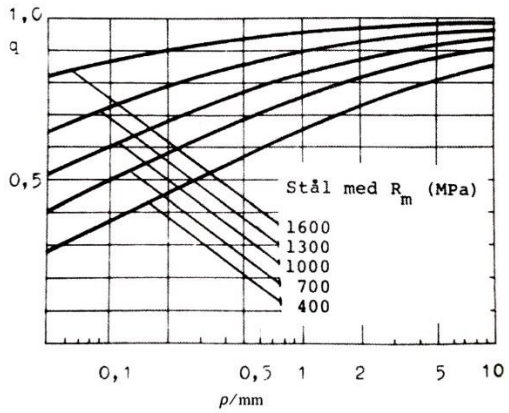

Figure 8.5 The graph used for estimating the notch sensitivity *q*. [14, p. 298]

SS 2225-04 has two tabulated values of ultimate stress at 790 MPa and 930 MPa [14, p. 387]. Using an average of 860 MPa and linearly interpolating vertically in the graph[17] at the fillet radius determined in the shear stress calculations (3 mm), an approximate value of

$$q = 0{,}87$$

is read. The value of K_t has been established previously, which yields

$$K_f = 1{,}87$$

[17] Between ultimate stress lines 700 MPa and 1000 MPa.

The *deep not*ch stress concentration factor K_d only deviates from a value of 1 if there is exists no *general* stress concentration factor K_t, which as shown is present in this case. It is thus left unchanged.

The surface roughness correction factor K_r is established by consulting the graph shown in Figure 8.6.

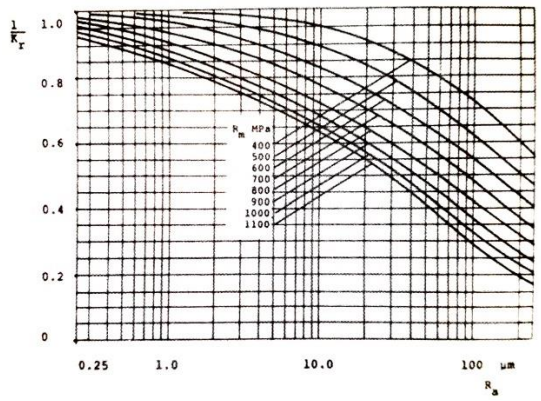

Figure 8.6 The graph used for estimating the surface roughness correction factor K_r. [14, p. 301]

Assuming a rough turned surface with $R_a = 10$ µm and linearly interpolating as previously done, the factor is approximated as

$$K_r = 1{,}429$$

This means that the total reduction factor is

$$\frac{\lambda}{K_f K_d K_r} = \frac{1}{4{,}299}$$

SS 2225-04 has a tabulated endurance limit for rotating bending of ±410 MPa [14, p. 387], which means the reduced endurance limit becomes

$$\frac{410}{4{,}299}\ \text{MPa} = 95{,}371\ \text{MPa}$$

A *fatigue safety factor* is now determined, at

$$\frac{95{,}371}{28{,}78} = 3{,}314$$

which means that the jackshaft has a large margin of safety against fatigue. For additional peace of mind, a 'Friday afternoon product' could also be evaluated. Assuming a *very* rough surface quality of $R_a = 20$ µm, in addition to the previously mentioned incorrectly milled keyseat, the total reduction factor becomes $\frac{1}{4{,}875}$. This results in a fatigue safety factor of 2,922, which is still within a very safe margin.

8.3 Bearings

Unless otherwise specified, all the following information has used the SKF catalogue for Y-bearings and Y-bearing units [22] as reference. ‘Y-bearing’ is the terminology used by SKF for their conventional ball bearing units.

The bearings will be seated in plummer block units. SKF mention that their Y-bearing units accommodate moderate initial misalignment, but normally no axial displacement. Axial displacement could arise from two effects in this case. The first is through bending forces from the chains pulling on—or being pulled by—the sprockets, causing the ends of the jackshaft to ‘pull inward’; the second is through thermal effects. The axial forces in the jackshaft due to bending are small, but still present, and occur during acceleration and regenerative braking, albeit to a lesser extent in the latter case. Considering the choice of material and axle diameter, the strain in the material caused by these forces is without a doubt small enough to not warrant a calculation. The forces do however warrant picking a bearing that can handle axial loads, such as a deep groove spherical ball bearing.

The thermal effects must still be evaluated. The relative change in length due to thermal expansion is estimated with

$$\frac{\Delta L}{L} = \alpha_L \Delta T$$

Assuming a temperature range of 70 °C in a worst-case scenario[18], a distance between set screws of roughly 383 mm, and SS 2225 (all variants) having a coefficient of thermal expansion of $\alpha = 11{,}1 \cdot 10^{-6}\ K^{-1}$ [14, p. 386], an absolute change in length of less than 0,3 mm is calculated, or more specifically 0,2976 mm. Considering a case where the jackshaft is assembled when the ambient temperature is 15 °C[19], the maximum change in length either by expansion or contraction then becomes half this value.

In conclusion, the left-side bearing should be a locating bearing, firstly since keeping correct alignment of the sprockets is important, and secondly since the proximity to the sprockets—and thus the chain forces—will expose it to higher loads. The right side could potentially be a non-locating configuration with a groove for the set screws. Set screw grooves are typically employed in cases where thermal expansion is an issue but should essentially accommodate axial displacement caused by bending forces just the same.

---

[18] Imagining an unheated garage during a cold winter dipping to negative 20 °C, to an extremely hot summer reaching 50 °C

[19] Directly in the middle of the temperature range given in the previous footnote.

9 Discussion

9.1 Reflections on design

The ‘plain carbon steel’ material was used in SW as this is what OMotion currently uses. It has similar yield strength to E220, a common cold-rolled steel used for rectangular tubing free of excessive loads [23] [24]. All the concerns regarding stresses in the swingarm close to yield limit would be reduced with an increase in said limit. Simply put, a doubling in yield strength equals a doubling in factor of safety. While a doubling might not be completely necessary, an increase is at the very least worth considering. Hopefully the discussion below helps OMotion decide what path to take.

The lateral force in the cornering case could possibly have been lowered significantly, as [11] shows the front tyre bearing a significantly larger load than the rear tyre during a skid pad run. The assumption in the cornering case was simply that the rear wheel would experience half of the lateral load during hard cornering, imagining a simple free body diagram where the CoG is located directly in the middle of the wheelbase. Unfortunately, the imagined sum of forces in this diagram did not take into consideration that a cornering—or, *turning*—vehicle actually *turns*…

The fact that the front tyres bear a larger lateral load when cornering is further explained by realising that it is the front wheels veering away from the current path of travel, and the rear tyres simply following. This attempt at an explanation seems disputed by Foale, however, in an example where the rear tyre experiences higher lateral, although for a cornering—and thus leaning—motorcycle [2, p. 6:43]. Another example showing this behaviour is a simulation of heavy-duty vehicles by Olofson in [25, p. 21], where she explains that the higher lateral forces are due to the mass being larger at the rear axle. For our purposes it is currently inconclusive, but since the lateral forces seems to have erred only slightly on the side of caution, the exact excess in force matters little.

With the large lateral forces causing a reconsideration in design luckily seems to have been a beneficial change overall. The only case that yielded worse results as a direct consequence of opting for a gusseted rectangular crossbar was the hard bump case, and the cornering case performed much better.

As mentioned in 7.4.1.4, the hard bump case could likely be improved with a more rearward mounting location of the suspension on the swingarm. The bending forces caused by the suspension placement currently used in this design, would instead become purely compressive in the small amount of material between suspension mount and wheel axle mount. An accurate coil-over shock absorber would likely have to be modelled to evaluate spatial concerns.

It must be remembered however that an angular change in the suspension also changes the internal forces within it; the vertical forces for example are countered by the suspension, mounted at an angle. The greater the angle, the greater the force. It seems however that the compressive forces that would result from the configuration in Figure 9.1 are much more manageable than the bending forces with a worse suspension fitting placement.

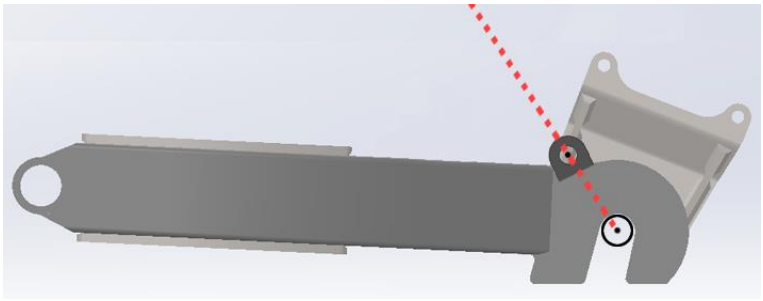

Figure 9.1 A simple visualisation of the suggested suspension mounting location, causing the otherwise bending forces it induced to instead become purely compressive.

On the same note, the placement of the steel tube to which the suspension fittings are mounted on the frame was not put in a highly specific position, but rather a general area where the suspension had a slightly forward tilt, to introduce a slightly progressive quality. Nonetheless, every simulation in this report has used values derived from the suspension angle in their respective boundary conditions. A more rearward placement of the bottom fittings, and/or a more forward placement of the upper fittings makes the suspension more progressive—which might be desirable. The exact magnitude of this *geometric* progressivity[20] was not actively decided in this report and was left for OMotion's further development.

Another method of improving the hard cornering case in addition to the widening of the longitudinal bars mentioned in 7.4.2 could be to triangulate the design more, meaning the frame fittings would be placed even further apart. More of the bending forces would become tensile and compressive forces in the longitudinal bars instead.

[20] There are also springs and dampers that are *intrinsically* progressive or regressive.

An analogy is that instead of hanging a weight onto a horizontal cantilever beam, it is instead hung from a similar beam, mounted at a predetermined downward angle. In the former case, we have a case of almost pure bending; in the latter case, depending on the angle we have converted some bending to tensile normal forces.

Chain tension adjustability at wheel mounting was unfortunately not regarded early enough in the design and as such, all simulations were already done at the time when it was considered. A suggested redesign is to instead use a locking mechanism similar to that usually found on many motorcycles, where the internal wheel axle is inserted from the side as shown in Figure 9.2.

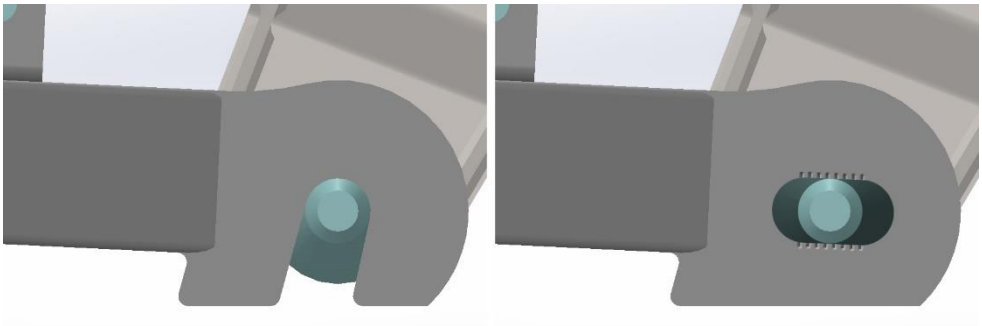

Figure 9.2 Wheel axle mounting plate. Left: 'current' design. Right: suggested redesign.

The wheel axle in this suggested redesign is instead removed laterally instead of lifting the rear of the vehicle (or just the swingarm) upward above the wheel. The notches seen on the suggested redesign in Figure 9.2 are intended for assisting in lateral alignment of the wheel.

9.2 Reflections on topology optimisation

9.2.1 **The topology optimisation study**

The TO design space might have benefitted from including a true-to-life protrusion modelling the fitting so that it would not be embedded into the rest of the volume. The exact geometry of the fitting could essentially have been used, but a simplification would make the study run faster without affecting the result much. In the TO in this project, the mounting location modelled the sides of the fitting, but did not hinder material from being built away from this location in a manner that later would not be feasible on the welded design. As mentioned, the crossbar in the TO result naturally created an arch on a slanted plane extending through the wheel

and suspension mounting points. If the design space had not allowed for a straight line to be built from the suspension mount location, a different angle of the crossbar in the TO result would have been likely.

The boundary conditions in the TO should probably have included a brake torque case, as it might have created a structure more resistant to bending.

9.2.2 Suitability of topology optimisation for weldments

The finished designs might not resemble the TO result to a great degree. The immediate, obvious reason being the difficulties regarding manufacturability. It is crucial on a swingarm that must withstand very high forces in extreme cases that the stress concentrations are minimised, especially near welds. Predicting these concentrations is not a trivial task and combating them required redesigns that ultimately made the design veer further from the TO result. It must be remembered that TO studies do not consider where future structural members will be welded together[21] (and might be weakened in a thermally affected zone), and constraints regarding dimensions and trade-offs in manufacturing. This is instead something the engineer would have to predict, slightly discrediting the use of TO for welded designs.

Ultimately, while using TO for a design that would eventually need to be weldable might not be the best choice of method, it did provide an interesting challenge, with an emphasis on ‘challenge’. In conclusion, TO is best suited for either cast, CNC-milled or 3D printed parts, as they can much more closely adhere to the result of the topology optimisation. With the exception of additive manufacturing, the result of a TO study is almost always used simply as an inspiration for a new part built from scratch. If used for parts that will be welded it is perhaps better used as a means of validating an existing design, or perhaps to suggest a radical redesign, and less effective when used as a tool whose results are to be followed closely.

[21] Well, at least not this one.

9.3 Other

- For factor of safety visualisations, the maximum plot value (where nodes that assume a value greater than it turn red) was halved, down to 110,3 MPa. This gave a clearer gradient of colours showing other parts that were close to the specified factor. At the time when the studies were run, this felt favourable to using the factor of safety plot function that SW offers, but it makes no real difference.
- All figures in this report of parts made in SW use an isometric view.
- The modified and newly created parts will all be supplied to OMotion, but drawings weren't included in the project, partly due to perhaps immediately being confidential, but also because alterations to the design—however small—are expected either way.

10 Future development

10.1 Regarding anti-squat

Consider what a change in anti-squat percentage entails. As 100% was specifically requested for this project, that is what was used. Some sources do however claim that a lower value is better in terms of feel, performance, etc. [26]. Whether or not the configuration designed in this project is satisfactory or not will ultimately be apparent upon prototyping it. If a small change in AS is requested, new TO studies are not necessarily warranted. New FEM simulations should of course be run as a safety measure but given the rather generic design there is not much doubt it would pass the scenarios tested in this project if everything else is kept unchanged.

A possible path to explore might be an adjustable AS percentage, allowing the end user to customise their own experience. With the current configuration there is an important thing to note, however. If the jackshaft and swingarm fitting move equal amounts vertically, the chain tension consistency during suspension travel is negatively affected. The degree of this effect gets larger with increasing vertical distance. The vertical separation varies with a tangent function as they have a fixed horizontal separation and move vertically while coincidental with a common line extending from the centre of the rear wheel axle. This is visualised below in Figure 10.1; note that this example shows an extremely exaggerated configuration, simply to aid in visualising the tangent function effect.

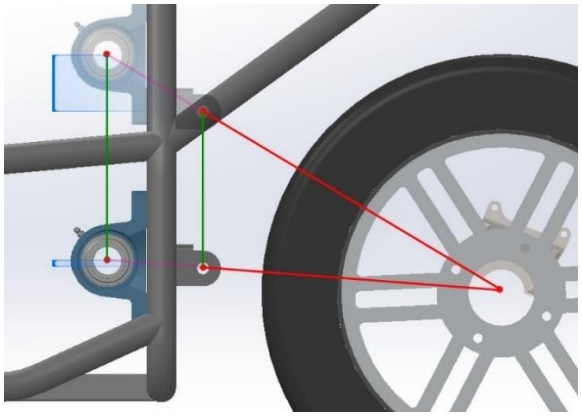

Figure 10.1 The difference in vertical distance visualised. The blue lines show the vertical separation of jackshaft and swingarm fitting for two different AS percentages that keep chain tension consistent. Red lines represent the swingarm, and green lines are vertical lines along which the centre of the bearing and fitting bolt hole move.

If the AS percentages offered are within a small margin, the chain tension consistency might not be an issue. Furthermore, if concept A is used for a future version this issue is eliminated, as this mounts the jackshaft and swingarm mounting location concentrically.

10.2 Other

The new battery compartment yet to be fully designed, and the motor placement, will influence the CoG. Determine what position is the most desirable if spatial constraints permit. It is worth keeping in mind that, while the longitudinal position of CoG does not affect the absolute value of load transfer in newtons [2, p. 9:1], it will affect the load transfer as a percentage of the weight normally supported under no acceleration.

As mentioned in 7.4.1.4 and 9.1, an evaluation of a suspension mounting that attaches to the swingarm further back is recommended. With the current suspension fitting used this probably will not work due to spatial concerns. Something like the fastening on the lateral face of the swingarm like on the Campagna T-Rex in Figure 10.2 might work.

Figure 10.2 The bolt fastening configuration on the lateral face of the swingarm used on some Campagna T-Rex models (adapted from [27]).

If for some reason a long axle jackshaft as suggested in this report turns out less than ideal, it might be worth looking into other configurations. One such configuration is simply to move the right vertical tube (which the right plummer block is mounted on) closer to the sprockets, shortening the distance between them. This could however cause asymmetrical frame strength, which must be evaluated. This method would lower the cost if the shaft were to be made with splines instead of a key for the torque transfer.

Investigate the factor of safety required. Ultimately, the safety margin is dependent on the uncertainty in the design[22]. With the limited knowledge of exact material properties, wear, the uncertainty of extreme cases during driving conditions, and other various outliers, it is hard to pinpoint a precise factor of safety value. With a more accurate value, cheaper materials might be viable, lower tolerances chosen, etc.

[22] If you know everything there is to know in your design, and if it will only be used in a controlled environment, you would barely need a margin of safety at all, as there would be no outlier cases. You could design to the exact maximum load that you know the structure will be affected by, and at what exact point.

10.3 Revisory comments

Upon completion of the project and review of the report by OMotion it was determined that there was a misunderstanding regarding the strength of the swingarm material. In this report, the material used has a yield limit of 220 MPa—in reality, the steel that will be used has a yield limit of 355 MPa. This of course means that the stresses in all edge cases are much more manageable. More precisely, the factor of safety for any given point, in any given scenario, has increased by a factor equal to the ratio of these two limits: 1,61. It is far from ideal to uncover something of this nature after the project has concluded, but at least the material that will be used in the real design has *higher* strength. A misunderstanding where the project used material with too high strength would have been far more troublesome.

References

[1] K. T. Ulrich, S. D. Eppinger and M. C. Yang, Product and Development, 7th ed., New York: McGraw-Hill Education, 2020.

[2] T. Foale, Motorcycle Handling and Chassis Design, Tony Foale, 2006.

[3] B. Mohan Redrouthu and S. Das, “Tyre modelling for rolling resistance,” Division of Vehicle Engineering and Autonomous System, Chalmers University of Technology, Gothenburg, 2014.

[4] J. Sabhadiya, “Shaft Key: Definition, Type, And Application,” Engineering Choice, 10 October 2020. [Online]. Available: https://www.engineeringchoice.com/what-is-shaft-key/. [Accessed 28 October 2022].

[5] Kullager.se, “Kedjehjul 5/8 x 08 S,” Kullager.se, [Online]. Available: https://www.kullager.se/kedjehjul-5/8x8-s. [Accessed August 2022].

[6] SKF, “SY 20 TF,” SKF, [Online]. Available: https://www.skf.com/group/products/mounted-bearings/ball-bearing-units/pillow-block-ball-bearing-units/productid-SY%2020%20TF. [Accessed October 2022].

[7] SKF, “FYTJ 40 TF,” SKF, [Online]. Available: https://www.skf.com/id/products/rolling-bearings/ball-bearings/angular-contact-ball-bearings/single-row-angular-contact-ball-bearings/productid-FYTJ%2040%20TF. [Accessed October 2022].

[8] J. D. da Cal Ramos, “Front and Rear Swing Arm Design of an Electric Racing Motorcycle,” Técnico Lisboa, Lisbon, 2016.

[9] Santa Fe Garage, “Skid Pad Testing,” Santa Fe Garage, [Online]. Available: https://www.santafegarage.com/precision-alignments/skid-pad-testing/. [Accessed 30 September 2022].

[10] J. Chen, A. Hope and J. Tate, “g Masters - Lateral Acceleration Testing,” MotorTrend, 15 June 2007. [Online]. Available: https://www.motortrend.com/news/0708-sccp-lateral-g-skidpad-testing/. [Accessed 13 October 2022].

[11] M. V. Bartolomeo, A. Lombardo, M. Colella and G. J. Delagrammatikas, "Measuring the Traction Limits and Suspension Forces of a Formula SAE," American Society for Engineering Education, New York, 2019.

[12] [Forum discussion], "Assumed Lateral and Longitudinal Acceleration for 1st year team," FSAE, 19 December 2010. [Online]. Available: http://www.fsae.com/forums/showthread.php?8312-Assumed-Lateral-and-Longitudinal-Acceleration-for-1st-year-team.&s=1f04b7dfa8fe76c88ae717b291ae1538. [Accessed 21 October 2022].

[13] B. P. Wiegand, "MASS PROPERTIES AND AUTOMOTIVE DIRECTIONAL STABILITY," Society of Allied Weight Engineers, Inc., Long Beach, 2021.

[14] Institutionen för hållfasthetslära, KTH, Handbok och formelsamling i Hållfasthetslära, Stockholm: KTH, 2016.

[15] Brake Experts, "Front vs. Rear Brakes: Does it Even Matter?," Brake Experts, [Online]. Available: https://brakeexperts.com/front-vs-rear-brakes-does-it-even-matter/. [Accessed 24 October 2022].

[16] RepairSmith, "What Is Brake Bias And How Does It Affect Braking Performance?," RepairSmith, [Online]. Available: https://www.repairsmith.com/blog/brake-bias/. [Accessed 25 October 2022].

[17] N. Kudarauskas, "Analysis of emergency braking of a vehicle," *Transport*, vol. 22, no. 3, pp. 154-159, 2007.

[18] Queensland Government, "Stopping distances: speed and braking," Queensland Government, 14 November 2016. [Online]. Available: https://www.qld.gov.au/transport/safety/road-safety/driving-safely/stopping-distances. [Accessed 26 October 2022].

[19] F. Eklund, "Design Study of Welded Beam Bracket According to Stress Concentrations in the Weld," KTH, Stockholm, 2021.

[20] M. Melters Pedersen, "Introduction to Metal Fatigue," Aarhus University, Aarhus, 2018.

[21] P. Kuhn and H. F. Hardrath, "An engineering method for estimating notch-size effect in fatigue tests on steel," NACA, Hampton, 1952.

[22] SKF Group, "Y-bearings and Y-bearing units," SKF Group, Gothenburg, 2013.

[23] Harris (Steels), "E220 Spec," Harris (Steels) Limited, [Online]. Available: https://www.harrissteels.co.uk/e220-standards-specification/. [Accessed 28 October 2022].

[24] AB Montano, "Fyrkantsrör stål," AB Montano, [Online]. Available: https://montano.se/product.html/fyrkantsror-stal. [Accessed August 2022].

[25] H. Olofson, “Rolling resistance during cornering - impact of lateral forces for heavy-duty vehicles,” KTH, Stockholm, 2015.

[26] Suspension Secrets, “GEOMETRY > ANTI GEOMETRY,” Suspension Secrets, [Online]. Available: https://suspensionsecrets.co.uk/anti-squat-dive-and-lift-geometry/. [Accessed July 2022].

[27] The Car Guide, “2017 Campagna Motors T-Rex 16S,” The Car Guide, 2017. [Online]. Available: https://www.guideautoweb.com/en/makes/campagna-motors/t-rex-16s/2017/gallery/?im=3. [Accessed 28 October 2022].

Appendix A Topology Optimisation Study Results

Views are shown in the following orientations (camera pointed *from* this direction):

Angled (top-left-behind)

Top

Behind

Left

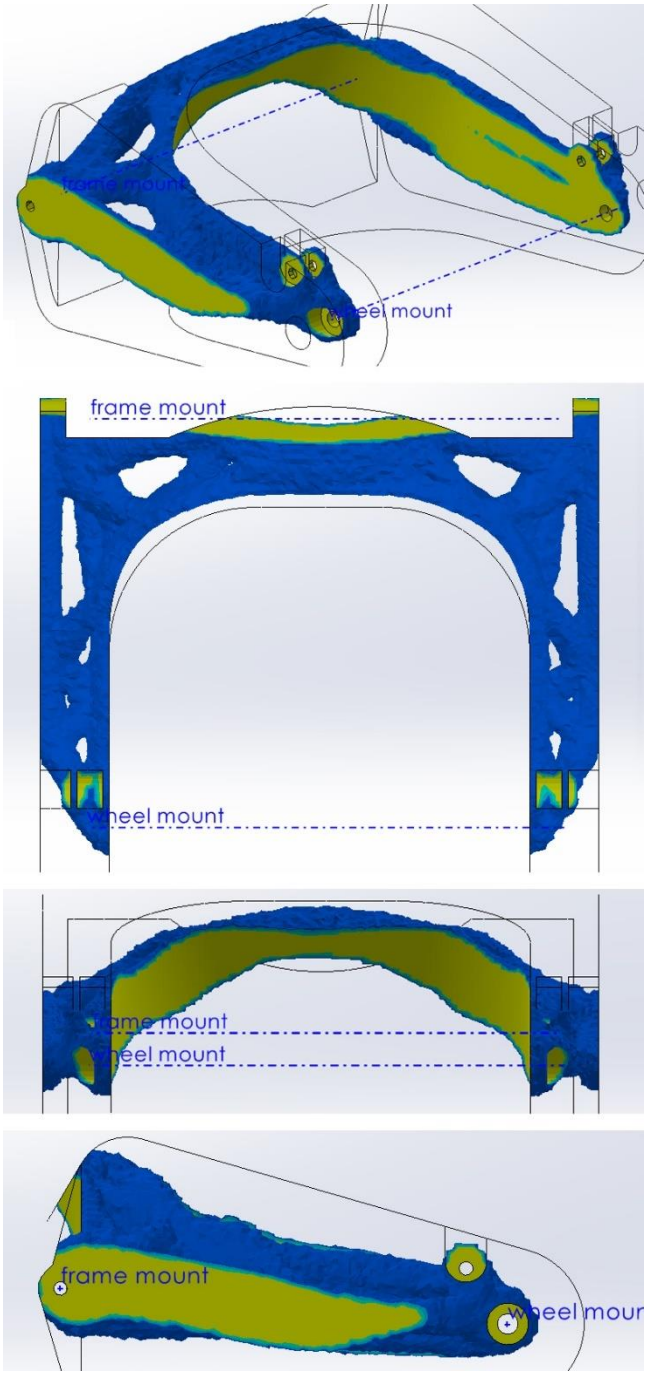

Figure A.1 Topology optimisation study result for configuration 1. Note that this figure shows a result where a large amount of material was kept, making the inner 'skeleton' less apparent. This is corrected in the results for the two other configurations.

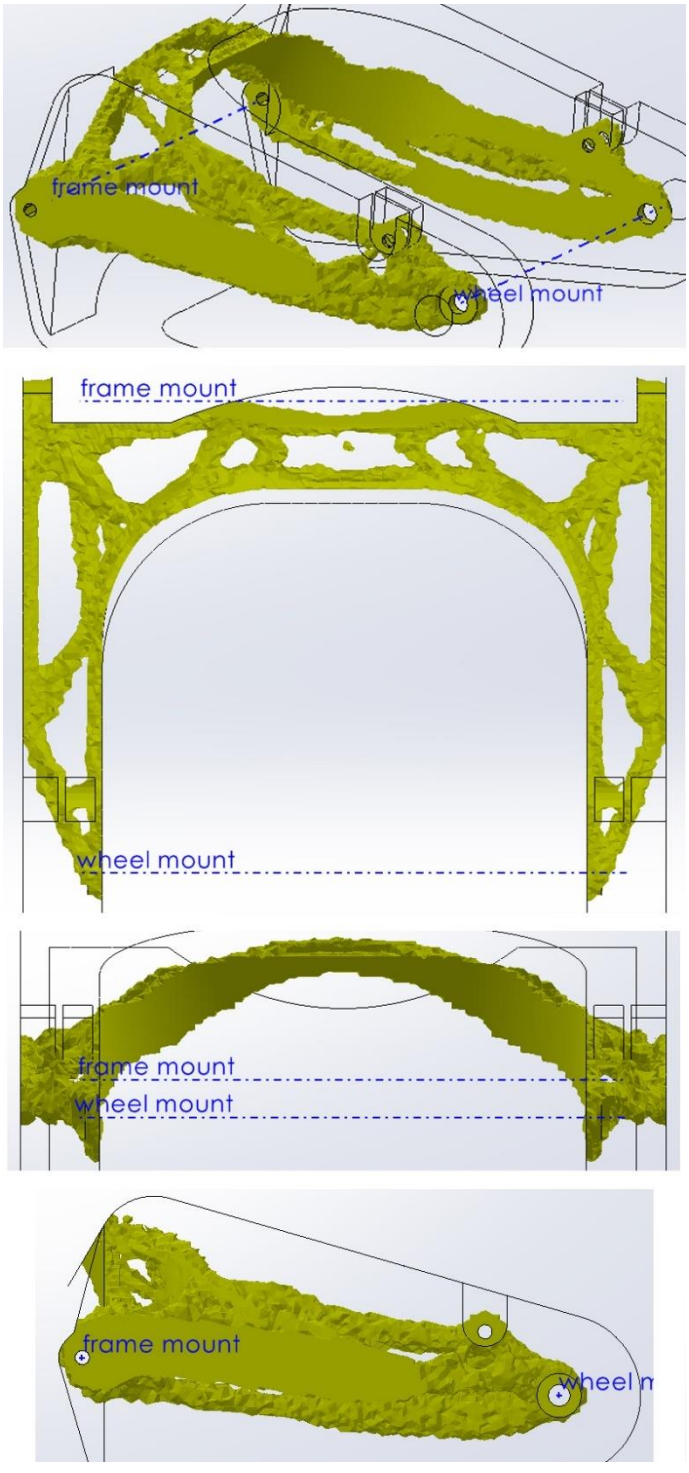

Figure A.2 Topology optimisation study result for configuration 2.

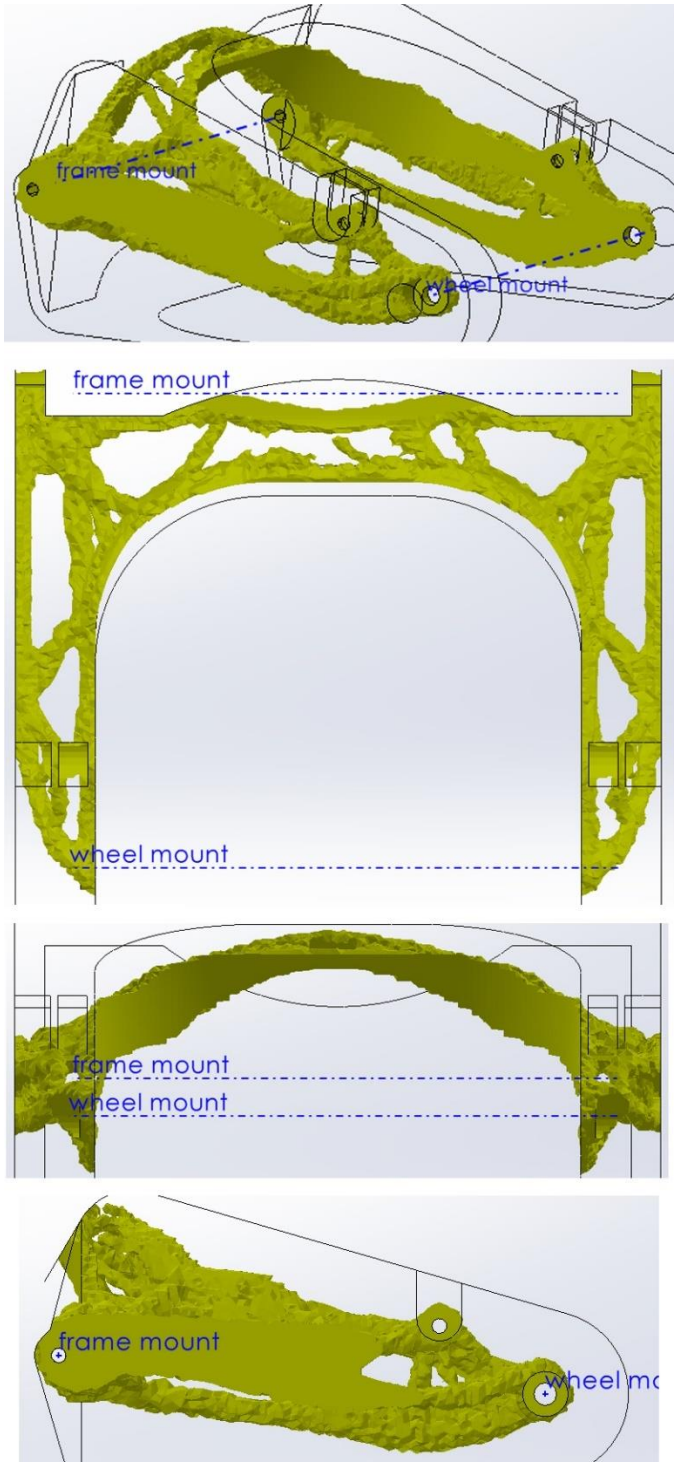

Figure A.3 Topology optimisation study result for configuration 3.

Appendix B FEM Results, First Iteration

Views are shown in the same manner as Appendix A.

The stress results are shown with a maximum plot value of 220,6 MPa, the yield limit of ‘plain carbon steel’ in SW.

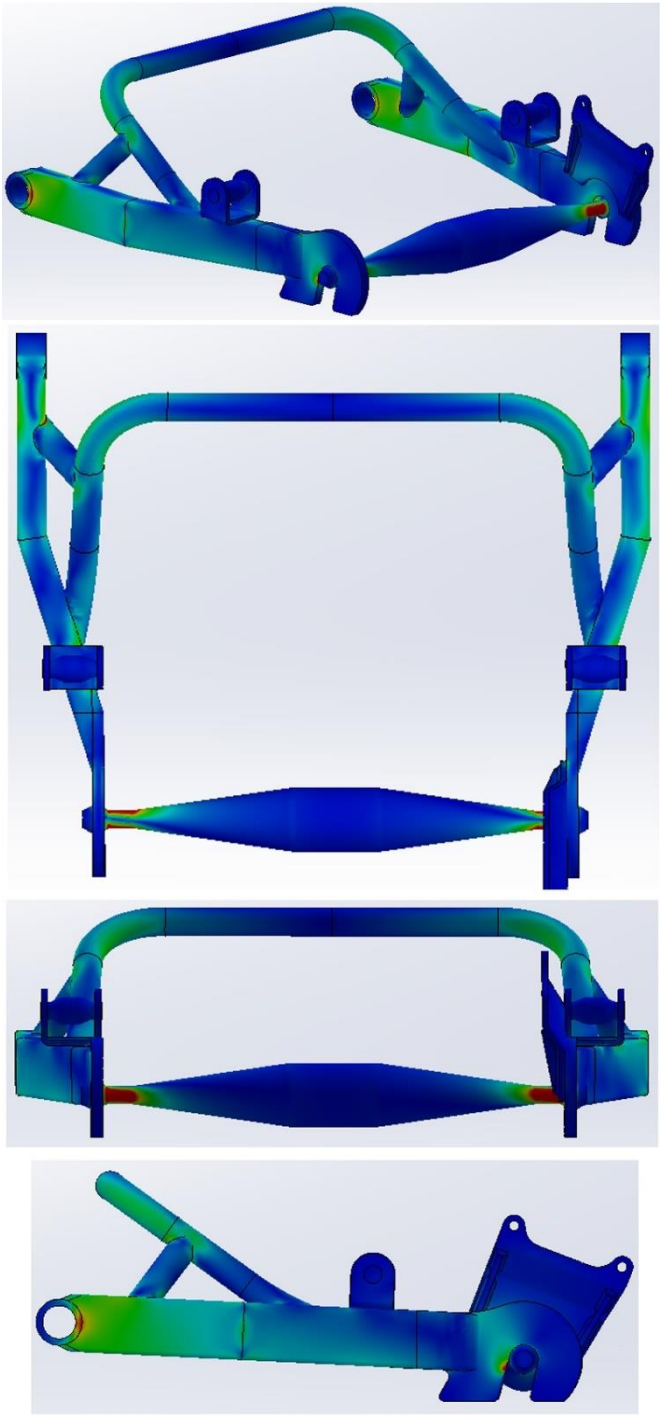

Figure B.1 The stress results from the hard cornering case, high crossbar variant.

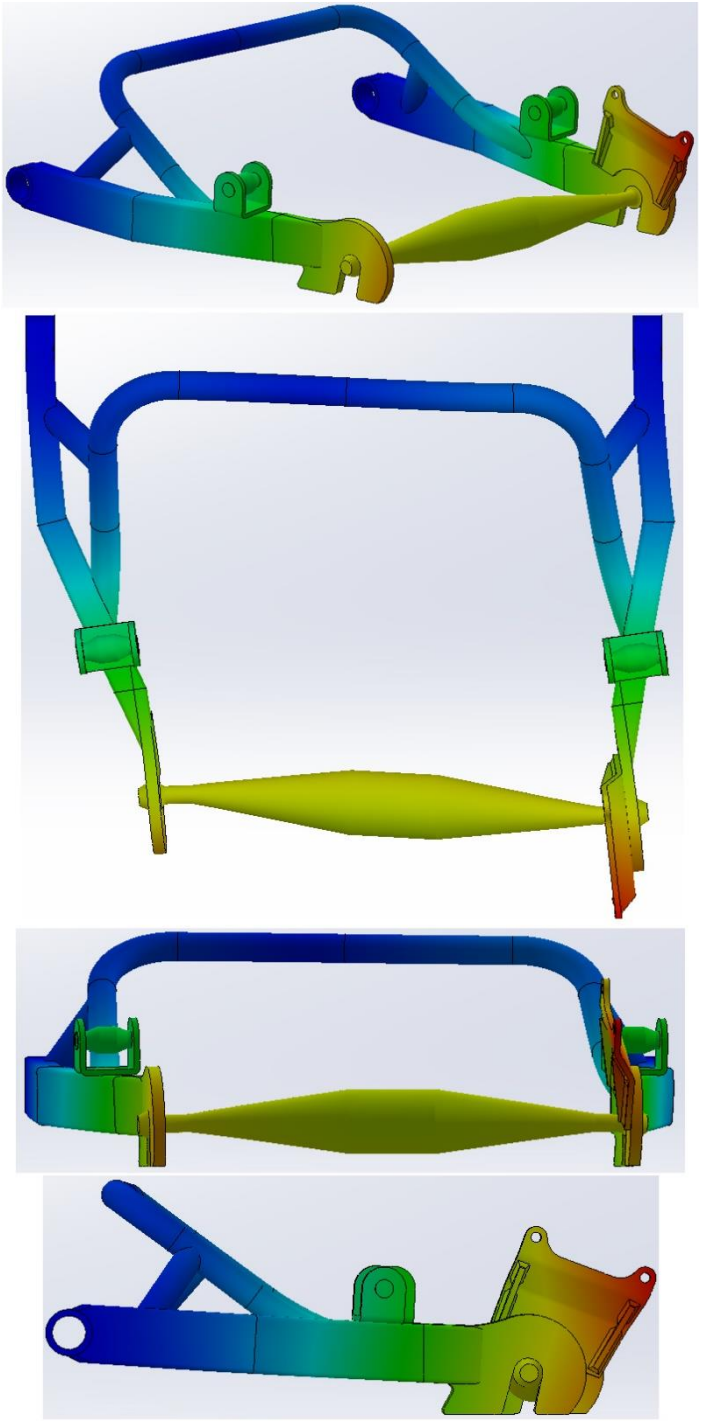

Figure B.2 The displacement results from the hard cornering case, high crossbar variant. Deformation scale 20,8 (results are amplified 20,8-fold). The reddest node moved 2,1 mm.

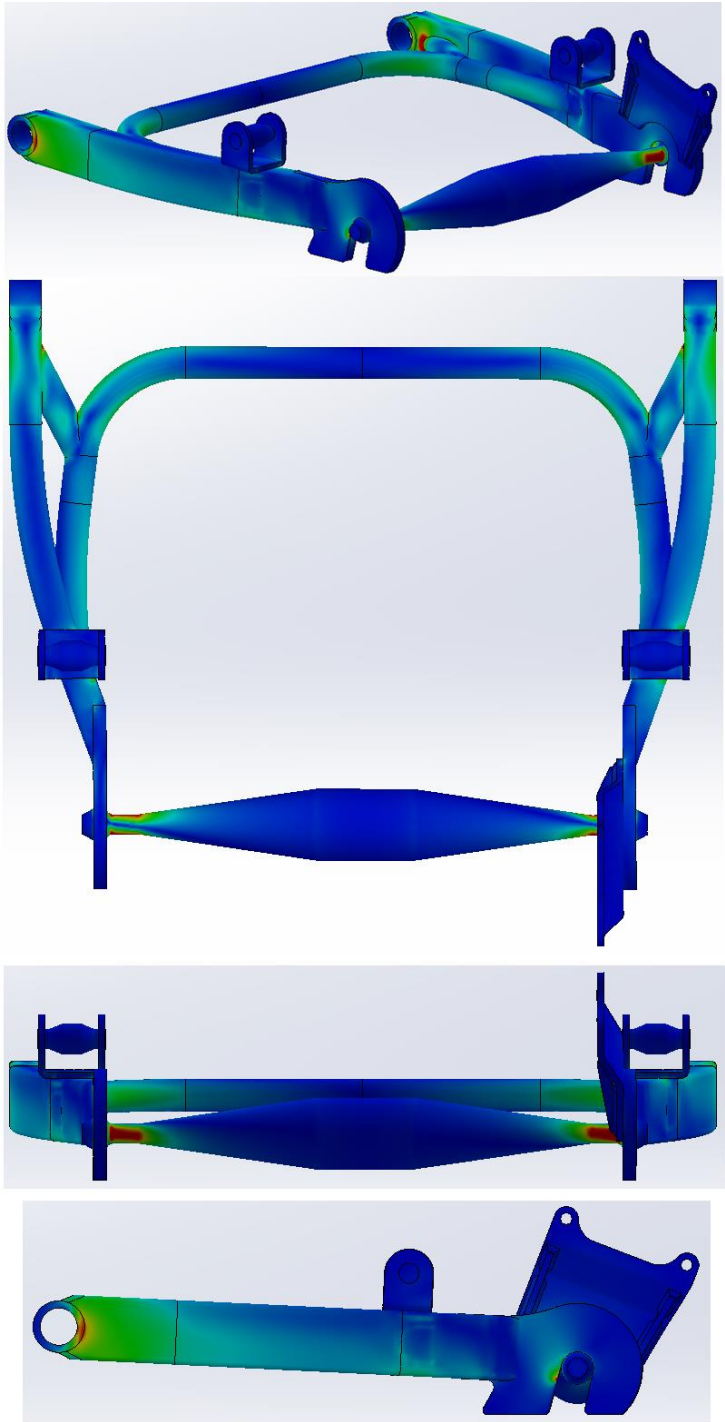

Figure B.3 The stress results from the hard cornering case, flat crossbar variant.

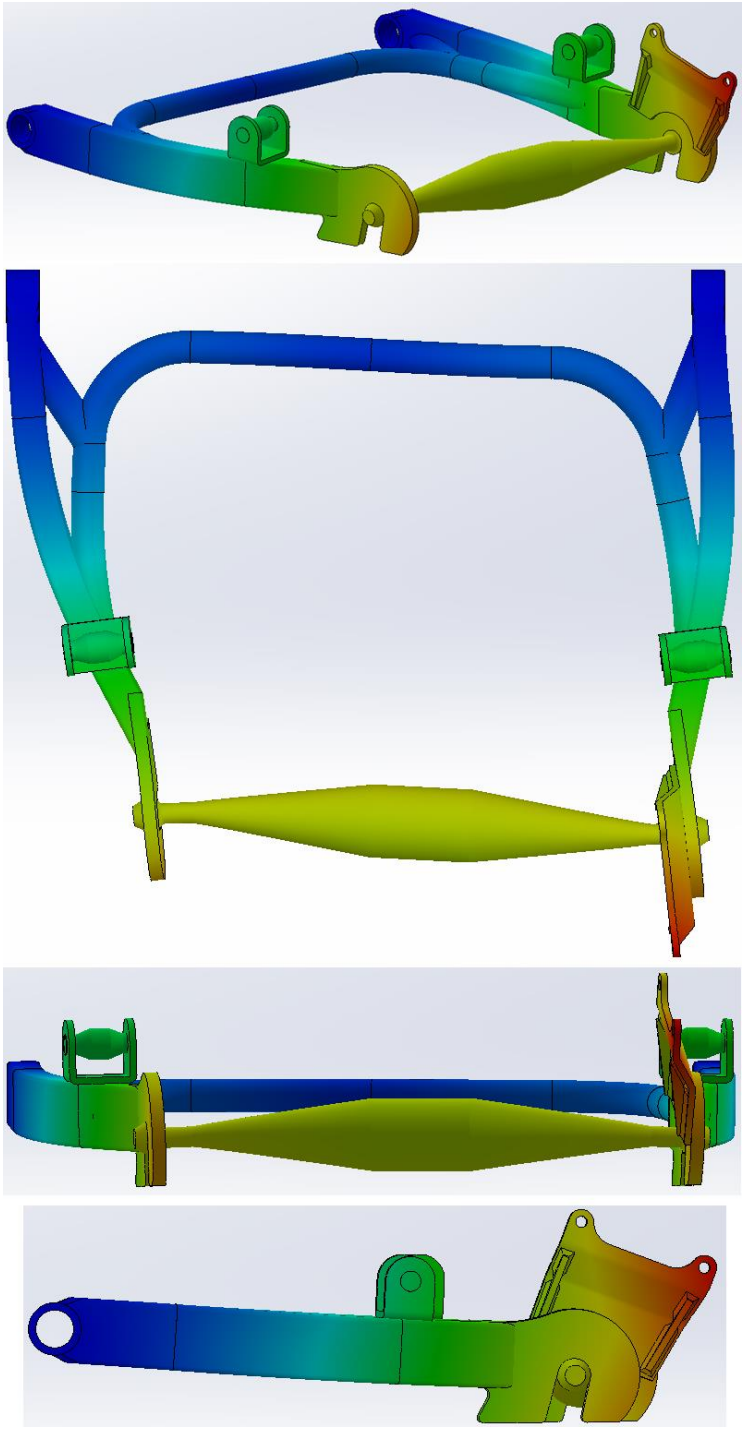

Figure B.4 The displacement results from the hard cornering case, flat crossbar variant. Deformation scale 25,3. The reddest node moved 1,75 mm.

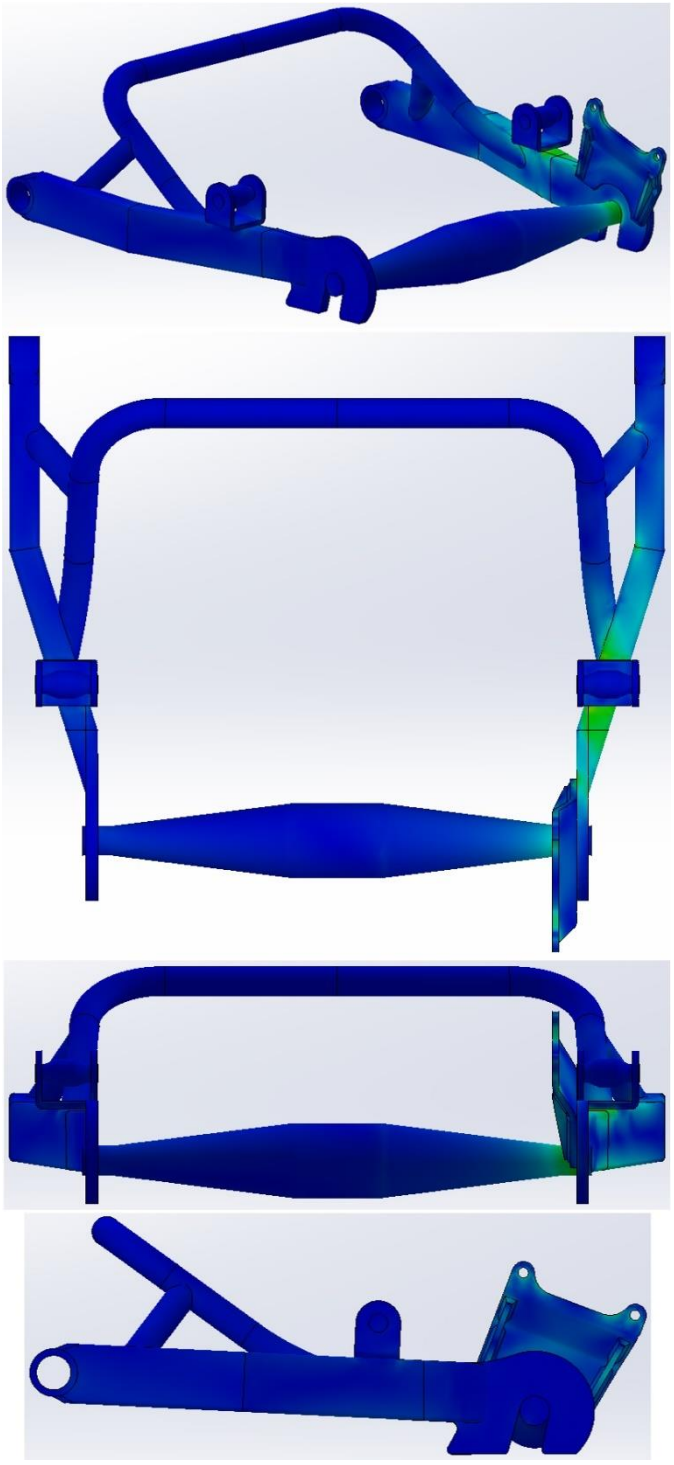

Figure B.5 The stress results from the hard braking case, high crossbar variant.

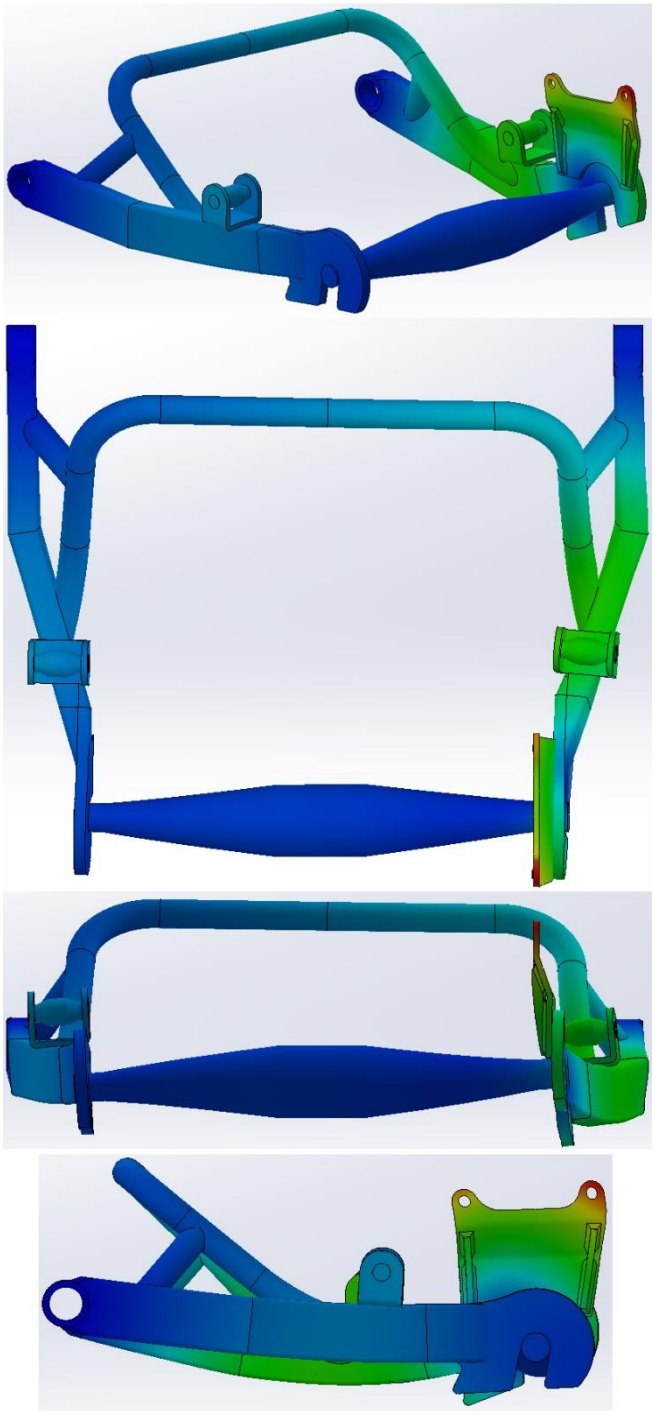

Figure B.6 The displacement results from the hard braking case, high crossbar variant. Deformation scale 180. The reddest node moved 0,281 mm.

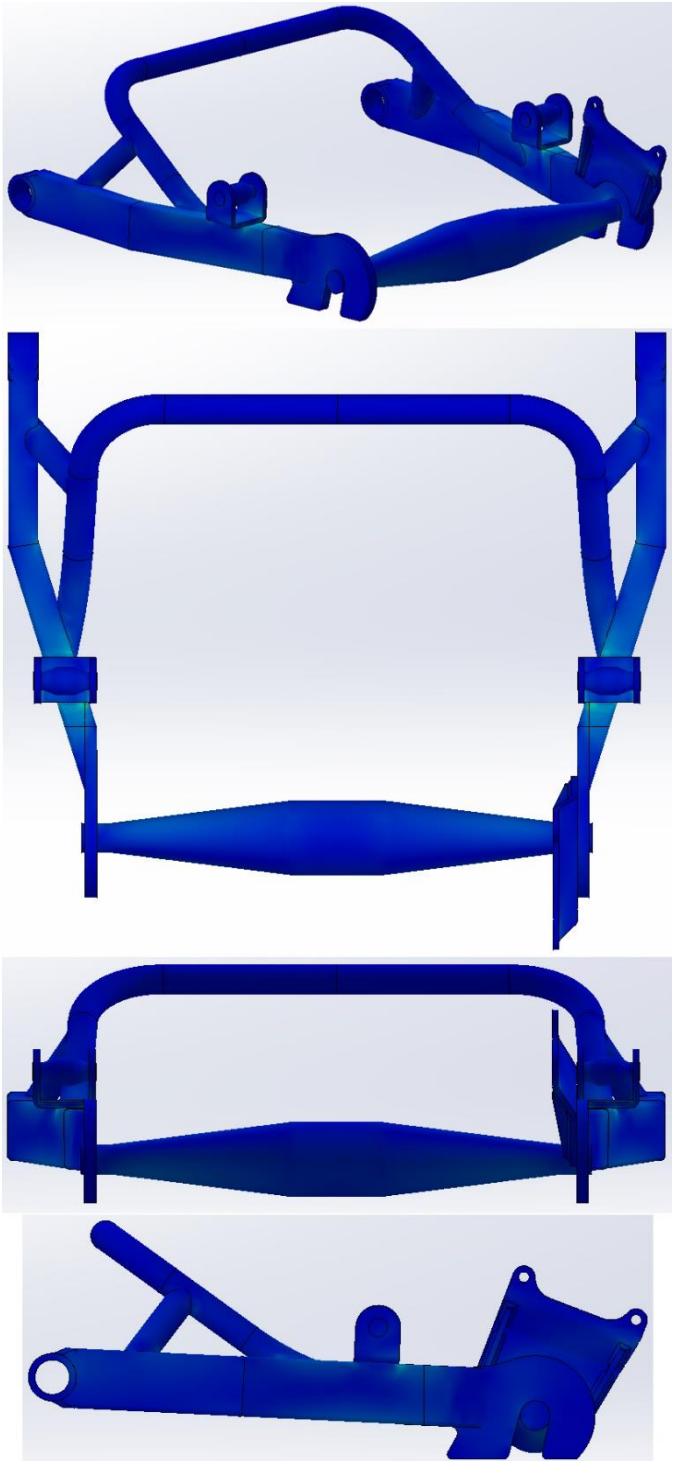

Figure B.7 The stress results from the maximum acceleration case, high crossbar variant.

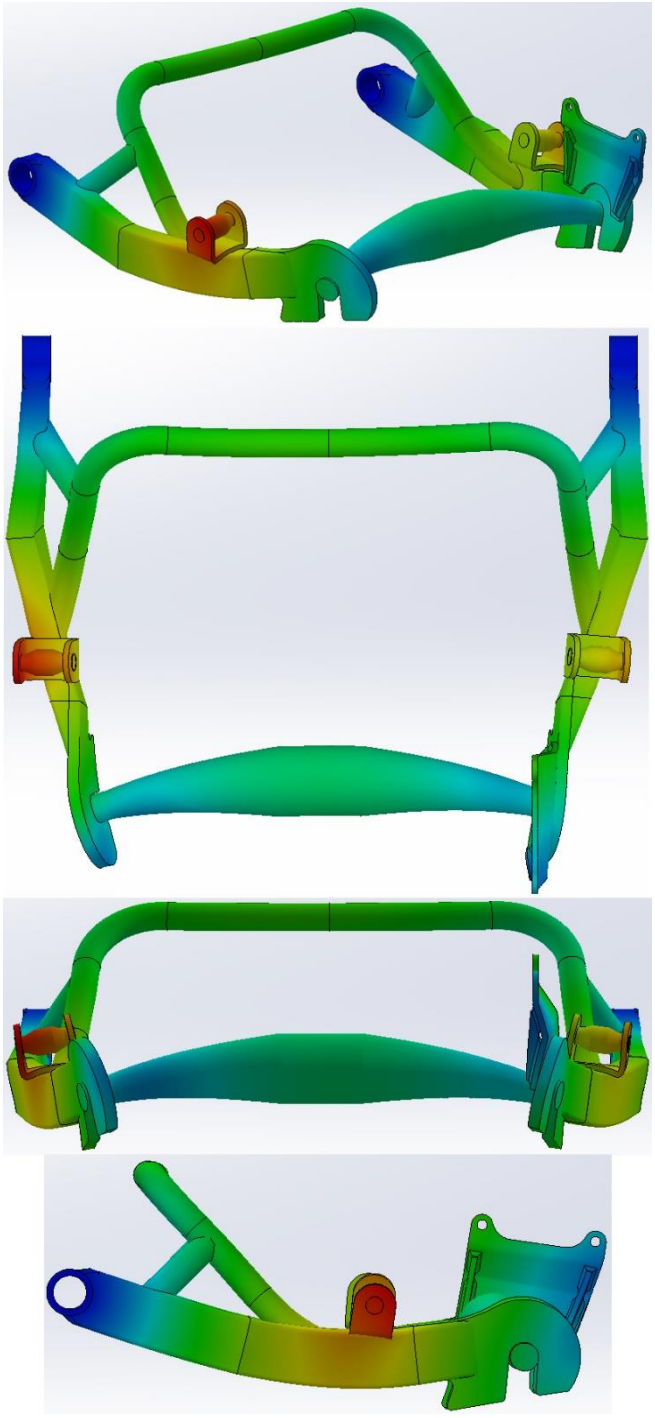

Figure B.8 The displacement results from the maximum acceleration case, high crossbar variant. Deformation scale 390. The reddest node moved 0,127 mm.

Appendix C FEM Results, Final Iteration

Views are shown in the same manner as Appendix A and B.

The stress results are shown with a maximum plot value of 220,6 MPa, the yield limit of ‘plain carbon steel’ in SW.

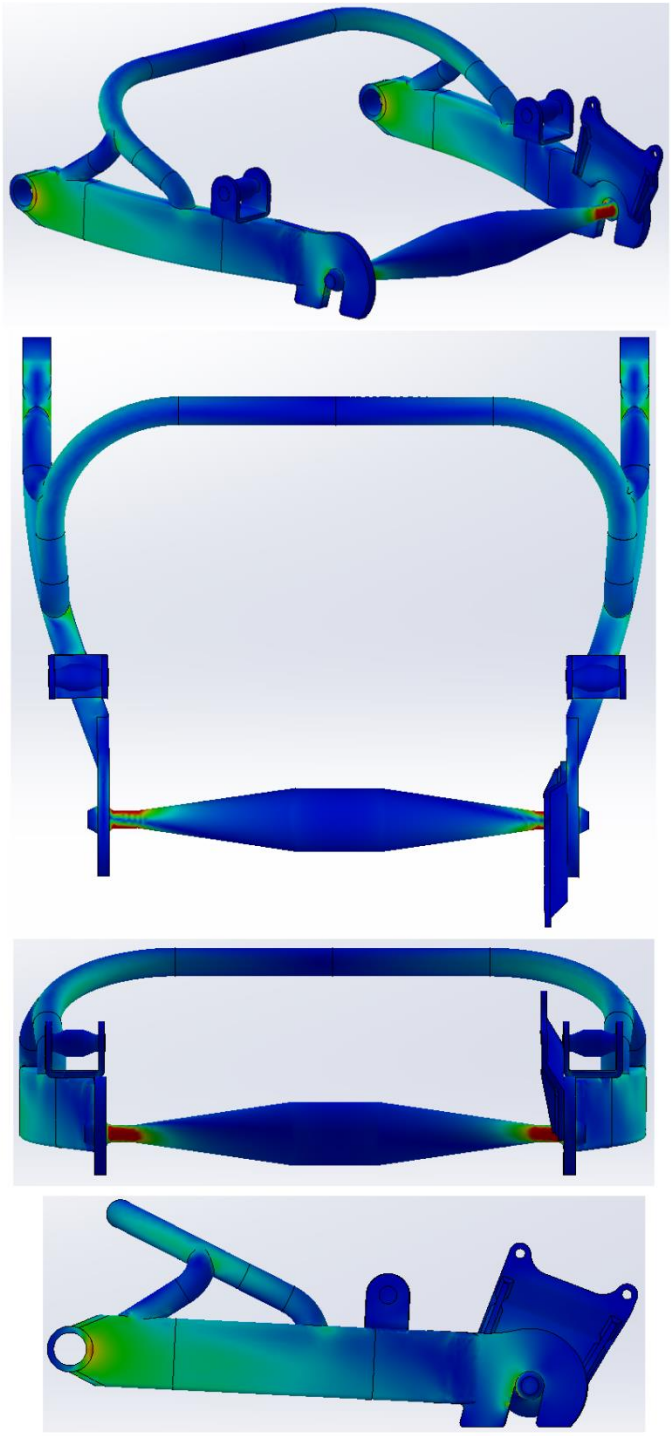

Figure C.1 The stress results from the hard cornering case, high crossbar variant.

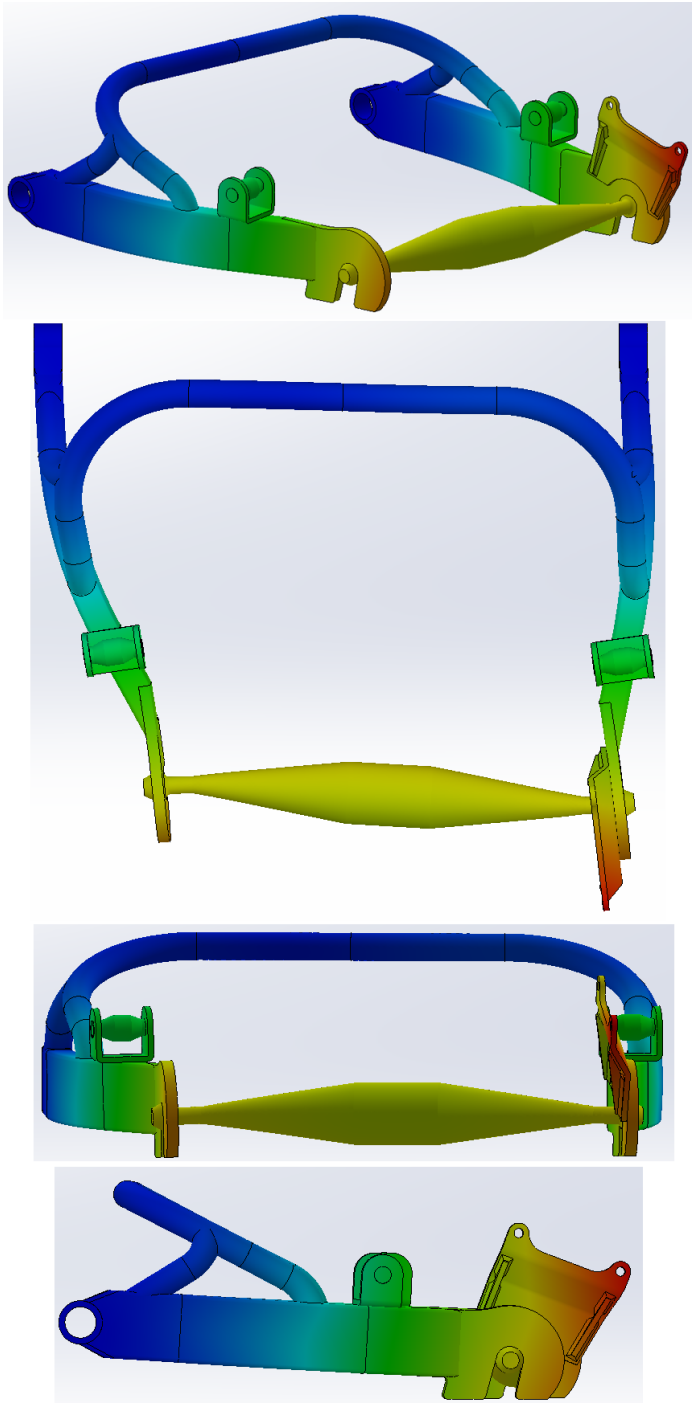

Figure C.2 The displacement results from the hard cornering case, high crossbar variant. Deformation scale 20,6. The reddest node moved 2,17 mm.

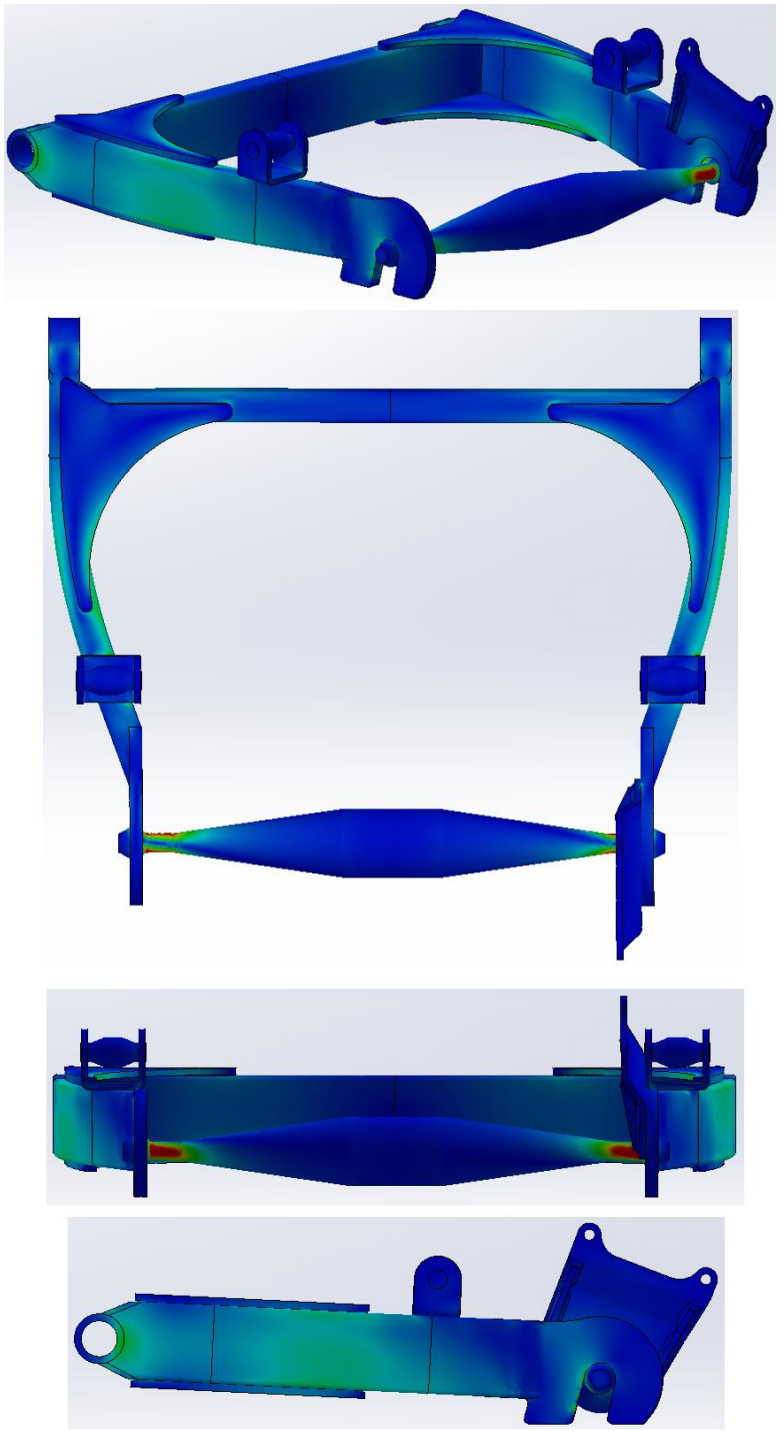

Figure C.3 The stress results from the hard cornering case, flat crossbar variant.

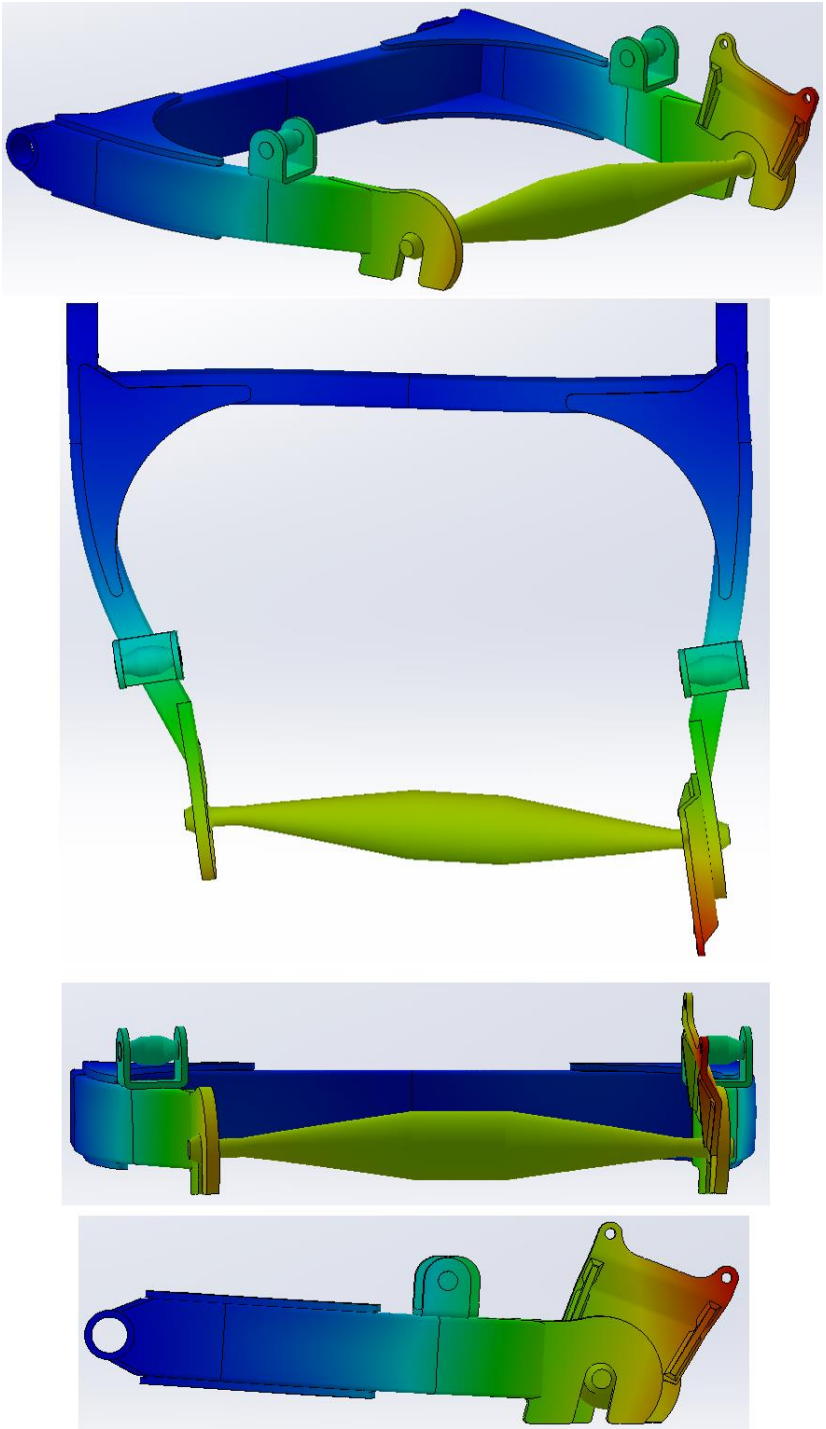

Figure C.4 The displacement results from the hard cornering case, flat crossbar variant. Deformation scale 29,1. The reddest node moved 1,54 mm.

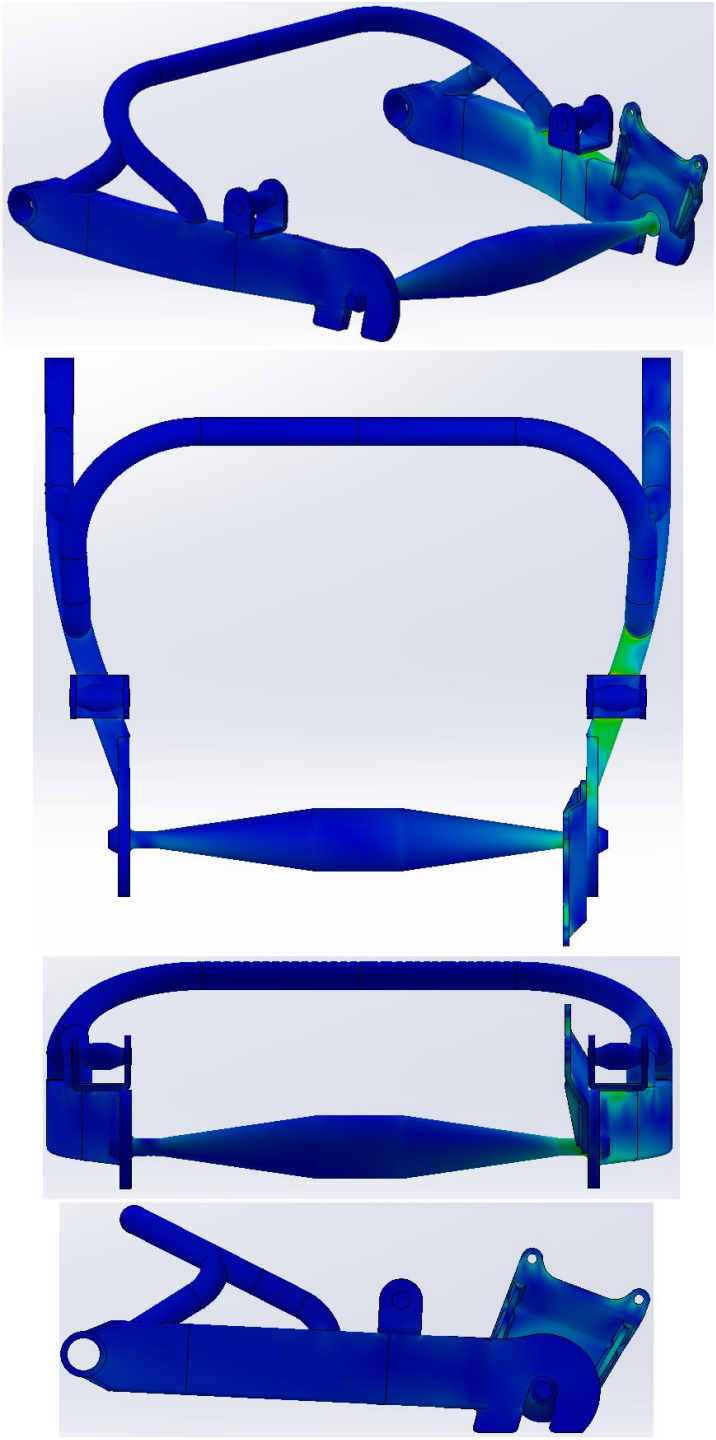

Figure C.5 The stress results from the hard braking case, high crossbar variant.

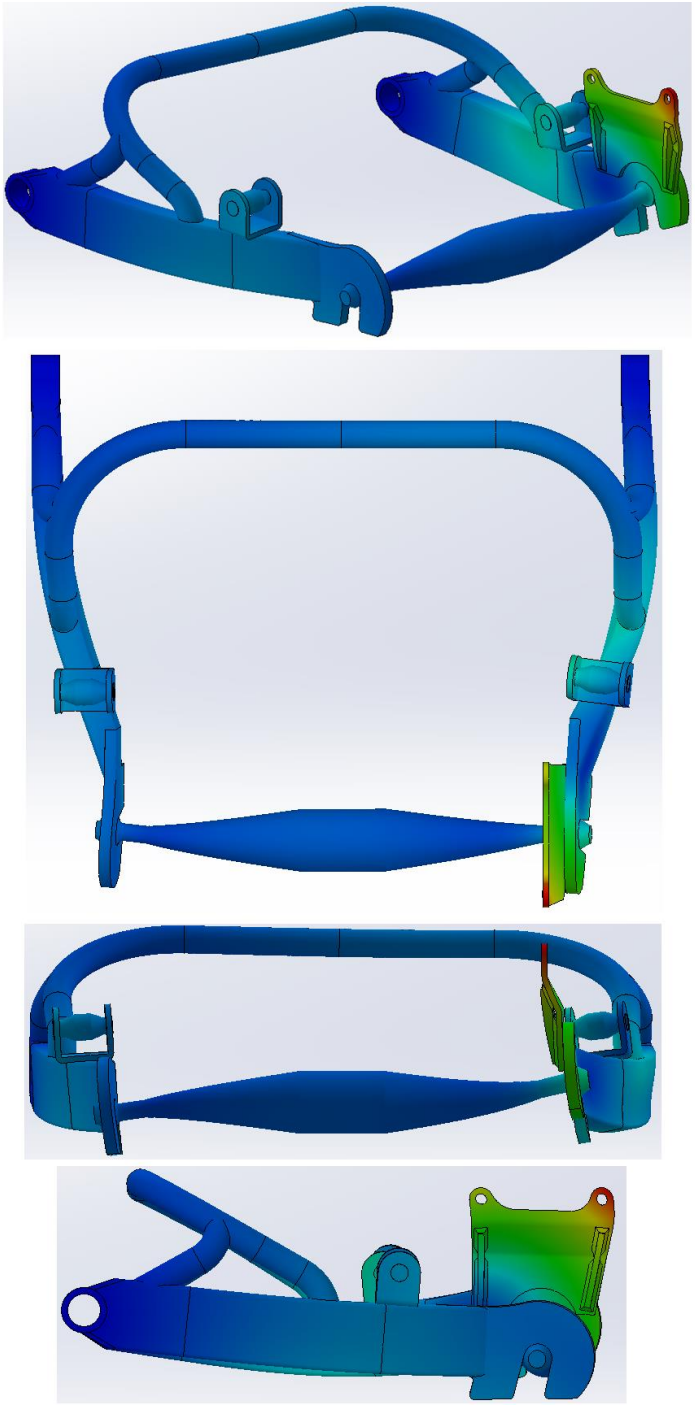

Figure C.6 The displacement results from the hard braking case, high crossbar variant. Deformation scale 154. The reddest node moved 0,321 mm.

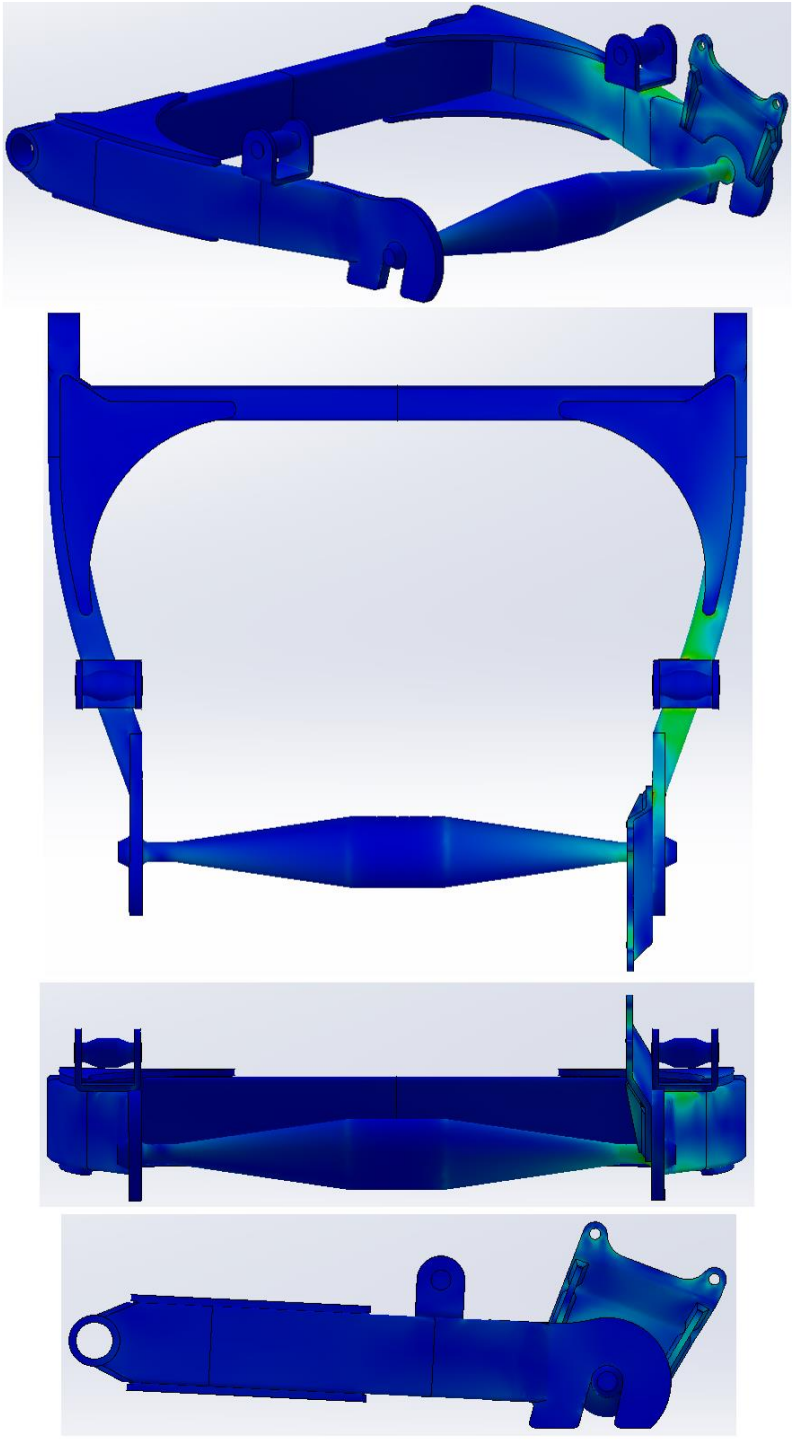

Figure C.7 The stress results from the hard braking case, flat crossbar variant.

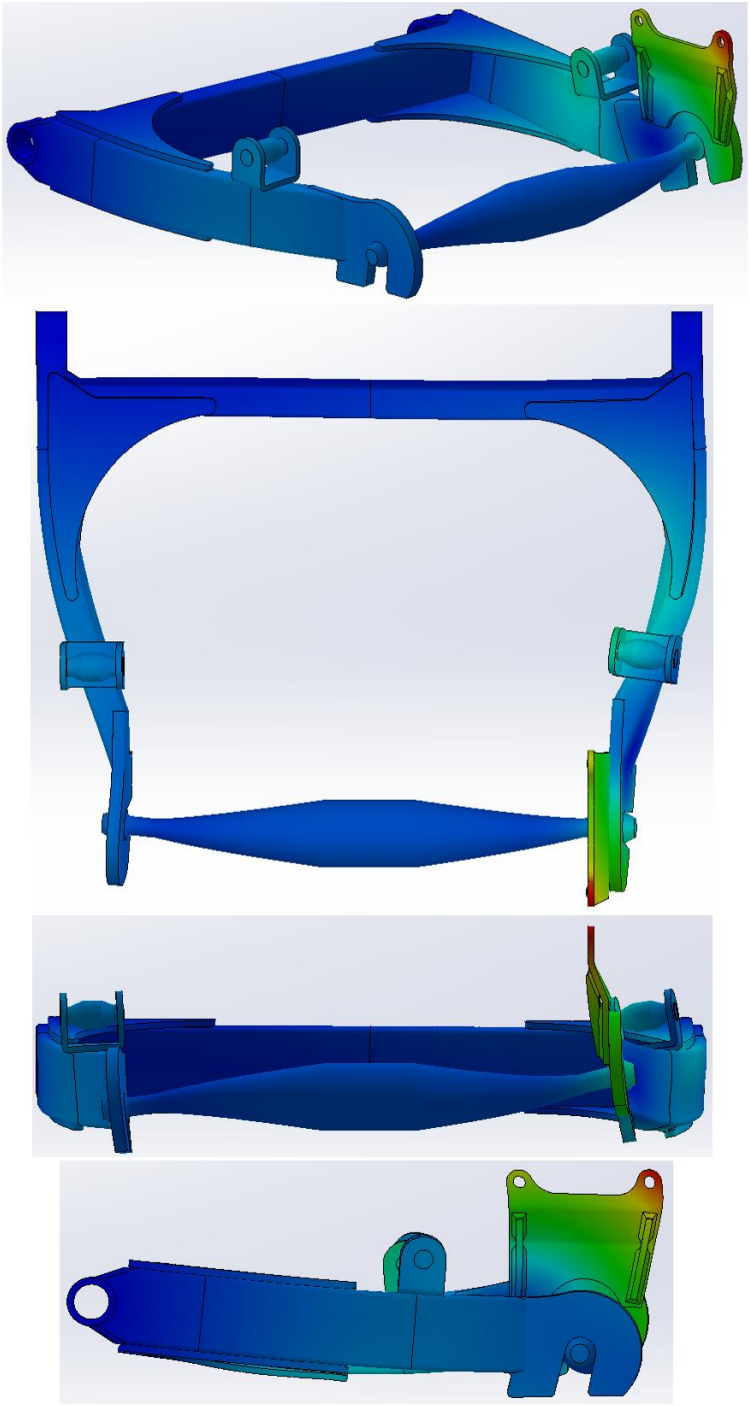

Figure C.8 The displacement results from the hard braking case, flat crossbar variant. Deformation scale 161. The reddest node moved 0,306 mm.

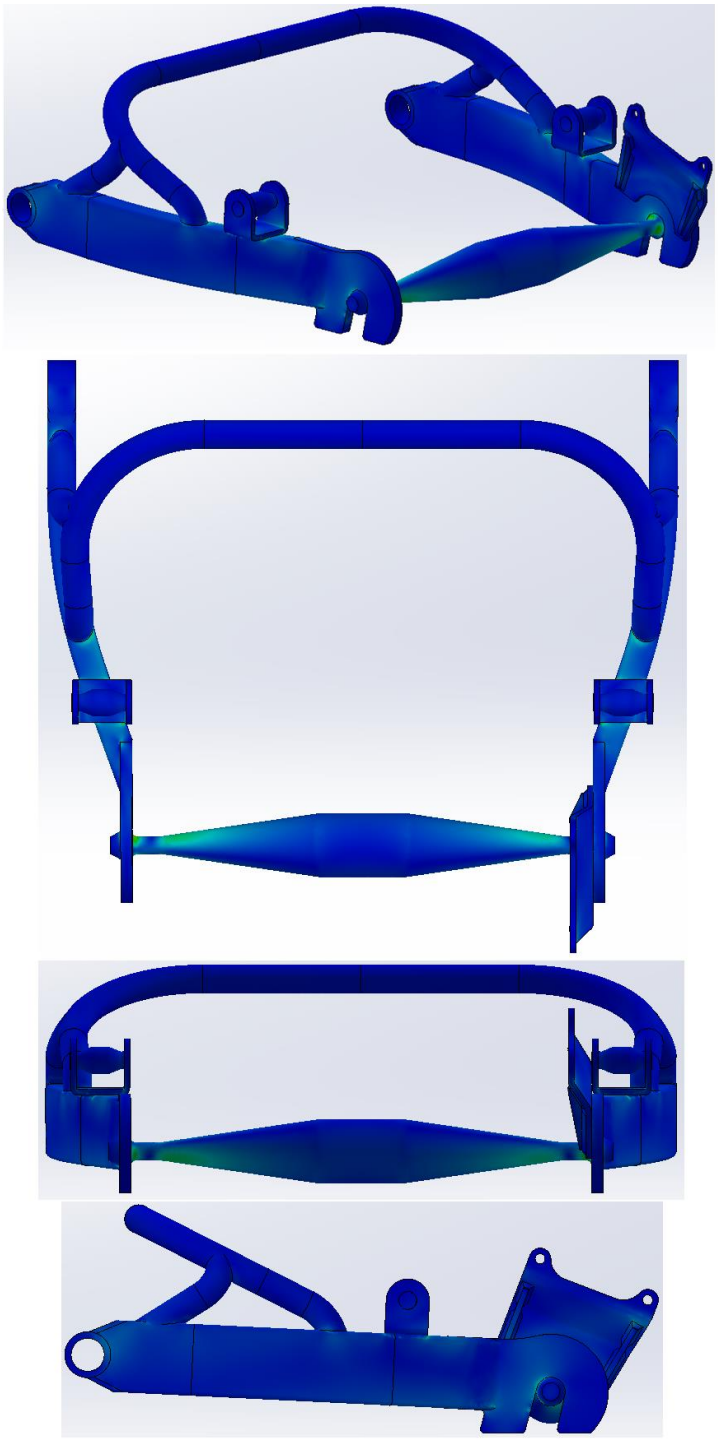

Figure C.9 The stress results from the maximum acceleration case, high crossbar variant.

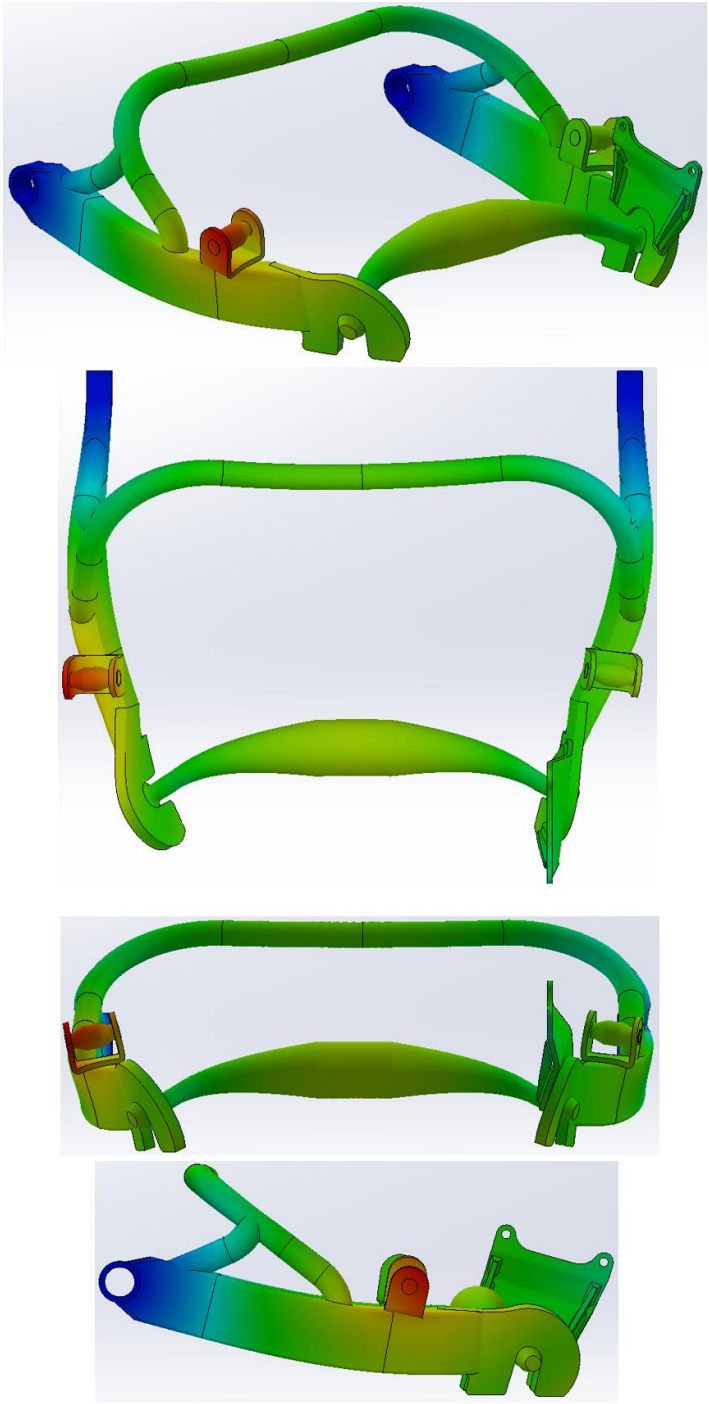

Figure C.10 The displacement results from the maximum acceleration case, high crossbar variant. Deformation scale 303. The reddest node moved 0,186 mm.

Figure C.11 The stress results from the maximum acceleration case, flat crossbar variant.

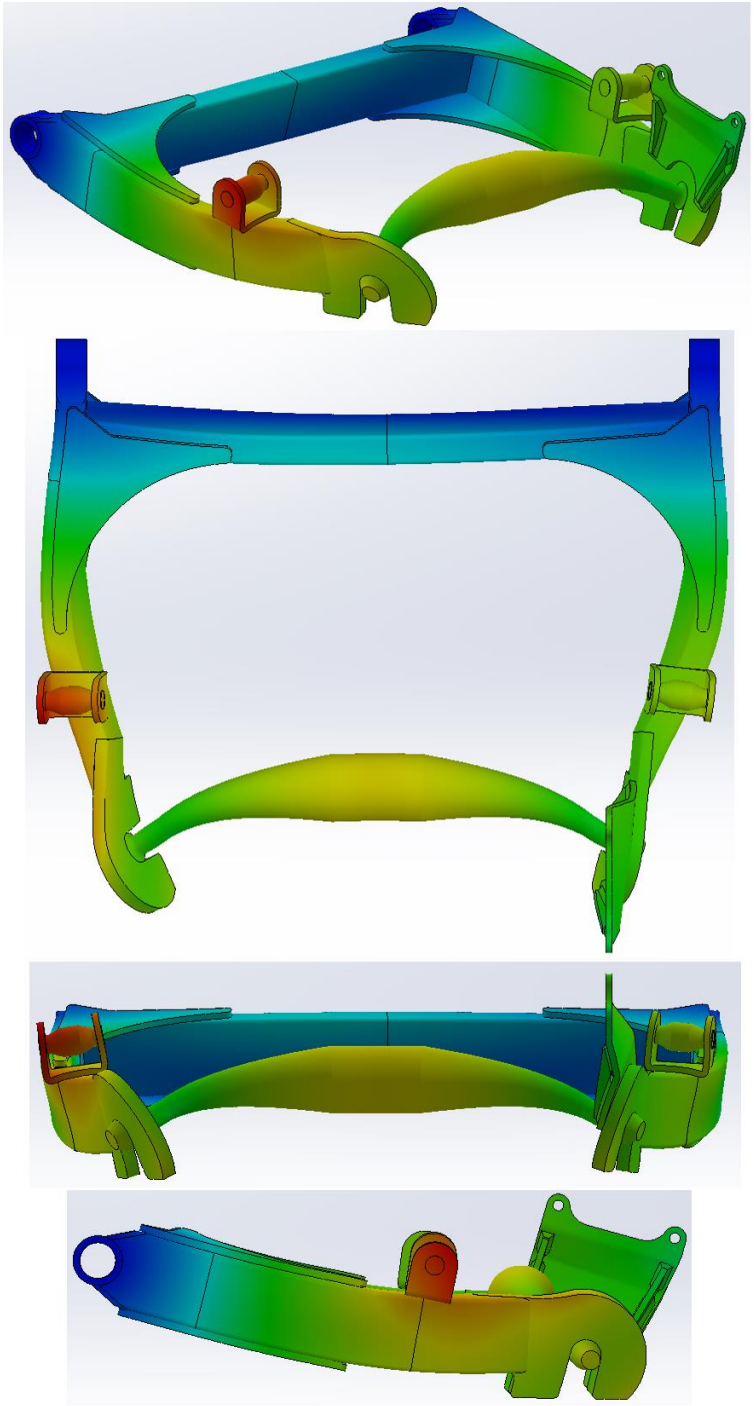

Figure C.12 The displacement results from the maximum acceleration case, flat crossbar variant. Deformation scale 326. The reddest node moved 0,162 mm.

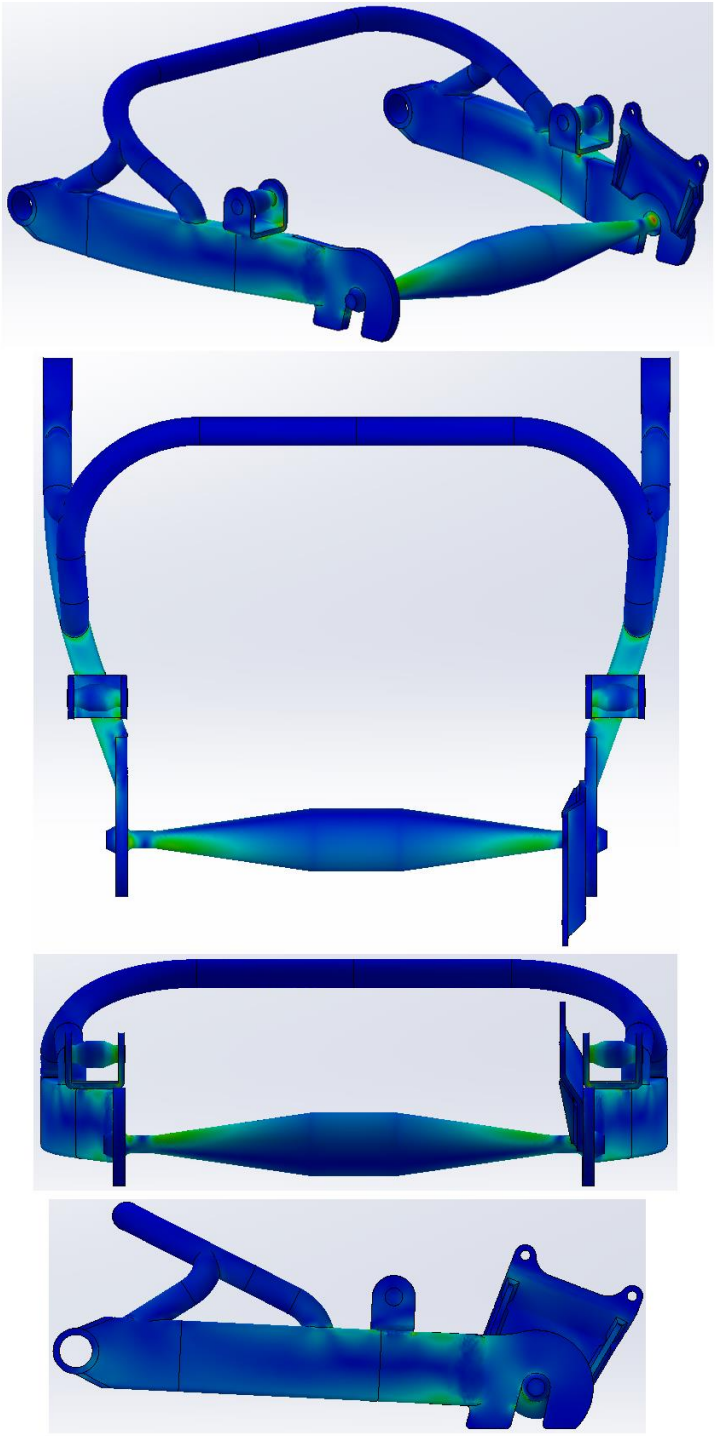

Figure C.13 The stress results from the road bump case, high crossbar variant.

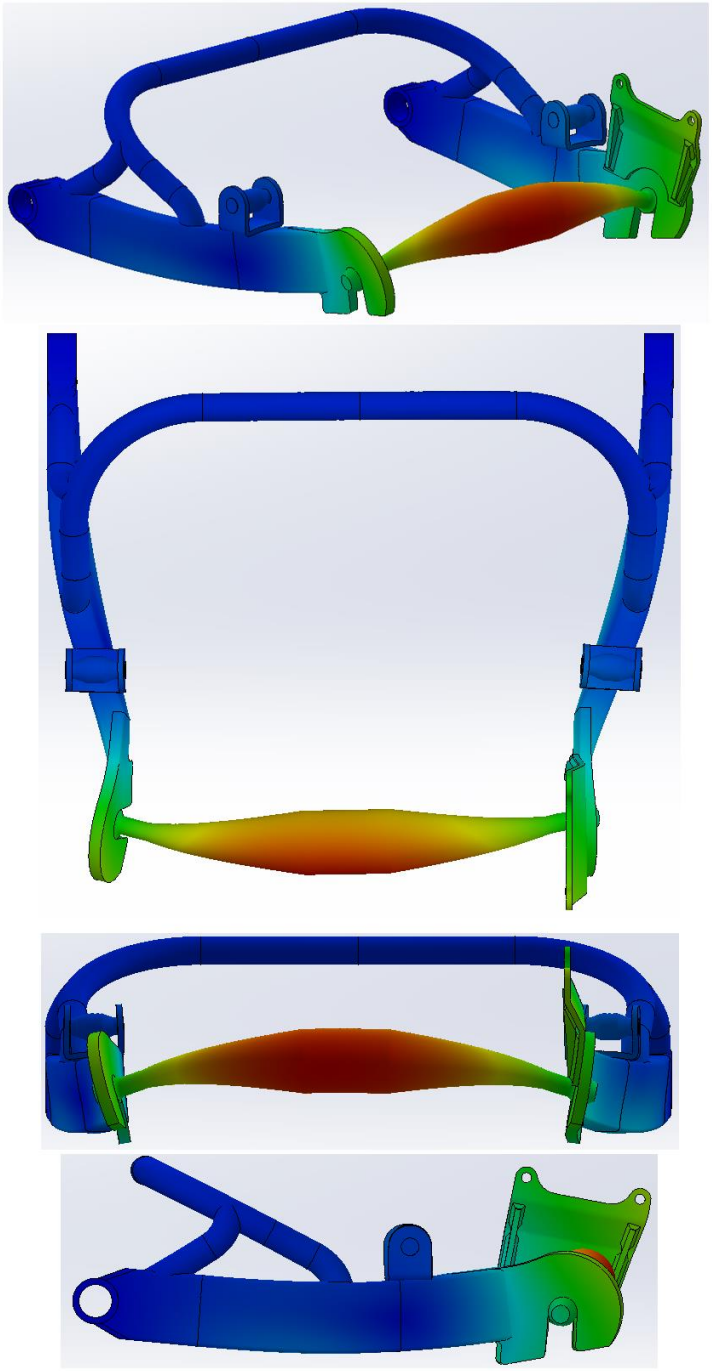

Figure C.14 The displacement results from the road bump case, high crossbar variant. Deformation scale 109. The reddest node moved 0,450 mm, but this information is of little value since its almost entirely due to the deflection of the simulated wheel axle.

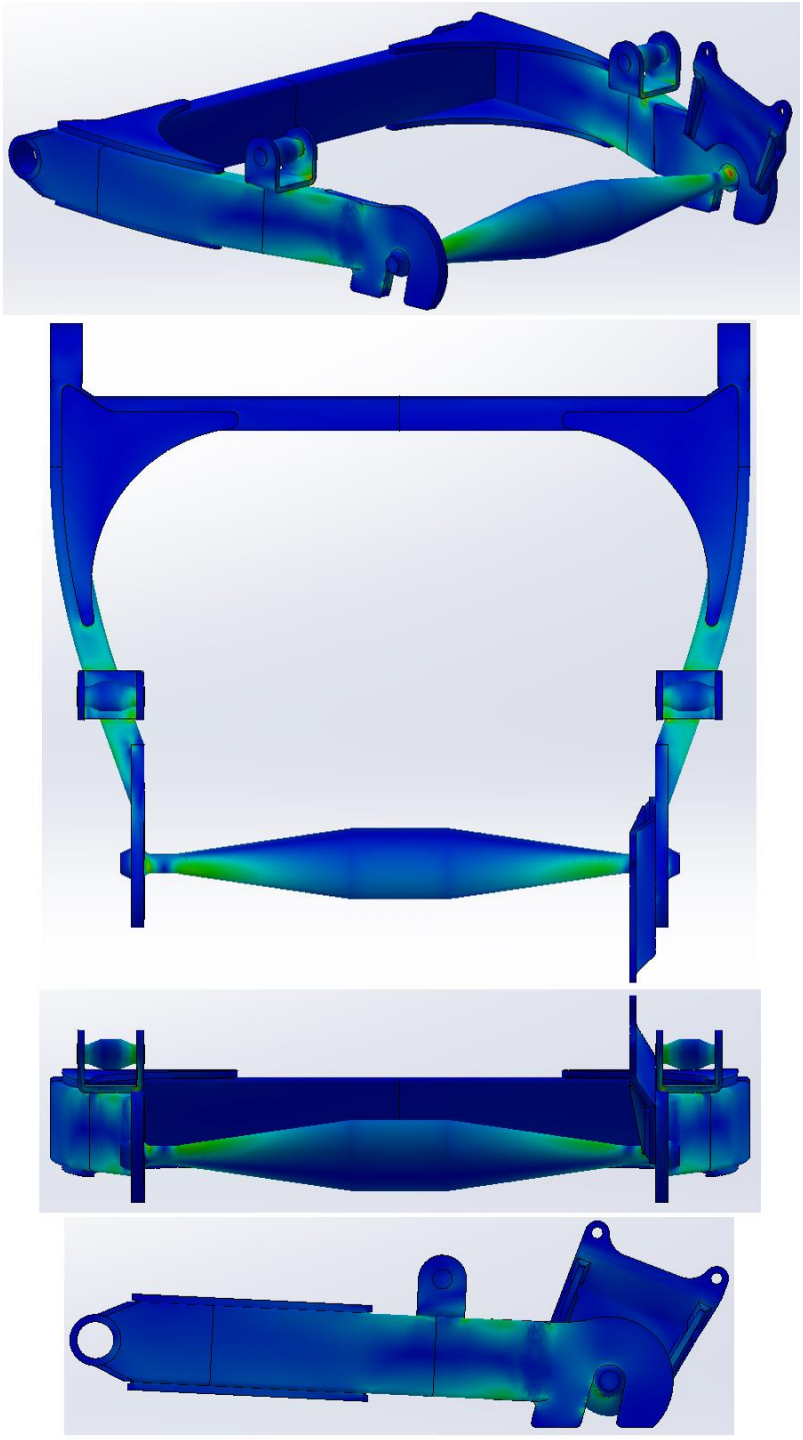

Figure C.15 The stress results from the road bump case, flat crossbar variant.

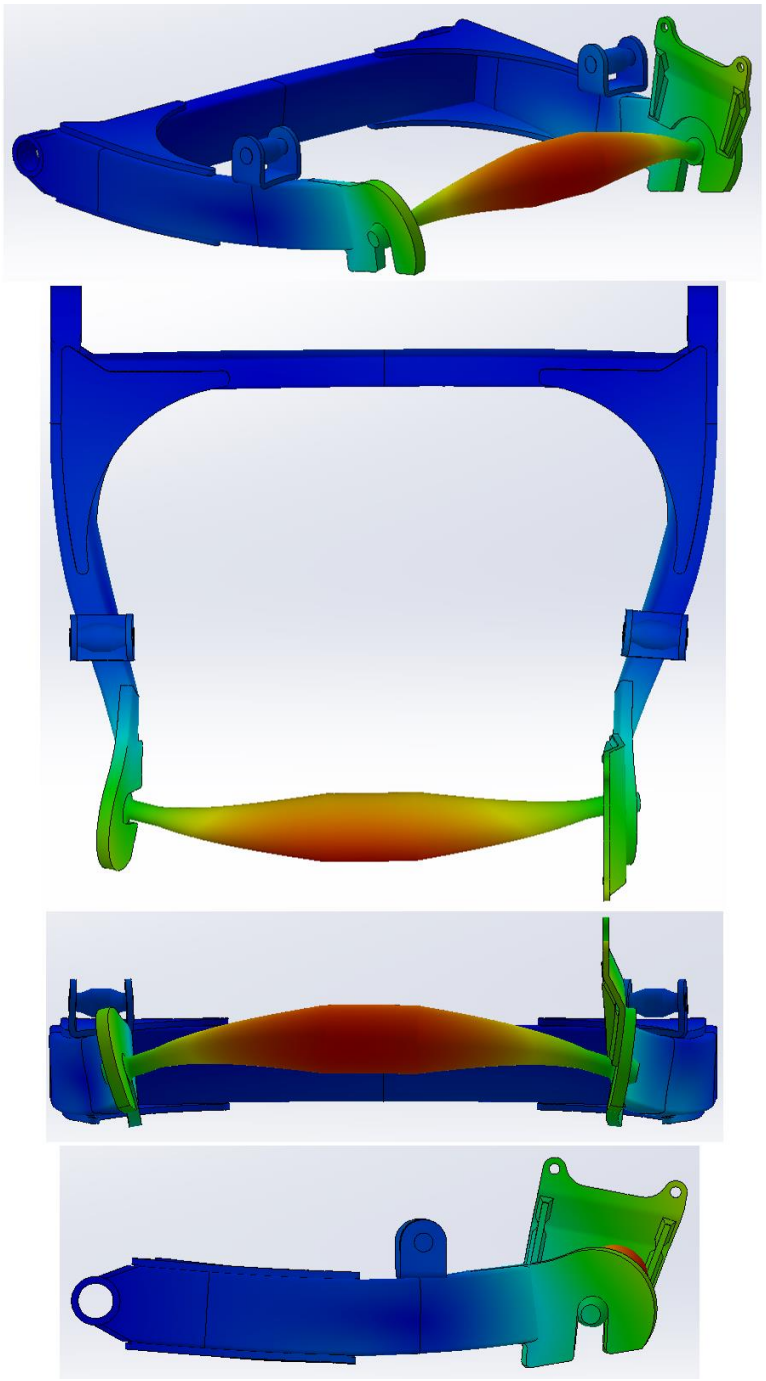

Figure C.16 The displacement results from the road bump case, flat crossbar variant. Deformation scale 109. The reddest node moved 0,448 mm (equally meaningless information as in Figure C.14).

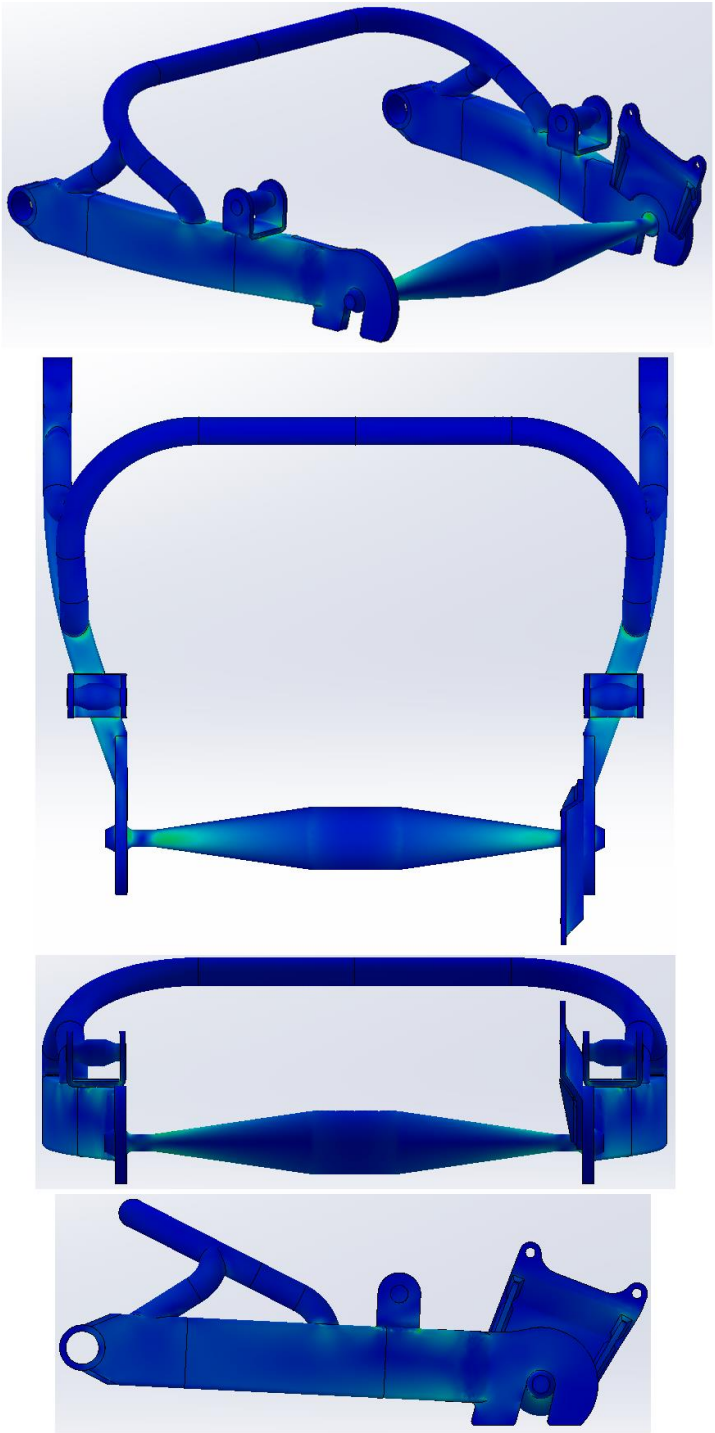

Figure C.17 The stress results from the full weight case, high crossbar variant.

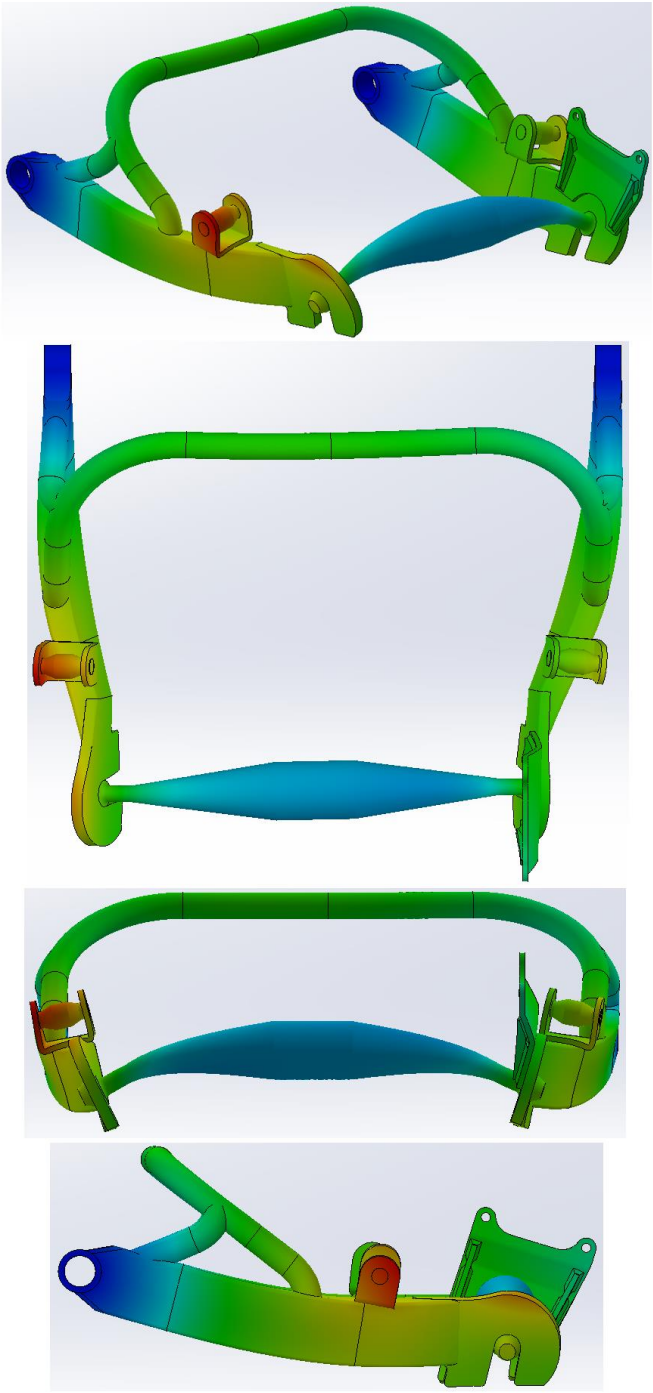

Figure C.18 The displacement results from the full weight case, high crossbar variant. Deformation scale 198. The reddest node moved 0,256 mm.

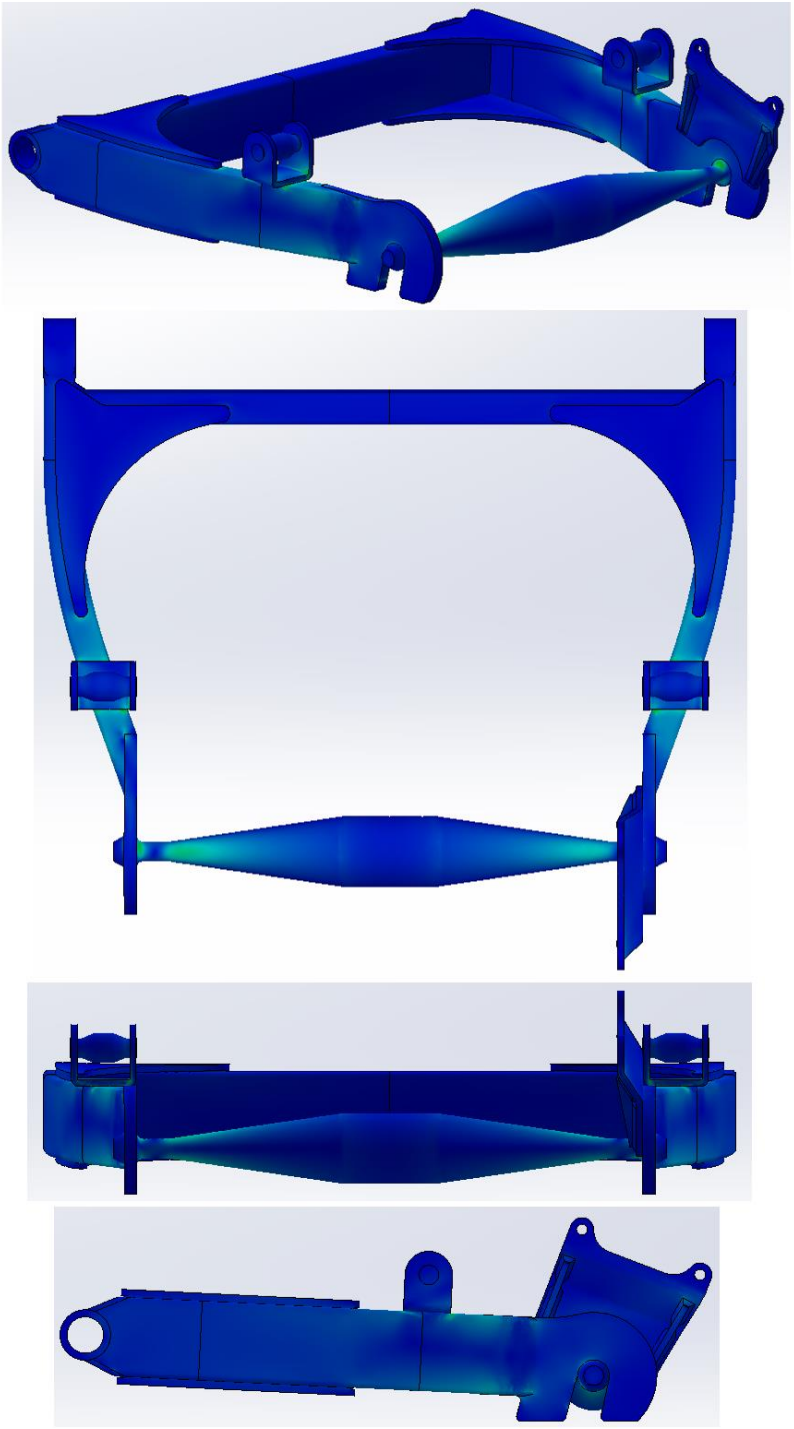

Figure C.19 The stress results from the full weight case, flat crossbar variant.

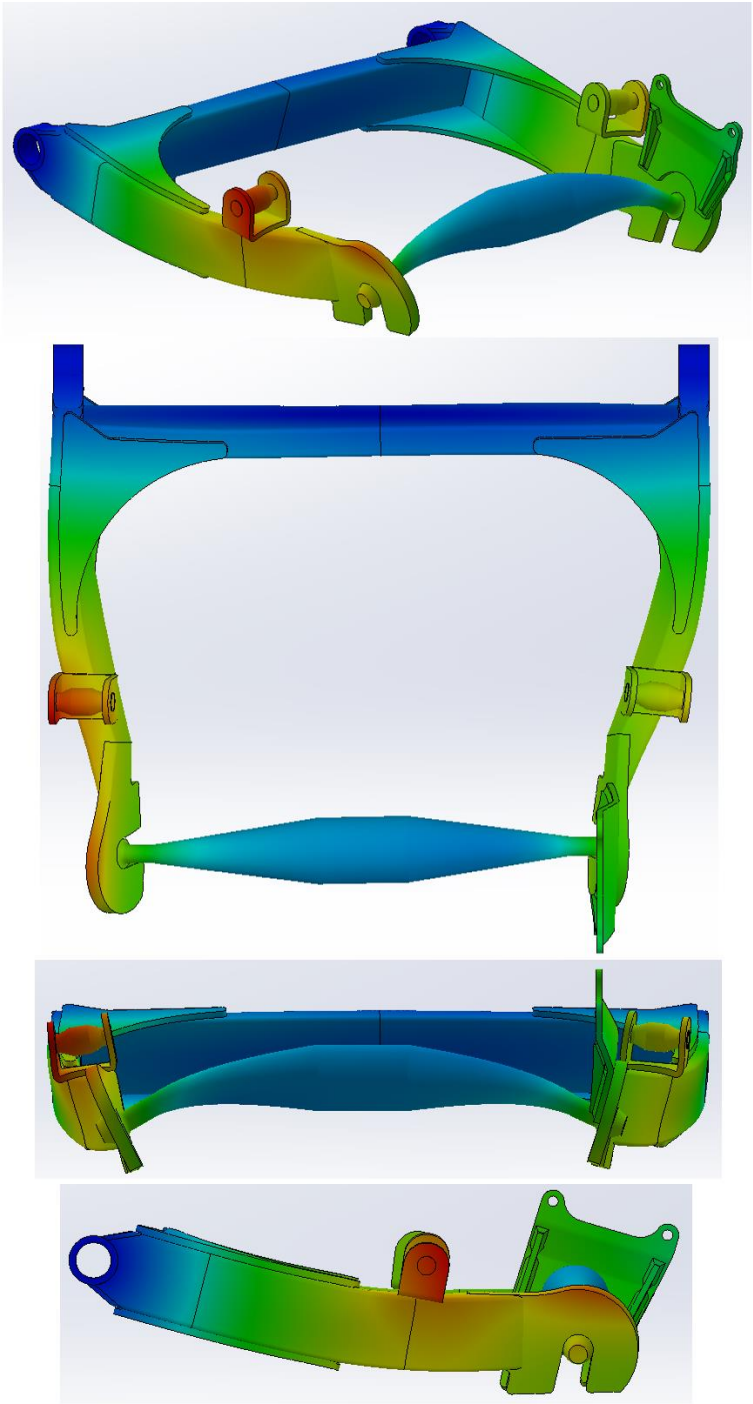

Figure C.20 The displacement results from the full weight case, flat crossbar variant. Deformation scale 219. The reddest node moved 0,221 mm.